AN ABSTRACT OF THE DISSERTATION OF

Alan J. Telecky for the degree of Doctor of Philosophy in Chemistry presented on May 1, 2012.

Title: Photoresist and Ion-Exchange Chemistry of HafSOx

Abstract approved: _____

Douglas A. Keszler

The chemistry of hafnium oxide based and materials are described in the context of ion exchange and lithography. HafSOx, represented by the composition $HfO_{2-x}(SO_4)_x$, is described to possess a significant capacity towards ion exchange in acidic and basic solutions, enabling films of HafSOx to be cleanly and readily be converted to oxide films by neutralization. The optical properties, composition and morphology of these oxide films are characterized. The fabrication of mixed metal oxide films is demonstrated via solution and ion exchange routes.

This thesis also explores the photoresist chemistry of HafSOx resists. A photoreaction mechanism based on the decomposition of peroxide is proposed. In addition, the patterning of HafSOx films by 193 nm, extreme ultraviolet (EUV) and electron beam radiation is described, and the influence of composition on its photoresist properties is studied.

Photoresist and Ion-Exchange Chemistry of HafSOx

by

Alan J. Telecky

A DISSERTATION

submitted to

Oregon State University

in partial fulfillment of
the requirements for the
degree of

Doctor of Philosophy

Presented May 1, 2012

Commencement June 2012

Doctor of Philosophy dissertation of Alan J. Telecky presented on May 1, 2012.

APPROVED:

_____

Major Professor, representing Chemistry

_____

Chair of the Department of Chemistry

_____

Dean of the Graduate School

I understand that my dissertation will become part of the permanent collection of Oregon State University libraries. My signature below authorizes release of my dissertation to any reader upon request.

_____

Alan J. Telecky, Author

ACKNOWLEDGMENTS

First and foremost I must thank my advisor Prof. Douglas A Keszler for the integral part that he has played towards the work contained within this thesis and during the course of my graduate career. His knowledge and intellect have always astounded me, and because of his guidance and support I was afforded ample supplies, resources, and opportunities that I otherwise would have not. Thus, my immense gratitude for his charitable and invaluable support cannot be understated.

The role and influence of Prof. Anthony Diaz also must be acknowledged. My potential interest in materials science and solid state chemistry lay unexplored before engaging in research in his lab, and the experience and knowledge gained therein proved to be life changing. His insight and viewpoints were always welcomed, and his lasting friendship continues to bear fruits, not the least of which are found in the form of snare drums and electric guitars.

I would be remiss to fail to recognize the members of the Keszler Research Group. Chris Knutson and Wei Wang, in particular, have vitally contributed to my interpretation and knowledge of chemistry through countless discussions in and out of the office, and of whom I have nothing but respect. Bill Cowell, an honorary member of the Keszler Group, deserves recognition here as well, as a valued colleague, friend, and engineer.

I am likewise indebted to the team of scientists at Inpria, most notably Andrew Grenville, Jason Stowers and Jeremy Anderson, for their support and

wisdom. The internship and collaboration with Inpria provided me with experience, knowledge, and education that are invaluable, and it is a relationship that I am eager to continue.

I also extend much gratitude to my committee members Dr. John Wager, Dr. Michael Lerner, Dr. Mas Subramanian, and Dr. William Warren for the time and knowledge they generously shared with me. I only hope I can retain a fraction of the information they had to give.

My friends and family deserve mention. My parents, Annamae and Alan, provided me with unfailing support and encouragement, and they bear more responsibility than anyone for nurturing my interest in the sciences. Their contributions to my life and career are incalculable. Similarly, my friends have shaped my interests and personality in many ways, and have made me the person I am today. They are my wolf pack.

I must also thank the other central influence on the completion of this thesis: my wife Kelsey. Her friendship has supported me through its entire course, and her love remains unconditional. Her beauty and affection is matched only by that of our lovely daughter, Elia, who is a remarkable and unending source of joy, pride, and hope for the both of us. I can only hope Elia grows up to appreciate the sciences as I have.

Lastly, I need to thank the Rolling Stones and Neil Young for providing what has largely been the soundtrack of my academic career.

CONTRIBUTION OF AUTHORS

A number of people have contributed to the work contained within this thesis. Jeremy Anderson developed the HafSOx system with which this thesis concerns itself and, together with Jason Stowers, has laid the foundation and basis for the patterning of HafSOx.

Deidre Olynick contributed to Chapter 2 in the form of facility and instrumental support, while Ben Clark contributed through data collection and analysis. Wei Wang provided manpower for conducting the TOF-SIMS analyses described in Chapter 5.

Chapter 3 is taken from a joint publication with co-authors Peng Xie and Bruce Smith from the Rochester Institute of Technology, Jason Stowers and Andrew Grenville from Inpria, and from Prof. Douglas Keszler.

Prof. Douglas Keszler has contributed to every chapter through suggestions, observations, and interpretations contained within this thesis.

TABLE OF CONTENTS

TABLE OF CONTENTS (Continued)

TABLE OF CONTENTS (Continued)

TABLE OF CONTENTS (Continued)

LIST OF FIGURES

LIST OF FIGURES (Continued)

LIST OF FIGURES (Continued)

LIST OF TABLES

PHOTORESIST AND ION-EXCHANGE CHEMISTRY OF HAFSOX

CHAPTER 1

INTRODUCTION

Moore's Law and the Importance of Lithography

In a way, and perhaps very unsurprisingly, Moore's Law has been a motivating factor for the research contained within this thesis. Moore's Law, derived from a statement by Intel co-founder Gordon Moore in 1965, predicts that every two years the density of transistors on an integrated circuit will double.[1] The consequences of this statement are profound when one thinks about the evolution of a chip and its journey from a single crystal of silicon to a modern quad-core processor or similar device. It is immediately obvious that the success of Moore's Law depends on the concerted and complementary efforts of physicists, chemists and engineers. Nowhere in the microfabrication process is this coordination of disciplines more evident than in the photolithographic process in which the patterning of the wafer occurs to create discrete active elements such as a transistor.

The modern photolithographic process is a highly complex and refined technology. An ArF excimer laser is used to produce 193 nm light that is then directed at a photoresist-coated substrate through a photomask. The photoresist converts this aerial distribution of light into a 3D spatial distribution of solubility. In a subsequent etch step the photoresist pattern is then transferred into the underlying substrate or layer. This step is referred to as pattern transfer. Figure 1.1 illustrates a simplified photolithographic process flow. Such a process is often repeated on a single wafer up to 50 times.

The chemistry and performance of the photoresist is of the upmost importance for achieving performance in the overall process. For nanometer sized patterns to be imaged the photoresist material it needs possess a good contrast between soluble and insoluble areas. A low roughness, especially, is highly important when one considers the implications of a roughness of a few nanometers of a feature with a critical dimension on the order of nanometers.

In addition to the photoresist itself a number of other layers are often needed to aid pattern transfer. For example, hardmasks, which are typically vacuum-deposited inorganic oxides or spin-coated Si-containing polymers, can substantially increase the etch budget of a standard polymer resist. The hardmask itself, however, must be patterned via an overlying polymer resist before pattern transfer to the substrate. Hence, such hardmask patterning considerably increases the complexity of the photolithographic process. The introduction of a sensitive spin-coatable and photopatternable hardmask alone would reduce the complexity of the entire process considerably.

The primary focus of this thesis deals with the chemistry of HafSOx and ZircSOx as photoresists for 193-nm, extreme-ultraviolet (EUV) and electron-beam lithographies. HafSOx and ZircSOx are members of a more general MSOx system represented by the formulas $HfO_{2-x}(SO_4)_x$ and $ZrO_{2-x}(SO_4)_x$, where the ratio between metal and sulfate is varied across the range $0.5 < x < 0.9$.[2] These material systems possess a number of advantages for process integration: they are deposited via spin coating of aqueous precursors, the films are X-ray amorphous and their

surfaces are atomically smooth. These properties enable low line width roughness and high resolution. Additionally, their precursor chemistries are extendable to other metals. Therefore a wide range of properties can be realized by the MSOx system by simply controlling the identity of the constituent metals and manipulating the ratio of sulfate to metal.

In this chapter, I will provide brief descriptions of some chemistries and histories relevant to the unique chemistry of HafSOx and its implications, including a background of metal oxide solution chemistry, an introduction to ion exchange, and a description of lithography and photoresists. On the surface these topics may not seem correlated, but this thesis attests otherwise. Lithography is a multi-step process where numerous chemical considerations need to be taken into account, such as the chemical and physical changes that occur during exposure, and the implications of aqueous base development, particularly of an inorganic resist like HafSOx.

The exposure of HafSOx resists by 193 nm light and electron beams will be investigated in Chapters 2, 3 and 4. First, chapter 2 will demonstrated the use of Raman spectroscopy to explore the exposure mechanism of HafSOx resists during electron beam irradiation. Next, chapter 3 highlights the versatility of MSOx resists with respect to the relationship between composition and optical properties. Additionally the use of MSOx resists as photopatternable hardmasks and in double patterning approaches is described. Chapter 4 examines the effects of metal

substitution in HafSOx with respect to the resolution, line width roughness, and sensitivity when exposed to electron beams.

Chapters 5 and 6 will elaborate on the ion-exchange chemistry of HafSOx resists. The ion-exchange chemistry of HafSOx resists plays an important role in the development step in the lithographic process, and the mechanisms and processes involved have a direct impact on the performance of HafSOx as a resist.

Solution Deposition of Metal Oxides

Metal oxides are of paramount importance to the continued success and integration of modern technology. From ceramics to solar cells, and windows to medicine, metal oxides have enabled the progress of a wide range of industries, and their importance will only increase as new and varied forms of technology continue to integrate into our daily lives. For example, the proliferation of smart windows, smart phones, photovoltaics, flat panel displays and other devices has been driven and enabled by the integration of thin film oxides such as zinc oxide (ZnO), indium tin oxide (ITO), and hafnium oxide (HfO_2).

Many of these oxides are prepared as high-quality films through vacuum methods such physical vapor deposition (PVD), chemical vapor deposition (CVD), or atomic layer deposition (ALD).[3,4,5] These techniques, however, require high vacuum, they are slow, and they are inefficient with respect to energy and material utilization. On the other hand, solution processing of metal oxide films can offer certain advantages. For example, solution-based approaches are readily scalable.

In wafer processing, spin-coating can be integrated on a conventional track system. For large area applications, aerosol CVD, capillary coating, and ink-jet printing offer options of limiting material use and enabling processing in air. Despite these advantages, it remains a challenge for solution processed materials to meet or exceed the performance of their vapor-deposited counterparts.

A vast library of solution routes for deposition of metal oxide thin films can be found in the literature. A common theme of these routes involves the use of metal-organic based precursors.[6,7] These routes employ chemistries where metal-oxide bonds are formed by hydrolysis and condensation of metal alkoxides or similar metal-organic species:

<u>Hydrolysis:</u> M-OR' + H_2O → M-OH + HO-R'

<u>Condensation:</u> M-OH + M-OH → M-O-M + H_2O

Dense films useful for electronics are difficult to prepare by sol-gel methods. It is generally a difficult task to effectively control the hydrolysis of metal alkoxides. It is common for these hydrolyses to produce large sol particles that pack into low density, rough films. At the same time, rapid or incomplete hydrolysis followed by condensation can trap organic components in the sols and films. To eliminate the trapped organics, it is necessary to resort to post-processing methods, such as slow diffusion processes or rapid combustion. Elimination through diffusion is performed in vacuum or air, and at slightly elevated

temperatures (50 ^{o}C < T < 200 ^{o}C) for an extended period of time (12-96 hrs) to allow for the expulsion of the undesired species. Rapid combustion methods, on the other hand, employ a high temperature anneal to combust the incorporated organic material, a process that often results in, or coincides with, crystallization of the metal oxide. As the film crystallizes, grain boundaries, voids or other defects are formed that lead to significant complications for film performance such as high leakage currents for insulators in capacitors and transistors, hampered mobilities in semiconductors, hindered conductivities in transparent conductors, decreased transparency in optical films, and other issues.[8,9,10]

Therefore, an all aqueous and non-organic sol-gel route is an attractive alternative over organic sol-gel techniques. The tendency of metal-aquo cations to hydrolyze and condense is well known. After all, it is the great propensity for metal-hydroxide and oxo-hydroxide formation that underlies organic sol-gel techniques. In aqueous solutions there is a strong tendency for metal-aquo cations to condense into dense hydroxides and oxo-hydroxides, a property that can be exploited to control morphology and composition through the proper choice of precursors. Both amorphous and crystalline products can also readily be obtained. Water, because of its capacity to participate in the formation of metal-oxide networks, should therefore be embraced as a desirable solvent.

Condensation of metal-aquo complexes proceeds via olation and oxolation: olation the formation of hydroxide bridges between metals, oxolation the formation of oxide bridges between metals:

Olation: $M\text{-}OH + M\text{-}H_2O \rightarrow M\text{-}OH\text{-}M + H_2O$

Oxolation: $M\text{-}OH + M\text{-}OH \rightarrow M\text{-}O\text{-}M + H_2O$

It should be noted that for condensation to occur by either process, deprotonation of a metal-aquo species must occur to form metal-aquo-hydroxo species, which indicates that pH is an important consideration. High-valent metals are often acidic in aqueous solution because of their small size and high charge, and thus their aqua complexes rapidly deprotonate. In turn, this initial deprotonation creates an active site for further condensation, which can lead to a variety of ionic species depending on metal electronegativity, solution pH, and concentration. For example, $Fe(H_2O)_6^{3+}$ will condense in aqueous solutions to $FeOOH(H_2O)_4^{+}$, whereas $Zr(H_2O)_8^{4+}$ will condense into tetramers of $Zr_4(OH)_8(H_2O)_{16}^{8+}$. Upon rapid and significant pH changes, such as is seen in base titrations of acidic metal solutions, condensation processes can occur irreversibly to form a metal hydroxide or hydrous metal oxide precipitate. The precipitates and films derived from aqueous solution deposition can also possess significant chemical properties in their own right.

History of Ion Exchange Materials

Of particular relevance to the photoresist and development chemistry of HafSOx is the process of ion exchange. During the development step of the

lithographic process, highly basic aqueous solution of tetramethylammonium hydroxide (TMAH) is used to transfer the pattern of exposure into a physical pattern. The large pH gradients that exist between the film and the developer solution lead to the phenomenon of ion exchange.

Ion exchange is hardly a recently discovered phenomenon, and in fact has been described since at least Aristotle's time when he noted that sea water loses part of its salt content when passed through certain sands.[11] More rigorous studies of ion exchange came in 1850 when the British chemists Thompson and Way observed the ion-exchange action of soils. In a straightforward experiment, Thompson passed a solution of ammonium sulfate through a column of soil and observed the formation of calcium sulfate at the end of the column.[12] In this process the ammonium cations in the eluted solution is exchanged with calcium cations in the soil. A bit later, Way demonstrated the generality of this behavior in soils by exchanging cations such as NH_4^+, Na^+, K^+ with stoichiometric amounts of Ca^{2+}.[13]

The sources of ion exchange in soils were later identified by Lemberg and Wiegner to be due to the presence of clays, glauconites, zeolites, and humic acids.[14,15,16] Zeolites, in particular, make up a well-known and important class of natural ion-exchange materials. They were among the first synthetic ion exchangers. Permutits, as they were termed, were commonly prepared by fusion of mixtures of soda, potash, feldspar, and kaolin, or similar components, and by basic precipitation of an acidic solution of aluminum sulfate and sodium silicate.

Attempts were made in some plant operations to use permutits in water softening processes, though widespread implementation was not realized. Nevertheless, the promise of ion-exchange materials led a number of chemists to envision extraordinary applications for the technology, such as recovery of gold from sea water.[11]

While synthetic materials could mimic a composition that closely resembled that of natural zeolite, synthetic methods yielded materials with highly irregular and random structures and were troublesome with respect to their reproducibility. The gelatinous permutits were also unstable in acidic solutions, severely limiting their usefulness. Additionally, permutits failed to achieve similar performance to their naturally occurring counterparts, which lead to permutits having little importance outside of their historical regard.

After the early research on natural and synthetic inorganic ion exchange materials, a spectacular breakthrough occurred in organic chemistry, when two chemists, Adams and Homes, discovered that crushed phonograph records exhibited ion-exchange properties.[17] This initial discovery led to the development of synthetic organic ion-exchange resins that outperformed any of the previous ion exchangers and allowed for the synthesis of ion exchangers with varied properties. These organic ion-exchange resins could outperform even nature and her mineral ion exchangers and were a landmark achievement for chemistry.[18]

Today ion exchange is a well-known and well-studied phenomenon. Many materials are now known to possess ion exchange capability, and their use

permeates a great number of industries, from the food and beverage industry to the semiconductor industry. For example, ion exchange materials are commonly used to produce high purity water for a variety of applications, and they are even found in common commercial laundry detergents as water softening agents.

Chemistry of Inorganic Ion Exchange Materials

Though ion-exchange behavior was originally thought to be isolated only to naturally occurring zeolites and clays, it is now known that a wide variety of inorganic materials possess ion exchange capability. While an exhaustive list of these materials and compounds is beyond the scope of this thesis, a brief discussion of a few representative types of ion exchange materials will be presented to illustrate the general principles behind ion exchange.

Many of the species identified by Wiegner and Lemberg to be responsible for the ion-exchange action of soils are metal oxides in the form of clays and zeolites,which are types of layered exchangers and cavity exchangers, respectively. These materials are generally lamellar structures comprised of anionic layers or planes of metal oxide stacked on top of each other with exchangeable charge compensating cations, such as H^+, Na^+ or Mg^{2+}, sandwiched between the layers. In these materials the bonds within the metal oxide layers are generally strong and covalent, whereas the bonds between layers are generally weak and ionic. As a consequence the layers can move in relation to each other

depending on the size and solvation of the interlayer cations, thus enabling high cation mobilities and allowing the interlayer cations to be readily exchanged.

Clays are classic examples of layered ion exchange materials and generally consist of stacked aluminum and silicon oxide layers with alkali or alkaline cations between the layers. The ion exchange behavior of clays arises from the presence of negatively charged hydroxyl groups associated with the metal oxide layers. A fixed negative charge arises in the metal oxide layers due to the replacement of Si^{4+} by Al^{3+}, or Al^{3+} by Mg^{2+}, etc, without a net change in oxygen coordination, allowing charge compensating cations to associate with the oxide layers.

Beyond layered exchange materials, many structures have cavities or tunnels in which labile and exchangeable cations reside. Zeolites, for example, are aluminosilicates materials that consist of SiO_4 and AlO_4 tetrahedra that share oxygens to create a negatively charged oxide framework with large cavities. Charge balancing alkali or alkaline cations can reside in these cavities. These materials often exhibit high selectivities towards specific cations. This selectivity tracks with solvated ion size, as exchangeable species must pass through a structure of well-defined pore and cavity sizes.[19]

Hydrous oxides are another important class of ion-exchange materials. They are exemplified by insoluble crystalline or semi-crystalline materials that exist within the metal oxide – H_2O system, as represented by the general formula MO_2xH_2O. They can be categorized into two main types: framework hydrates and particle hydrates.[20] Framework hydrates are analogous to zeolites and other porous

ion-exchange materials in that they possess cavities and tunnels in which exchangeable species can reside. Particle hydrates, however, are materials where exchange occurs only at the surfaces of the constituent oxide particles.

In general, particle hydrates contain a significant level of surface hydration that facilitates exchange of protons and hydroxides at surfaces, enabling cation or anion exchange, respectively. They are typically prepared by base-induced precipitation of the soluble salt, a process that generally leads to amorphous or poorly crystalline solids through rapid condensation processes.[21] Depending on the pK_a of a metal complex, or rather the strength of the metal-oxygen bond in comparison to that of the oxygen-hydrogen bond in OH^-, and the solution's pH, either cation and anion behavior can be observed. This leads to anion exchange (A^- for OH^-) typically being observed in acidic conditions, while cation exchange (X^+ for H^+) is displayed at high pH, according to the following general reactions:

$$M\text{-}OH + A^- \rightarrow MA + OH^-$$

$$M\text{-}OH + X^+ \rightarrow M\text{-}OX + H^+$$

Therefore hydrous oxide exchange materials can exhibit both cation and anion behavior as a function of pH. Examples of such materials include ZrO_2xH_2O and SnO_2xH_2O, both of which have been shown to exhibit amphoteric ion exchange behavior.[22]

Hydrous zirconia itself consists of small particles with dense anhydrous oxide cores. These cores adopt the fluorite structure where Zr^{4+} ions are coordinated by eight oxygen atoms, and each oxygen is coordinated by four Zr

atoms. A much different environment exists at the surface. Here, oxygen atoms are partially bound to protons in the form of terminal water and hydroxide groups.. At high pH these surface protons can be removed, leading to particle growth through condensation.[23]

HafSOx and ZircSOx As Ion Exchange Materials

HafSOx and ZircSOx are amorphous gels and behave as hydrous oxide exchangers because of their pseudo particle hydrate form. In this work, films deposited from HafSOx and ZircSOx solutions are considered to consist of highly hydrated domains of low molecular weight and lightly polymerized oxide particles with a size on the order of 1 nm or smaller. These small cluster-like oxide particles are bound together by a hydrated network of hydroxide and sulfate bridges, a network that also contains a significant amount of hydration in the form of water voids and surface hydroxyls. Annealing the films drives off excess hydration and drives condensation between metal ions and the formation of bridging sulfates.

ZircSOx and HafSOx are also quite acidic due to the presence of surface and sulfate bound protons.. Essentially, these excess protons at surfaces function as active sites where extensive acid-base chemistry can occur. When the films are immersed in basic solutions these protons and associated anions are rapidly lost through the thickness of the film due to low film densities. The anions are replaced in favor of oxide and hydroxide. This neutralization process is extremely rapid at low film densities because the presence of water voids between particles enables

rapid diffusion of protons and ions through the film. Loss of acid then promotes condensation through olation and oxolation pathways. A more detailed look at the morphology of both HafSOx and neutralized HafSOx films will be presented in Chapter 2.

This ion-exchange process in HafSOx and ZircSOx films is also highly dependent on solution pH. At high pH the films undergo rapid base-catalyzed condensation, while at neutral or acidic pH little condensation occurs. Therefore, and as this thesis will show in Chapter 3, HafSOx and ZircSOx films are rather similar to hydrous oxide exchangers, such as hydrous zirconia, which display the uptake of anions at low pH and uptake of cations at high pH. The ion exchange chemistry of HafSOx is therefore an important consideration with respect to the development step in the lithographic process.

The Invention of Photolithography

The first major milestone in lithography can be traced back to 1798 when, like many great scientific discoveries, it was somewhat of an accident. Its start occurred when a playwright named Alois Senefelder found that he was able to transfer wax letters written on a limestone plate by immersing it in nitric acid. He saw that the wax was unaffected by the nitric acid while the limestone was etched, allowing for a transfer of the wax pattern into the stone.[24] Following this discovery he quickly realized that he could then in turn use this relief printing method to create a template for duplicating a pattern. By writing on a plate of limestone with

an oily ink and applying a mildly acidic solution of gum arabic he could create a slight relief image. When an ink roller was then rolled across the limestone surface the ink would adhere only to the areas of the stone where the oily ink was applied. This image could then be transferred to a piece of paper laid face down on the stone, thereby demonstrating the basis for both contemporary lithographic printing and chemical lithography.

A few decades later, in 1825, another major milestone was realized when the process of photolithography was invented in France by Joseph Nicephore Niepce.[25,26] Niepce had been experimenting with using a camera obscura to expose images onto silver chloride paper, but he ran into problems related to aging and weathering of the silver chloride. He then decided to move to stone-plate lithography where he was successful in transferring an image from a camera obscura into a latent image in a film of asphalt on a pewter plate. Through this method the unexposed regions of the asphalt could be dissolved in turpentine oil to reveal a topographic image. Niepce named this process heliography, literally "writing by the sun", and it marked the beginning of photolithography.

Modern Lithography Overview

The modern lithographic process has evolved into a complex series of steps, and its importance is paramount to the success of modern semiconductor – based technologies. Every device, computer, or other electronic gadget around us is, at its heart, a collection of microprocessors and integrated circuits. It is also

apparent for a cursory consideration of these technologies over the last few decades that not only has the size of electronic devices decreased considerably, but the speed at which these devices operate has increased with each successive generation. Both of these observations are manifestations of Moore's Law, which dictates that as the density of transistors on an integrated circuit increases, the size of a single transistor decreases. The ability to decrease the size of transistors has largely been dependent on the advancement of the processes of lithography.

Today, lithography is still quite similar to Niepce's process in that an optical pattern is translated into a physical pattern. Modern lithography, however, uses highly advanced exposure sources, e.g., electron beams, extreme ultraviolet (EUV, λ=13.5 nm), and 193 nm laser light. The general photolithographic process consists of the following steps: adhesion promotion, coating, post-application bake (PAB), exposure, post-exposure bake (PEB), development, hard bake, pattern transfer and strip. A brief explanation of each step is as follows:

Adhesion promotion is done to ensure the surface to be coated, such as a bare silicon wafer, is clean and sufficiently suited for the application of the resist. Without proper adhesion the resist coating will not properly coat, will not cover the entire wafer, or will have a significant number of defects. Obviously, a poor resist coating will result in a poor pattern and a sub-optimal lithographic process. To ensure proper adhesion, a silicon wafer typically undergoes a thorough cleaning in piranha solution (a mixture of sulfuric acid and hydrogen peroxide) to remove any organic contaminants. This cleaning is then typically followed by a

high temperature (>800 ^{o}C) anneal to drive off any remaining surface contaminants and to drive off any surface hydroxyls or dangling bonds. For organic-based resists, adhesion promotion is done to create a hydrophobic surface, while for aqueous or other polar resists a hydrophilic surface is required. Hexamethyldisilazane (HMDS) is often used to produce a hydrophobic surface by reacting and destroying any hydroxide or dangling bonds that may remain after both the oxidative cleaning and high temperature anneal. When a hydrophilic surface is necessary, the wafer can treated with a piranha solution again or exposed to an oxygen plasma.

After adhesion promotion, the resist material is coated through spin-coating followed by a low temperature (~100 ^{o}C) post-application bake (PAB), which is performed to drive off excess solvent from the resist. The PAB serves to densify and thin the photoresist and to promote more stable adhesion of the photoresist to the substrate. Driving off excess solvent is also important because it can dampen the intensity of the incident light in the exposure step. A thicker resist will absorb more light near its surface, which may cause incomplete exposure at the substrate-photoresist interface.

Next, the resist is exposed by projecting an optical image onto the resist. This can be done achieved by exposing the photoresist through a mask or with an interference tool. The exposure step plays an integral role in determining the resolution of the material and is based on the Rayleigh Equation:

$$R = k_1 \frac{\lambda}{n \cdot \sin \theta_{max}}$$

where R represents the minimum resolution; k_1 is a constant unique to the lithographic process (typically in the range of 0.5 – 1.0); λ is the exposure wavelength; n is the index of refraction of the medium between exposure source and resist; and θ_{max} is the maximum half-angle of light that can enter the lens.

The Raleigh Equation highlights why the exposure wavelength has decreased with each generation of lithography, with the evolution from ultraviolet emission of mercury vapor lamps (λ=365 nm) to ArF excimer lasers (λ=193 nm) to extreme ultraviolet (EUV, λ=13.5 nm). As the demands of device microfabrication and Moore's Law push device dimensions smaller, smaller wavelengths are needed to resolve their features.

After exposure, a second low-temperature, post-exposure bake (PEB) is performed. The PEB serves to stabilize the exposed area by essentially smoothing out the latent exposed image within the resist. With chemically amplified resists, which will be covered in the next section, the PEB plays the vital role of activating the chemical amplification reactions.

Development occurs following the post-exposure bake. Development is the step in which the projected optical pattern is physically transcribed into the photoresist material. There are two types, or tones, of photoresists: negative tone resists which become insoluble upon exposure, and positive tone resists which become soluble upon exposure. During development of a positive tone resist, the exposed region is dissolved away leaving only the unexposed areas. Development is typically conducted by immersing the wafer in a low concentration

tetramethylammonium hydroxide (TMAH) solution, though other developers can be used. A thorough rinsing with ultra-pure water is done to cease development and to wash away any remaining TMAH. The wafer is then dried, usually by spinning, and then it is moved onto the next hard bake step.

A hard bake at a moderately high temperature (>200 ^{o}C) is necessary after development to solidify the remaining resist. Because the subsequent step is an etch to transfer the photoresist pattern into the substrate, the photoresist needs to be dense so that it can sufficiently withstand an etch plasma and provide a high etch budget. Without a suitable hard bake, the resist will not be resistant to etching, resulting in an inadequate pattern transfer into the substrate.

Pattern transfer is performed through a plasma etch. The photoresist shields the substrate directly underneath it, while the exposed substrate is subjected to the etch. When complete, the photoresist is destroyed, but it has effectively served as a stencil for the substrate. Plasma etches, such as SF_6/Ar plasmas or O_2 plasmas, typically etch away the photoresist much quicker than the underlying substrate. It is for this reason that photoresists have traditionally been on the order of 100 nm thick so that enough photoresist is present to transfer only 10-25 nm into the substrate. Lastly, a strip step is needed to remove any remaining photoresist.

Conventional Organic Resists

While the photolithographic process has evolved considerably since Niepce's time, the fundamental method of exposing a material with energy to

create a solubility difference is still at its heart. The majority of these materials are represented by a vast collection of organic polymers and resins that either harden or soften when exposed to light, known as negative tone and positive tone behavior, respectively.

A hugely successful scheme for creating photoresists is demonstrated by doping, or mixing, a polymer resin with a photoactive sensitizer molecule. The polymer resin itself is either soluble or insoluble in some developer until the sensitizer molecules are activated by the absorbed radiation energy. The activated sensitizer molecules then react with the polymer resin to either enhance or decrease its solubility.

An example of this scheme can be traced back to the early 20^{th} century with diazoquinone salts. Diazoquinone salts such as diazonapthoquinone (DNQ) had been known for some time to be photoactive and had been used in conjunction with azo coupling agents as early as 1917 for producing blueprints. The blueprint process exposure uses light to induce decomposition of the diazoquinone salts. Subsequent treatment with ammonia drives the reaction of the azo coupling agent and the remaining diazoquinone salt to form a blue compound, thereby giving it the name blueprint.

Eventually researchers went looking for effective DNQ binding agents for production of continous films that could be used to produce images. Initial success was achieved with novolac resins. Quite remarkably, it was observed that DNQ/novolac mixtures are highly insoluble in aqueous base, but after exposure to

light they became highly soluble. The DNQ molecules decompose under illumination and their photodecomposition products react with the novolac resin to form soluble species.[24]

The ultimate resolution of these materials was not originally of importance, because their resolution far exceeded the minimum feature sizes that were being produced at the time. In the 1970s when microfabrication demands intensified, it became necessary to improve both the resolution and sensitivity of the materials. Additionally, the DNQ/novolac resists were not sufficiently sensitive enough to shorter wavelength exposure radiation, such as with deep ultraviolet (λ=193 nm) or extreme ultraviolet (λ=13.5 nm) sources. To achieve the sensitivity necessary to make photoresists viable for the new generations of lithography, chemically amplified resists (CARs) were developed.

Chemically amplified resists (CARs) contain a catalyst that can act on the surrounding matrix to induce chemical or physical changes that can be exploited for image formation. Most CARs are based on organic polymers that include moieties called photo-acid generators (PAGs), which produce acid upon exposure. In general, these acids then affect the surrounding matrix during the subsequent post-exposure bake. During the PEB the photo-generated acids diffuse through the surrounding area and react with the polymer, inducing chemical changes that manifest in the development step as either increased or decreased solubility. For example, a successful CAR for deep ultraviolet (λ = 256 nm or 193 nm) lithography is based on a formulation of poly(t-butoxycarbonyl oxystyrene)

(PBOCST) polymer and triphenylsulfonium hexafluoroantimonate molecules (photoacid generators). Upon exposure, photolysis of the onium salt occurs, producing acid. During the PEB, the photogenerated acid diffuses through the matrix and reacts with the hydrophobic PBOCST polymer to form hydrophilic poly(hydroxystyrene) (PHOST), along with the subsequent regeneration of the acid.[27] The hydrophilic PHOST can then be dissolved in an aqueous base developer. A generalized CAR reaction scheme is shown in Figure 1.2. In this way CARs can take relatively weak incident radiation and chemically amplify the effect of exposure. Chemical amplification has been virtually responsible for the success of modern generations of photolithography, including 193 nm and 193 nm immersion (193i) lithography.

The same processes that enable chemical amplification are also disadvantages. The reactions responsible for chemical amplification occur during the PEB step, and are reliant upon diffusion of the acid through the resist to reaction sites in the matrix. Thus, diffusion lengths of these acids, play a critical role in determining the ultimate resolution of the resist; they are resolution limiting.[28,29] It has been shown that the diffusion length of photogenerated acids in some ArF resists can be as high as 11 nm.[30] This resolution limitation is known as resist blur.

Another problem with CARs is encountered with respect to EUV lithography: the outgassing of molecular organic byproducts during exposure. EUV exposure tools necessitate that the resist chamber and exposure source exist

within the same vacuum chamber, and contamination related to outgassing of reactive species is known to be problematic. Outgassed species can coat and react with the optics and mirrors within the instrument, necessitating complicated and expensive cleaning procedures or repairs.

Inorganic Resists

Inorganic photoresists have a number of desirable resist properties, though they have yet to find much wide-scale application for a number of reasons. For example, inorganic resists have been responsible for the highest resolution yet achieved with electron beam lithography, but they suffer from low sensitivity. Additionally, inorganic materials possess an inherently higher etch resistance than organic materials, an important consideration for pattern transfer with small aspect ratios at higher resolutions. Furthermore, the fundamental unit size in inorganic materials can be much smaller than that of organic materials, which is beneficial for controlling line width roughness and resolution. Perhaps the biggest advantage to inorganic photoresists is that inorganic materials can serve dual functions, as hardmasks, for example, that can be directly patterned. A number of inorganic systems have been studied as inorganic photoresists including chalcogenides, lithium and aluminum fluorides, and polyperoxometallates.

A few amorphous chalcogenide glasses are known to be photosensitive, including As_2S_3, AsSe, and GeSe. These materials can be either positive or negative tone. They have a number of drawbacks, however. In addition to their

low sensitivity, exposure of these chalcogenides leads to structural changes that are accompanied by a photodarkening effect, therefore leading to a problematic increase in absorption near the top of the film.[31] Another approach employed with these chalcogenides is based on the exposure induced diffusion of silver ions into the chalcogenide to form insoluble species.[32] This is achieved by depositing a layer of Ag or AgTe on top of the chalcogenide film prior to exposure. Exposure then drives diffusion of the Ag into the chalcogenide to form an insoluble region. Chalcogenide resists, however, have never found much use despite their high resolution, most likely due to the toxicity of their constituents and the deleterious nature of silver as a dopant in silicon, which restricts its use for most lithography applications.

A few self-developing inorganic resists are also known. Of these, aluminum doped lithium fluorides ($LiF\text{-}AlF_3$) deposited via evaporation are the most documented and are responsible for the highest resolution achieved using electron beam lithography.[33] Self-development occurs due to the radiolysis and volatilization of the metal halide upon exposure to electron beams in high vacuum. This self-development occurs in situ, and leads to positive tone behavior. Although very small features sizes on the order of 1 nm can be imaged with such resists, they suffer from low sensitivity and fail to warrant serious consideration as an electron-beam resist.[34]

Peroxopolymetallates, particularly of molybdenum and tungsten, have also been studied as electron and ion-beam resists. Aqueous based solutions of

peroxopolymetallates are prepared by dissolving tungsten, molybdenum or other desired metal, in concentrated H_2O_2, followed by catalytically decomposing the excess peroxide. These solutions can then be deposited through spin-coating to deposit films that consist of poorly polymerized and hydrated networks of $MO_x(OH)_y(O_2)_z$ polyhedra. These polyhedra undergo polymerization upon exposure due to peroxide-decompostion, which catalyzes network formation.[35,36] Exposure can also lead to an amorphous to crystalline phase transformation, where the crystalline phase is more soluble in aqueous base developer.[37] In both cases negative tone behavior is exhibited.

Today the most commonly used inorganic resist is hydrosilsequoxine (HSQ), marketed by Dow Chemical as Flowing Oxide (FOx). HSQ is a silicon-containing organic polymer dissolved in methyl iso-butyl ketone (MIBK). It exhibits negative tone behavior under both electron beam and EUV exposure. Solutions of HSQ consist of cage-like structures of various sizes represented by the general formula $(HSiO_{3/2})_{2n}$; exposure drives polymerization through the opening and crosslinking of these cage structures.[38] The resolution of HSQ is known to be quite high: 10 nm dense lines have been patterned using e-beam lithography, though a dose of 33 mC/cm^2 was required.[39] The main advantages of HSQ are its low roughness, which arises from its small unit size and its amorphous nature. These features enable the ability to readily resolve sub-20-nm features and reasonable contrast.

Recently HafSOx has been shown to be a high resolution negative tone resist with sensitivity to 193 nm and EUV photons, as well as electron beams.[40,41] Similar to HSQ, HafSOx is an amorphous oxide consisting of a weakly polymerized network of metal oxide. Exposure leads to the densification of the oxide through radiation–induced cross-linking and network formation, which renders the exposed area insoluble in developer. HafSOx resists contain Hf-peroxo groups that decompose upon exposure and drive polymerization. The high sensitivity of HafSOx can be partially attributed to this radiation induced decomposition. Using electron beam lithography 18-nm dense lines were imaged at 244 uC/cm^2, and 60 nm dense lines were patterned at a dose of 25 mJ/cm^2 using 193 nm interference lithography. A particular advantage of HafSOx resists is their high electron density in comparison to organic resists. According to a modified Bethe Equation proposed by Joy and Luo,[42] the electron stopping power of a material is proportional to its electron density. More energy is then deposited in a smaller volume of high electron density materials. This relationship is especially important with respect to EUV and electron beam patterning because of the nature of the processes that occur during exposure to high energy radiation and electron beams.

Radiation and Photochemistry of Resists

During the exposure step of the lithographic process, the resist film is illuminated by radiation to induce a solubility change within the resist. As

exposure radiation interacts with the resist distinct processes occur that result in chemical and physical differences between exposed and unexposed regions of the film. These differences create a contrast of resist solubility in developer solution and enable the patterning of resist materials.

The radiation used to expose photoresists can fall within a wide range of energies. Wavelengths from visible to x-rays and ions such as electrons and He^+ can be used to expose resists. Although all of these exposures can create solubility contrasts within resists, the exposure mechanisms leading to such changes differ depending on the energy of the exposure radiation.

The mechanism of exposure of a resist is determined by the nature of the interaction between the incident radiation with the constituent atoms and species within the resist. When the exposure radiation is relatively low energy, such as with visible or ultraviolet photons, the exposure mechanism is mediated by photon absorption by chromophores within the resist. Absorption of photons promotes these chromophores into excited states and initiates chemical changes within the film, resulting in chemically distinct products that differ from the unexposed regions. This is the realm of photochemistry: localized adsorption and excitation.

Radiation chemistry, on the other hand, occurs when the energy of the radiation is high enough to induce ionization events within the material.[43] These ionization processes are rarely limited to specific species or sites within the material, but rather occur throughout the solid. The reason for this is because the energy of the incident radiation is much higher than the bond energy of the

chemical bonds within the material. It is also much higher than the ionization potential of the resist's atoms, and thus inelastic scattering of the incident radiation occurs and induces ionization events within in material as illustrated in the following scheme:

$$X \rightarrow X^{+} + e^{-}$$

This process is known as the photoelectric effect. The ejected photoelectron is imparted with a portion of the energy of the incident radiation, and rapidly moves away from the ionization site. As it travels it loses energy by scattering inelastically with the material's constituent atoms, inducing further ionizations and excitations along its path and creating a cascade of Auger and secondary electrons in its wake. These secondary electrons can then initiate more ionization and excitation events themselves.[44,45] Eventually, as these processes continue, electrons are produced of low enough to energy to be absorbed, and results in subsequent promotion of a species into an excited state from which it can decay through numerous pathways, including:

$$X^{+} + e^{-} \rightarrow X^{**}$$

$$X^{**} \rightarrow X + hv$$

$$X^{**} \rightarrow X^{+} + e^{-}$$

$$X^{**} \rightarrow R_1^{*} + R_2^{*}$$

$$X^{**} \rightarrow X^{*}$$

which represent the absorption of a secondary electron, the emission of radiation, the emission of a lower energy electron, the fragmentation into ions or radicals and

internal conversion, respectively. This collection of processes that follow the ionization of a solid by a primary beam is known as a secondary electron cascade, and is illustrated in Figure 1.3.

The products produced after these ionized and excited species decay are responsible for the solubility contrast between the exposed and unexposed regions of a resist in a developer. Many of the excited or ionized species are unstable and will thus undergo chemical changes that result in more stable products through dissociation, bond scission or formation mechanisms. Therefore it is the secondary electrons that lead to the exposure of the resist rather than the primary radiation. The primary radiation simply ionizes the medium, setting in motion secondary electron cascades that then lead to further ionizations and excitations that eventually result in distinct exposure products that determine the material's solubility in a developer. These secondary electron cascade processes not only occur as a result of exposure of EUV or x-ray photons, but also occur due to exposure to electron or ion beams. In all cases, as the incident photon or ion impacts the resist, secondary electron cascades are generated that then go on to induce exposure events.

Advantages of HafSOx as an E-Beam and EUV Resist

Because the exposure of a resist in EUV or electron-beam lithography is due to the action of secondary electrons and their associated interactions, it is obvious that the resolution of the resist is limited by the ability of the material to

contain the electrons within the smallest area possible. This measure is known as it stopping power, and is usually described in terms of energy losses per unit distance in a solid. The modified Bethe equation describes such a process and is represented by the following formula:[42]

$$\frac{dE}{ds} = -785\frac{\rho Z}{AE}ln(\frac{1.166(E+kJ)}{J})$$

where E is the instantaneous energy of the electron, s is the electron's path length, ρ is the mass density of the solid, Z is its atomic number, A is its atomic weight, J is its mean ionization energy and k is a constant unique to the material that is close to unity. From this formula it can be seen that an electron will deposit more energy in a shorter distance in materials with a high atomic number and a high density. The Bethe equation also indicates that lower energy electrons, such as those produced during the secondary electron cascade processes, will travel farther before losing energy through a scattering event, presenting, with respect to ultimate resolution, another advantage to high density and high Z materials for EUV and electron-beam resists.

The potential advantage to HafSOx over organic-based resists is therefore evident. The latter half of this thesis, chapters 5, 6 and 7, will describe and compare the use of HafSOx as a resist for 193 nm, EUV and electron beam lithography, and the effect of composition upon lithographic performance will be highlighted.

References:

(1) Moore, G. E. *IEEE Solid-State Circuits Newsletter* **2006**, *20*, 33–35.

(2) Anderson, J. T.; Munsee, C. L.; Hung, C. M.; Phung, T. M.; Herman, G. S.; Johnson, D. C.; Wager, J. F.; Keszler, D. A. *Advanced Functional Materials* **2007**, *17*, 2117–2124.

(3) Gusev, E. P.; Cabral, C.; Copel, M.; D'Emic, C.; Gribelyuk, M. *Microelectronic Engineering* **2003**, *69*, 145–151.

(4) Yu, H. Y.; Li, M. F.; Kwong, D. L. *Thin Solid Films* **2004**, *462-463*, 110–113.

(5) Leskelä, M.; Kukli, K.; Ritala, M. *Journal of Alloys and Compounds* **2006**, *418*, 27–34.

(6) Schwartz, R. W.; Schneller, T.; Waser, R. *Comptes Rendus Chimie* **2004**, *7*, 433–461.

(7) Mitzi, D. B. *Solution processing of inorganic materials*; Wiley: Hoboken, N.J., 2009.

(8) Aoki, Y.; Kunitake, T.; Nakao, A. *Chemistry of Materials* **2005**, *17*, 450–458.

(9) Choi, J. H.; Hwang, S. M.; Lee, C. M.; Kim, J. C.; Park, G. C.; Joo, J.; Lim, J. H. *Journal of Crystal Growth* **2011**, *326*, 175–178.

(10) Lee, K. D. *Thin Solid Films* **1997**, *302*, 84–88.

(11) Helfferich, F. G. *Ion exchange*; Dover Publications: New York, 1995.

(12) Thompson, H. S.; Roy, J. *J. Agric. SOC. Engl.* **1850**, *11*, 68.

(13) Way, J. T.; Roy, J. *J. Agric. Soc. Engl.* **1852**, *13*, 12.

(14) Lemberg, J. *Z. deut. gel. Ges.* **1870**, *22*.

(15) Lemberg, J. *Z. deut. gel. Ges.* **1876**, *28*.

(16) Wiegner, G. *Landwirtsch* **1912**, *60*.

(17) Abrams, I. M.; Millar, J. R. *Reactive and Functional Polymers* **1997**, *35*, 7–22.

(18) Adams, B. A.; Holmes, E. L. *J. Soc. Chem. Ind. (London)* **1935**, *54*.

(19) Clearfield, A. *Inorganic ion exchange materials*; CRC Press: Boca Raton, Fla., 1982.

(20) England, W.; Cross, M.; Hamnett, A.; Wiseman, P.; Goodenough, J. *Solid State Ionics* **1980**, *1*, 231–249.

(21) Clearfield, A. *Chemical Reviews* **1988**, *88*, 125–148.

(22) Amphlett, C. B.; McDonald, L. A.; Redman, M. J. *Journal of Inorganic and Nuclear Chemistry* **1958**, *6*, 236–245.

(23) Clearfield, A. *Inorganic Chemistry* **1964**, *3*, 146–148.

(24) Okoroanyanwu, U. *Chemistry and lithography*; John Wiley: Hoboken, New Jersey, 2010.

(25) Gernsheim, H.; Gernsheim, A. *The history of photography from the camera obscura to the beginning of the modern era,*; Thames & Hudson: London, 1969.

(26) Reiser, A. *Photoreactive Polymers : The Science and technology of Resists*; John Wiley&Sons: New York [etc.], 1989.

(27) Willson, C. G. SPIE, 1997; Vol. 3048, pp. 28–41.

(28) Honda, T.; Kishikawa, Y.; Iwasaki, Y.; Ohkubo, A.; Kawashima, M.; Yoshii, M. *Journal of Microlithography, Microfabrication, and Microsystems* **2006**, *5*, 043004.

(29) Nakamura, J.; Ban, H.; Deguchi, K.; Tanaka, A. *Japanese Journal of Applied Physics* **1991**, *30*, 2619–2625.

(30) Honda, T. SPIE, 2006; Vol. 6154, p. 615422–615422–9.

(31) Shtutina, S.; Klebanov, M.; Lyubin, V.; Rosenwaks, S.; Volterra, V. *Thin Solid Films* **1995**, *261*, 263–265.

(32) Lavine, J. M. *Journal of Vacuum Science & Technology B: Microelectronics and Nanometer Structures* **1996**, *14*, 3489.

(33) Kratschmer, E. *Journal of Vacuum Science & Technology B: Microelectronics and Nanometer Structures* **1987**, *5*, 369.

(34) Isaacson, M.; Muray, A.; Scheinfein, M.; Adesida, I.; Kratschmer, E. *Microelectronic Engineering* **1984**, *2*, 58–64.

(35) Okamoto, H.; Iwayanagi, T.; Mochiji, K.; Umezaki, H.; Kudo, T. *Applied Physics Letters* **1986**, *49*, 298.

(36) Okamoto, H.; Ishikawa, A.; Kudo, T. *Journal of Photochemistry and Photobiology A: Chemistry* **1989**, *49*, 377–385.

(37) Hashimoto, M.; Watanuki, S.; Koshida, N.; Komuro, M.; Atoda, N. *Japanese Journal of Applied Physics* **1996**, *35*, 3665–3669.

(38) Grigorescu, A. E.; Hagen, C. W. *Nanotechnology* **2009**, *20*, 292001.

(39) Grigorescu, A. E.; van der Krogt, M. C.; Hagen, C. W.; Kruit, P. *Microelectronic Engineering* **2007**, *84*, 822–824.

(40) Stowers, J.; Keszler, D. A. *Microelectronic Engineering* **2009**, *86*, 730–733.

(41) Telecky, A.; Xie, P.; Stowers, J.; Grenville, A.; Smith, B.; Keszler, D. A. *Journal of Vacuum Science & Technology B: Microelectronics and Nanometer Structures* **2010**, *28*, C6S19.

(42) Joy, D. C.; Luo, S. *Scanning* **1989**, *11*, 176–180.

(43) Grigor'ev, E. I.; Trachtenberg, L. I. *Radiation chemical processes in solid phase : theory and application*; CRC Press: Boca Raton, Fla. [u.a.], 1996.

(44) Han, G.; Khan, M.; Cerrina, F. *Journal of Vacuum Science & Technology B: Microelectronics and Nanometer Structures* **2003**, *21*, 3166.

(45) Han, G.; Khan, M.; Fang, Y.; Cerrina, F. *Journal of Vacuum Science & Technology B: Microelectronics and Nanometer Structures* **2002**, *20*, 2666.

Figures

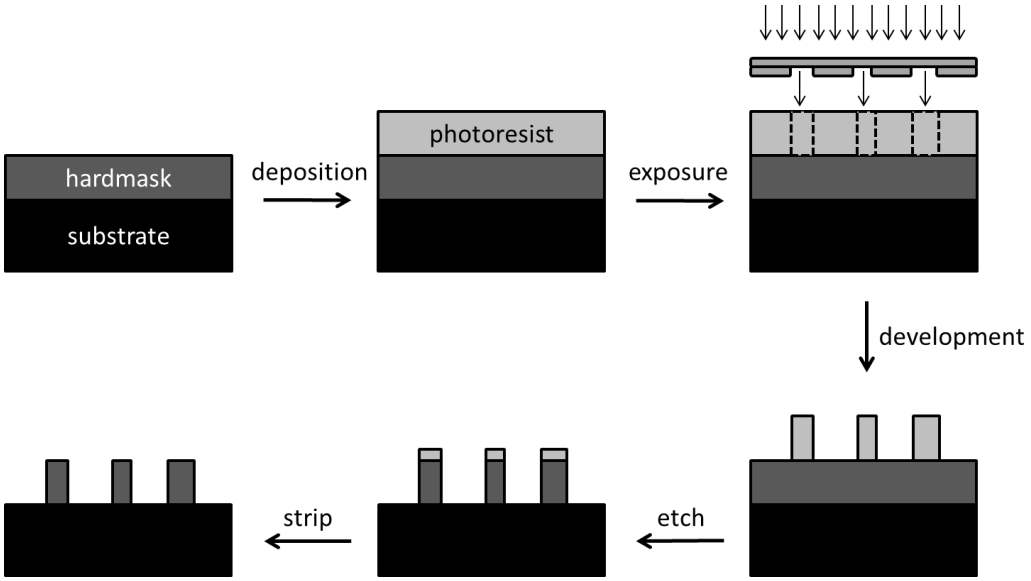

Figure 1.1: Simplified negative-tone photolithographic process consisting of the following steps: deposition of the photoresist, exposure through a mask, development and removal of unexposed photoresist, etch and pattern transfer into hardmask, and stripping of remaining photoresist.

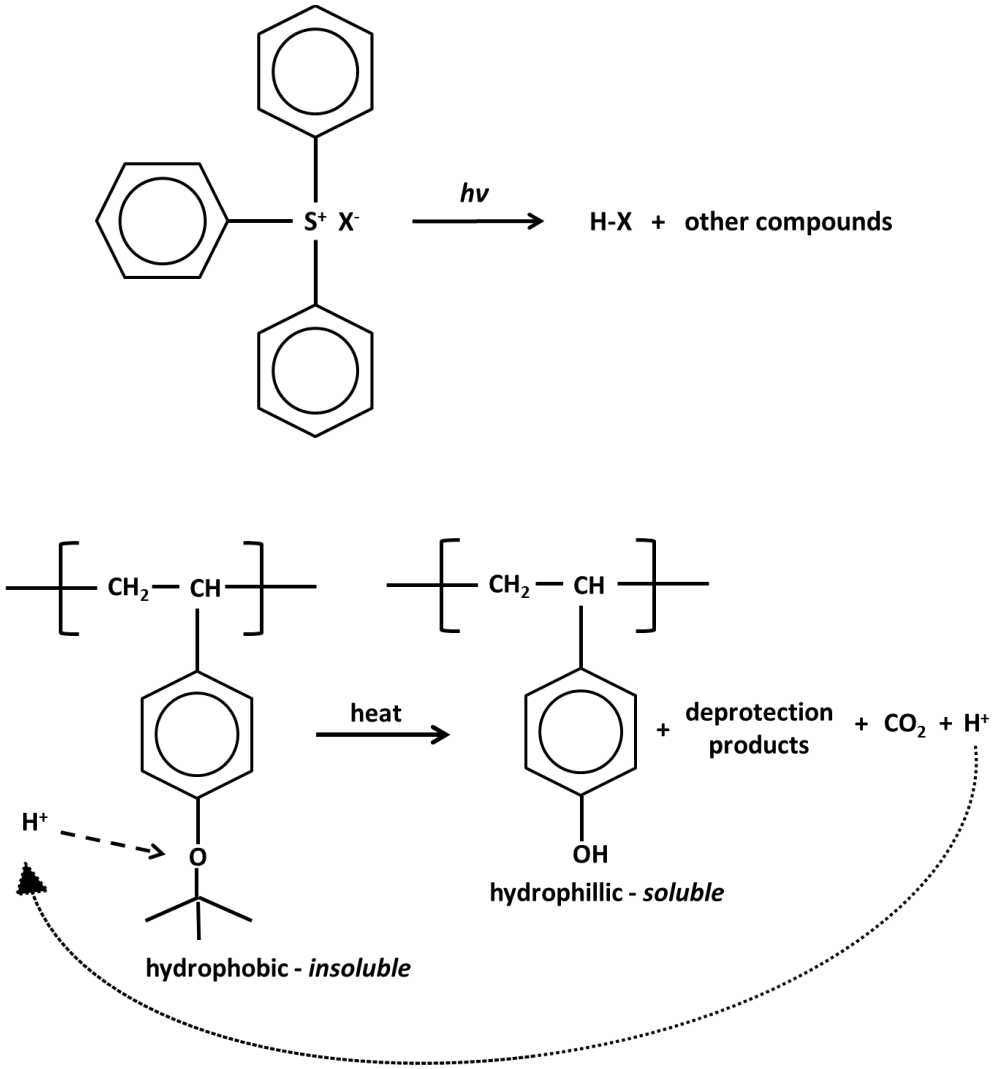

Figure 1.2: Generalized chemical amplification mechanism in chemically amplified photoresists: a) photoacid generation from a sulfonium salt upon exposure, b) reaction of photoacid with hydrophobic polymer to induce fragmentation and induce hydrophillicity along with regeneration of the acid.

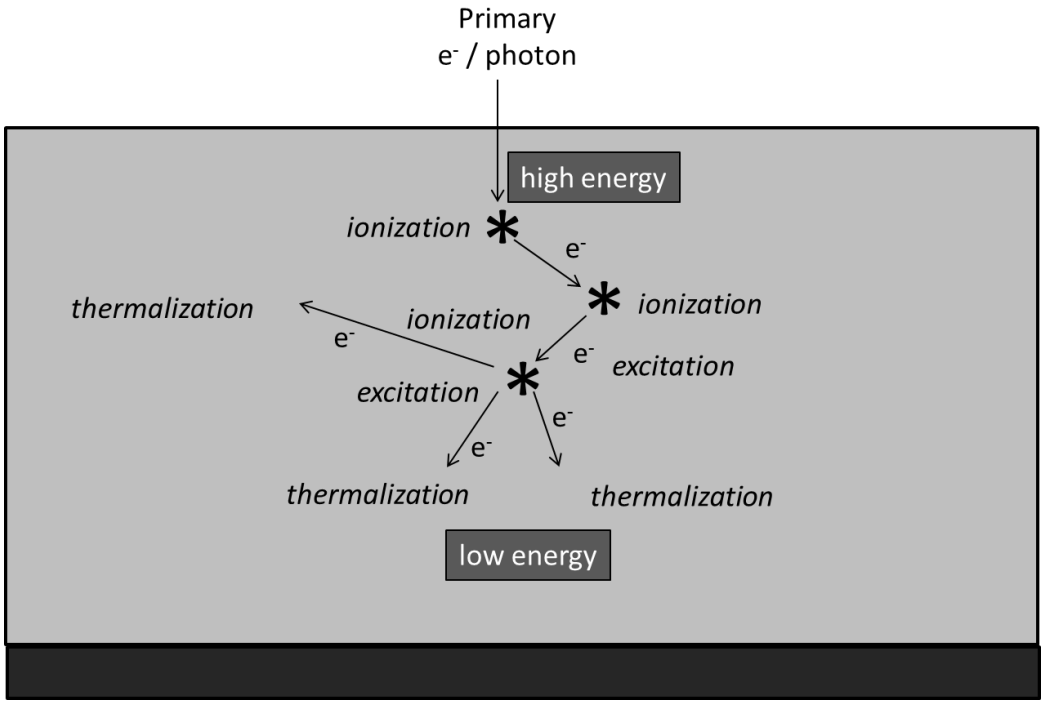

Figure 1.3: Schematic of the secondary electron cascade process. A primary high energy photon or electron impacts the material which results in an initial ionization event which produces a lower energy secondary electron. Both the primary electron and newly created secondary electron can continue to initiate other ionization and excitation events until, eventually, they lose enough energy to become thermalized by the material.

CHAPTER 2

RAMAN STUDY OF HAFSOX SOLUTIONS, THIN FILMS AND EXPOSURE MECHANISM

Abstract

Raman spectroscopy was conducted on solutions and films of HafSOx resists to determine the presence of hafnium peroxo species. A Raman band at 831 cm^{-1} was found to be unique to peroxide containing HafSOx solutions and was assigned to a Hf-peroxo species. For HafSOx films, a band at 840 cm^{-1} was correlated to Hf-peroxo species. HafSOx films were also exposed to an electron beam, and the decomposition of peroxide was confirmed with Raman spectroscopy. It was seen that a decrease in the O-O signal occurs with exposure.

Introduction

Inorganic resists have been demonstrated to possess the highest resolution of all resists used in electron beam lithography, a trait that can be attributed to both their smaller unit size and their higher densities when compared to organic or polymeric analogues.[1] Despite their high resolution and other advantages, inorganic resists still fail to see much success due to their relatively low sensitivity when compared to organic resists. Organic resists have evolved into high sensitivity materials due to the implementation of chemical amplification, a method where photosensitive moieties or ligands are doped into the organic polymer matrix and are then activated by incident radiation. A subsequent anneal then causes them to react with the polymer to either increase or decrease the material's overall solubility.[2,3,4] Inorganic resists, on the other hand, have had no such advances.

Recently, the peroxo-hafnium oxide sulfate (HafSOx) system has been shown to be a high resolution, high sensitivity inorganic resist.[5,6] The relatively high sensitivity of HafSOx compared to other inorganic resists is thought to be the result of the interaction of the incident radiation with unstable Hf-peroxo bonds which undergo rapid radiolysis, resulting in cross-linking and bridging between metal centers. Consequently as crosslinking and bridging occurs the material becomes insoluble in developer.

While early transition metals such as Ti, V, Mo, and W are known to readily form stable and observable metal-peroxo species in solutions and can be isolated in solids, Hf and Zr peroxo species are rarely isolated.[7,8,9] Examples of such species are the zirconium peroxo fluorides represented by $(NH_4)_3Zr(O_2)F_5$ and $M_3Zr_2(O_2)_2F_7$ ($M = K^+$, Rb^+, Cs^+, NH^{4+}), where the highly complexing and electronegative fluorine atom facilitates the stability of the Zr-peroxo complex and allows for crystallization.[10,11] There are also reports of large and highly complex 6-Zr-peroxo and 6-Hf-peroxo crown species with bridging peroxo groups coordinated to Keggin-like tungstosilicate ligands to form massive $[(M)_6(O_2)_6(OH)_6(SiW_{10}O_{36})_3]^{18-}$ (M = Zr, Hf) polyanions.[12] Additionally, a number of organic Zr-peroxo and Hf-peroxo species are known.[13,14]

Complexation of Zr and peroxide in aqueous solution has also been established. Thompson has proposed a peroxozirconium complex in highly acidic solutions with a composition of $Zr_4(O_2)_2(OH)_4^{8+}$, which is similar to the well-known $Zr_4(OH)_8^{8+}$ tetramer formed in acidic zirconium salt solutions.[15,16] An identical Zr-peroxo tetramer was also proposed by Gao et. al.[17] Still, though, there are no reports of structural characterization of these proposed peroxo-Zr or peroxo-Hf species.

While the isolation of well-defined Zr-peroxo or Hf-peroxo species is difficult, Raman spectroscopy can be employed to determine if such species are present in film or solution.[18] The absorption energy of the metal-bound O-O is

typically distinct from that of the O-O bond in aqueous H_2O_2. For example, the O-O stretch in H_2O_2 solutions occurs at 876 cm^{-1} whereas the O-O stretch in barium peroxide is seen at 842 cm^{-1}. With this knowledge, a Raman investigation of HafSOx was conducted to determine the presence of any Hf-peroxo species in films and solutions, and to elucidate on the mechanism of exposure of HafSOx by tracking the change in the O-O stretch with exposure dose.

Experimental

Solutions of HafSOx were prepared by mixing stoichiometric amounts of $HfOCl_2$, H_2SO_4 and H_2O_2, typically in a 1:0.7:3.0 ratio, respectively, followed by dilution with DI water to reach a total metal concentration of between 0.15M and 0.6M. Films were deposited on glass substrates and were prepared for deposition by a UV/ozone treatment for 30 minutes. Films of HafSOx were deposited by spin coating the as-mentioned HafSOx solutions at 2000 rpm for 45s, followed by a post-application hotplate anneal at 80 ^oC for 3 minutes.

Raman spectroscopy for solutions was conducted at Oregon State University on a Coherent Legend Elite Femtosecond Ti:Sapphire 1 KHz Laser Amplifier System. Films were analyzed on a Wi-Tech scanning near-field optical microscope equipped with a 535 nm laser and a 100X objective lens.

Results and Discussion

It is known that the presence of peroxide increases the shelf life of HafSOx solutions. Without peroxide HafSOx solutions readily form white precipitates in a matter of hours whereas precipitation can be delayed by up to two weeks at room temperature in the presence of peroxide, as shown in Figure 2.1. Such behavior suggests a stabilization of the hafnium species in peroxide containing HafSOx solutions, presumably by replacing condensable sites with non-condensable peroxo groups, e.g. replacing terminal hydroxyl with peroxo groups.

Raman spectroscopy was then employed to elucidate to presence of any Hf-peroxo species by looking for an O-O stretch that corresponds to bound peroxide in both solutions and films. Therefore solutions of water, 30% H_2O_2, peroxide free HafSOx and HfSOx with peroxide, were prepared and analyzed by Raman spectroscopy, with the data shown in Figure 2.2. The aqueous solution of H_2O_2 shows a strong bend at 876 cm^{-1} which corresponds to the O-O stretch, a peak which is also present in the peroxide-containing HafSOx solution. Comparing the spectra of HafSOx with and without peroxide, a peak at 831 cm^{-1} is present only in the peroxide containing HafSOx solution and can be assigned to a Hf-peroxo complex.

Next, films of HafSOx with and without peroxide were deposited by spin-coating on SiO_2 substrates. Figure 2.3 shows the Raman spectra of such films. While bands associated with the SiO_2 substrate are quite prominent, a peak in the

peroxide containing HafSOx film spectra can be seen at around 840 cm^{-1}. This peak is indicative of bidentate peroxo groups as a number of reports have established, such as in fluoroperoxozirconium compounds.[10] Therefore, it is likely that the presence of a band at 840 cm^{-1} indicates the presence of a Hf-peroxo complex.

Since the presence of a Hf-peroxo species was established in both solutions and films, the effect of exposure to an electron beam was analyzed. Figure 2.4 shows the Raman spectra of HafSOx before and after a 1 mC/cm^2 flood exposure. It can be seen that the peak at 840 cm^{-1} disappeared entirely after exposure indicating that of the decomposition of peroxide is indeed related to the exposure mechanism. It is known that the exposed regions of HafSOx become insoluble in aqueous base developer, and therefore densification and crosslinking must occur during exposure and in concert with or as a result of peroxide decomposition. Additionally, radiation induced peroxide decomposition is further supported by the fact that it has been found that HafSOx films expel O_2 gas and H_2O vapor upon exposure to radiation.[19]

A similar photoexposure mechanism has been proposed for peroxopolytungstic acid films by Okamoto et. al, where peroxo groups are decomposed by incident UV radiation to result in crosslinking of WO_6 and WO_7 polyhedra.[20] Additionally, water and oxygen liberation was detected from the films

during UV exposure, further supporting the peroxide decomposition exposure mechanism.

Based on the results obtained from Raman spectroscopy and with consideration of the behavior of peroxopolytungstic acid films, an exposure mechanism for HafSOx resists can be posited. Initially, peroxide containing HafSOx films are of low density and consist of molecular-like hydroxoperoxosulfato hafnium species of general formula $HfO_{2-x-z-y/2}(O_2)_x(OH)_y(SO_4)_z$. Mild heating after film deposition serves to drive off loosely bound water and slightly densify the film. Exposure induces decomposition of the peroxo species to produce water and O_2 gas while catalyzing polymerization due to the peroxide decomposition process.

Conclusion

Raman spectroscopy was conducted on HafSOx solutions and films to determine the presence of Hf-peroxo species. Solution Raman indicated the binding of peroxide to hafnium in aqueous solutions with an O-O stretch at 831 cm^{-1}. Films of HafSOx were also analyzed to determine the retention of such Hf-peroxo species, and also to track the disappearance of the associated Raman absorption band with exposure to an electron beam. A significant decrease of the Hf-peroxo peak was seen after a 1 mC/cm^2 electron beam exposure. These results, along with the drastic decrease in solubility of the exposed regions, indicate that the radiation induced decomposition of peroxo species and subsequent

polymerization of the metal oxide network is responsible for the solubility switch, and thus photoresist behavior, during exposure. Exposure driven metal-peroxo decomposition is an effective and potentially general route for inorganic photoresist development.

References

(1) Isaacson, M.; Muray, A.; Scheinfein, M.; Adesida, I.; Kratschmer, E. *Microelectronic Engineering* **1984**, *2*, 58–64.

(2) Ito, H. SPIE, 1999; Vol. 3678, pp. 2–12.

(3) Nakamura, J.; Ban, H.; Deguchi, K.; Tanaka, A. *Japanese Journal of Applied Physics* **1991**, *30*, 2619–2625.

(4) Kozawa, T.; Yoshida, Y.; Uesaka, M.; Tagawa, S. *Japanese Journal of Applied Physics* **1992**, *31*, 4301–4306.

(5) Stowers, J.; Keszler, D. A. *Microelectronic Engineering* **2009**, *86*, 730–733.

(6) Telecky, A.; Xie, P.; Stowers, J.; Grenville, A.; Smith, B.; Keszler, D. A. *Journal of Vacuum Science & Technology B: Microelectronics and Nanometer Structures* **2010**, *28*, C6S19.

(7) Schwarzenbach, G.; Muehlebach, J.; Mueller, K. *Inorganic Chemistry* **1970**, *9*, 2381–2390.

(8) Butler, A.; Clague, M. J.; Meister, G. E. *Chemical Reviews* **1994**, *94*, 625–638.

(9) Campbell, N. J.; Dengel, A. C.; Edwards, C. J.; Griffith, W. P. *Journal of the Chemical Society, Dalton Transactions* **1989**, 1203.

(10) Jere, G. V.; Santhamma, M. T. *Inorganica Chimica Acta* **1977**, *24*, 57–61.

(11) Schmidt, R.; Pausewang, G.; Massa, W. *Zeitschrift anorganische und allgemeine Chemie* **1986**, *535*, 135–142.

(12) Bassil, B. S.; Mal, S. S.; Dickman, M. H.; Kortz, U.; Oelrich, H.; Walder, L. *Journal of the American Chemical Society* **2008**, *130*, 6696–6697.

(13) Tarafder, M. T. H.; Miah, M. A. L. *Inorganic Chemistry* **1986**, *25*, 2265–2268.

(14) Dengel, A. C.; Griffith, W. P. *Polyhedron* **1989**, *8*, 1371–1377.

(15) Thompson, R. C. *Inorganic Chemistry* **1985**, *24*, 3542–3547.

(16) Clearfield, A. *Reviews of Pure and Applied Chemistry* **1964**, *14*.

(17) Gao, Y.; Masuda, Y.; Ohta, H.; Koumoto, K. *Chemistry of Materials* **2004**, *16*, 2615–2622.

(18) Griffith, W. P.; Wickins, T. D. *Journal of the Chemical Society A: Inorganic, Physical, Theoretical* **1968**, 397.

(19) Stowers, J. K.; Telecky, A.; Kocsis, M.; Clark, B. L.; Keszler, D. A.; Grenville, A.; Anderson, C. N.; Naulleau, P. P. 2011; p. 796915–796915–11.

(20) Okamoto, H.; Ishikawa, A.; Kudo, T. *Journal of Photochemistry and Photobiology A: Chemistry* **1989**, *49*, 377–385.

Figures

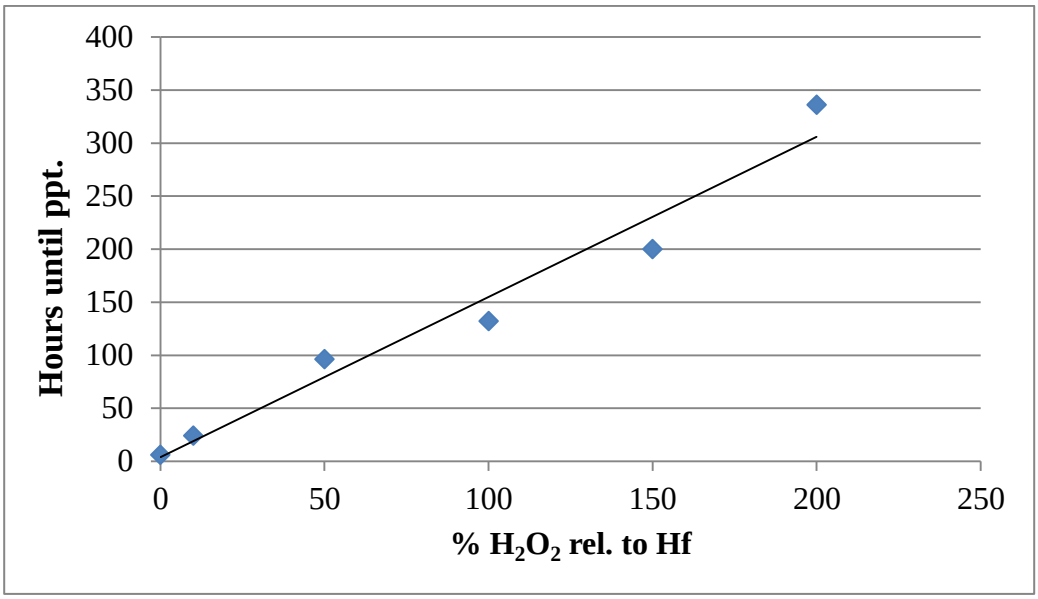

Figure 2.1: Influence of peroxide concentration on the time before HafSOx solutions precipitate.

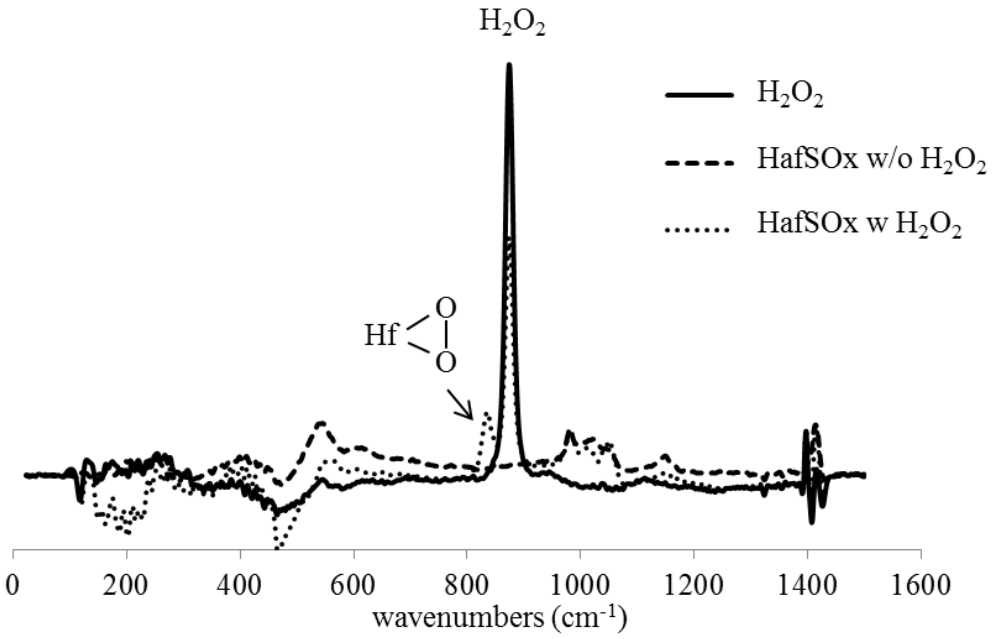

Figure 2.2: Raman of 1.2M H_2O_2 and 0.4M (by metal) HfSOx (1.2M H_2O_2) solutions.

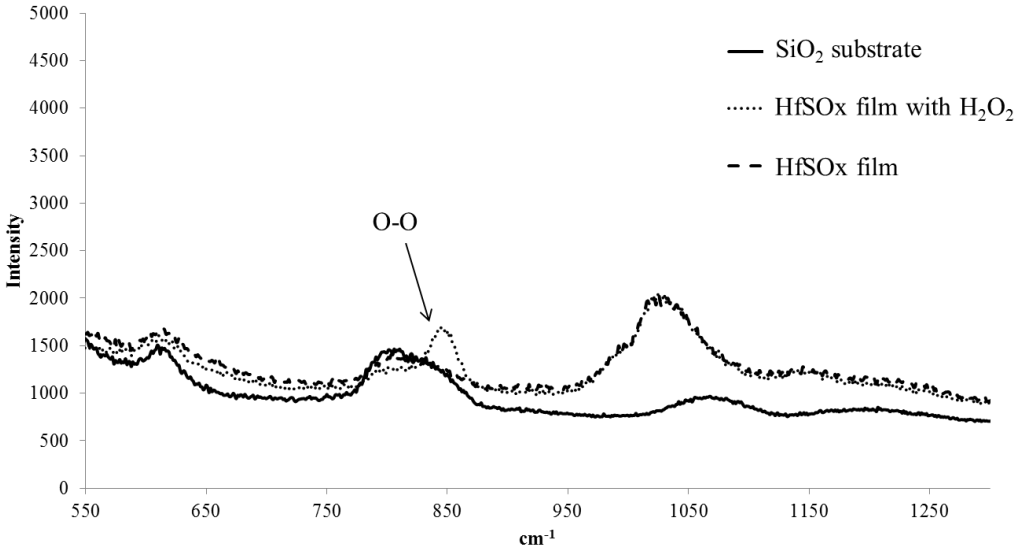

Figure 2.3: Raman spectra of HfSOx films with and without peroxide.

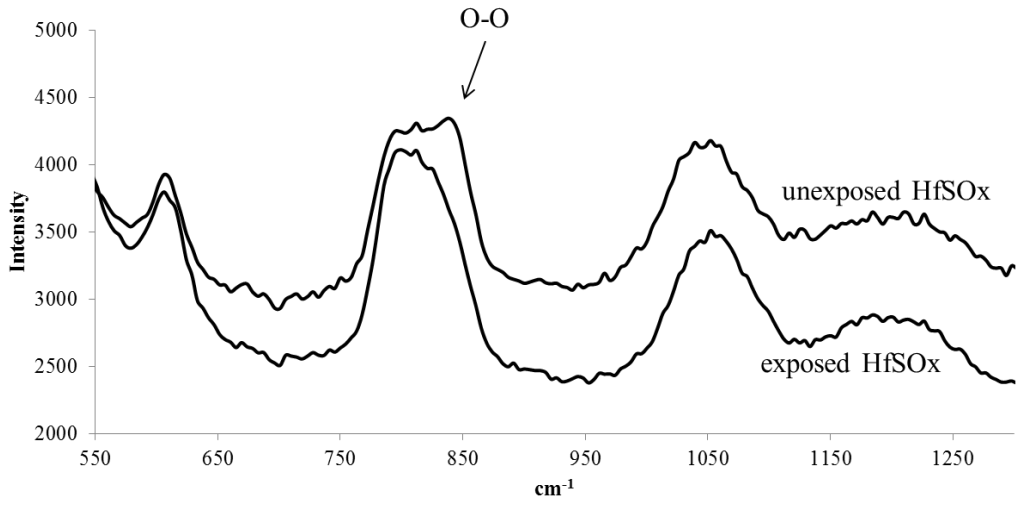

Figure 2.4: Raman spectra of HfSOx films before and after exposure to an electron beam at a dose of 1 mC/cm^2

CHAPTER 3

PHOTOPATTERNABLE INORGANIC HARDMASK

Alan Telecky, Peng Xie, Jason Stowers, Andrew Grenville, Bruce Smith, and Douglas A. Keszler

Published in *Journal of Vacuum Sciences and Technology B*. **28**, C6S19 (2010)

Abstract

We present here a directly photopatternable inorganic hardmask for 193-nm lithography based on solution-deposited dielectric metal oxide sulfate (MSOx) system. To demonstrate pattern fidelity, 18-nm half-pitch features were written at a dose near 240 μC/cm^2 (30 keV) with LWR values between 1.6 and 1.8 nm. Well resolved and uniform 30-nm contact holes were fabricated via a litho-freeze-litho-etch (LFLE) process employing electron beam exposure and a simple thermal freeze. ZircSOx has a high index of refraction approaching 1.9 at 193 nm, and the extinction coefficient, k, can be varied by an order of magnitude by substituting Zr with Hf. Optical interference lithography at 193 nm was used to realize 60-nm half-pitch lines in MSOx at a dose of 25 mJ/cm^2.

Introduction

To meet the needs for continued scaling and fabrication of nanoscale devices, electron-beam, 193-nm optical, nanoimprint, and extreme ultraviolet (EUV) lithography technologies need to meet increasingly demanding performance. The progress of lithography is highly dependent on the interplay between innovations in exposure-tool development and breakthroughs in resist chemistry, which together lead to advanced capabilities. Currently, 193-nm immersion (193i) optical lithography is being used in high-volume manufacturing of CMOS devices. Advanced approaches, e.g., 193i double patterning, and EUV lithography are currently being developed to address feature-size and resolution requirements beyond the 22-nm node. Both technologies share the need for high performance resists that must meet stringent requirements for sensitivity, resolution, line-width roughness, and etch resistance.[1] In this contribution, we describe a new inorganic resist chemistry for optical lithography that is firmly on the path to meeting many of these advanced needs.

Numerous chemically amplified resists (CARs) have been developed to address the sensitivity requirements for all forms of semiconductor lithography. Typically, CARs are polymer-based organic resins with high positive-tone (in some cases negative-tone) sensitivity that is achieved through the addition photo-acid generators (PAGs) designed for chemical amplification.[2,3] Amplification occurs in these systems when incident photons stimulate the release of an acid that

diffuses through the resist. The acid reacts with the crosslinked polymer, catalytically breaking many bonds and altering the solubility of the resin. Despite a high sensitivity, progress in CARs is hindered by acid diffusion, which contributes to feature blurring, high LWR, and limited resolution.[2,3,4,5]

During the past few decades, several inorganic materials have been examined as alternatives to organic resists. Work on these inorganic materials has been stimulated in part by the small, high-quality features that can be written with high-dose electron-beam lithography.[6,7] For example, the interdiffusion chemistry of various layered chalcogenides has been used to produce photoimagable materials.[8,9,10] Despite high contrast, the utility of these materials has been limited by vacuum-deposition requirements, material toxicity, and deleterious doping of silicon by constituent metals, e.g. silver. Peroxometalates, notably peroxopolytungstates, have also been examined as resists with sensitivity to ultraviolet, X-ray, and electron beams. These materials never garnered much interest because of their tendency to crystallize and their limited sensitivites.[11] More recently, sol-gel metal-organic resists have been developed. For these materials, exposure doses can exceed those of CARs by three orders of magnitude; they also suffer from high absorption, only modest feature-size capabilities, and poor LWR.[12,13] Outgassing of the organic constituents is also likely to be problematic for use in EUV systems, where lens contamination can rapidly occur.

To address many of the past limitations of inorganic resists, we have recently introduced peroxo modified forms of the materials zirconium oxide sulfate (ZircSOx) and hafnium oxide sulfate (HafSOx) as a new family of directly patternable metal oxide. They provide many advantages with respect both to CAR's and all other photopatternable inorganic resists.[14,15] Because many metal ions other than Hf and Zr can be used in the basic resist chemistry, the family is more generally designated as *MSOx*.

A sensitive, photopatternable inorganic resist could simultaneously address many issues in advanced semiconductor manufacturing. Current double-patterning techniques, for example, require a vacuum-deposited hard mask, e.g., $SiON_x$, that must then be patterned with a polymer resist. Additional layers are also often applied to aid in pattern transfer, which can add considerable complexity to the process.[16,17] Many processing steps – vacuum deposition, polymer processing, etching – could be eliminated with the introduction of a spin-coated, directly imageable hard mask having high sensitivity. Such materials would also enable complete hard-mask processing on efficient, low-cost wafer tracks.

Electron-beam lithography remains an enabling technology for other forms of lithography. EUV, 193i and nanoimprint lithography, especially, rely on masks and templates fabricated through the use of electron beam lithography. Therefore a continuing need exists for a high-performance electron beam resist possessing a high sensitivity and low line width roughness (LWR).

We describe below initial results on photopatterning the resists zirconium oxide sulfate (ZircSOx) and hafnium oxide sulfate (HafSOx). Before addressing the photoexposure of the MSOx resists, we consider new results on electron-beam patterning, demonstrating dense features at 18 nm half-pitch and implementation of a litho-freeze-litho-etch (LFLE) double patterning methodology.

Experiemental

Aqueous MSOx solutions were prepared using an Inpria proprietary formulation technique. Solutions were then spin coated onto silicon substrates at 3000 rpm for 30 s. Following spin coating, a 70 °C post apply bake was conducted for 3 minutes to partially dehydrate the film. The resulting film thickness from this procedure was typically 30 nm as measured by ellipsometry. A 1-minute 70 °C post-exposure bake was conducted on e-beam exposed samples, while 193 nm exposures were baked at 100 °C for 1 minute following exposure. The silicon substrates were prepared for spin coating by sonication in Decon Labs Contrad-70 solution at 45 °C for 60 min.

Ellipsometry measurements were collected using a J.A. Woollam VASE Ellipsometer and modeled with WVASE32 software. The modeling of MSOx resists involved collecting data over the wavelength range of 190 to 600 nm and fitting to a Cauchy-Urbach absorption model.

Electron-beam exposures for line and pattern formation were conducted at 30 keV on a Zeiss Ultra-55 SEM with a Nabity lithography system. Development

was conducted by immersion in 25 or 2.38% w/w tetramethylammonium hydroxide (TMAH) for 15 seconds; this step was followed by thorough rinsing with deionized water. The composition of MSOx was tuned for use with each developer. A final hardbake was performed at 220 °C for 5 min. Films were exposed at 193 nm by using an interference ArF tool at the Rochester Institute of Technology; exposure methods have been outlined elsewhere.[18] SEM images were collected by using a Zeiss Ultra-55 SEM operating at 5 keV except for 193 nm pattern images, which were collected using a LEO EVO 50 SEM operating at 5 keV. Line width roughness (LWR) values for electron-beam exposures were measured by using Hitachi Offline CD measurement software version 4.11 with an inspection length of 500 nm. LWR values for 193 nm exposures were not measured.

Results and Discussion

Electron Beam Results and Etch Resistance

Electron beam exposures at 30 keV have previously been reported for MSOx[14], where feature sizes of 28 nm on a 100 nm pitch were demonstrated. A contrast of 5.6 was obtained for MSOx with D_0 and $D_{0.8}$ doses of 200 μC/cm^2 and 400 μC/cm^2, respectively. A high etch resistance was also demonstrated by reactive ion etching with CHF_3; etch rates of 2.2 nm/min were reported, a rate 9x slower than thermally grown SiO_2 under the same conditions. Such a high etch resistance for MSOx enables the use of low aspect ratios features for pattern

transfer, and eases the constraints on resist contrast. As a result a relatively thin MSOx resist film can effectively be used to pattern transfer features of significantly higher aspect ratios into the substrate. Data and examples of pattern transfer into Si using MSOx resists will be presented in a subsequent publication.

Continued optimization of the MSOx system has resulted in improved resolution and contrast while maintaining similar sensitivity. An SEM image of 18-nm half-pitch lines for an exposure at a dose of 244 $\mu C/cm^2$ (30 keV) is shown in Figure 3.1. 21-nm lines on a 60-nm pitch at a dose of 436 $\mu C/cm^2$ can be produced with LWR values in the range of 1.6 to 1.8 nm (Figure 3.2), a value significantly lower that was first reported with hydrogen silsesquioxane (HSQ) and superior when compared to organometallic Zr/Hf nanoparticle-based resists. [12,13,19]

LFLE Double Patterning

The MSOx chemistry is directly amenable to a negative-tone litho-freeze litho-etch (LFLE) process. This process involves two consecutive lithographic steps and two resist coating steps. In the first lithography step, a resist layer is deposited, exposed, baked, and then developed. A freeze step follows, which involves rendering the developed pattern insoluble in the second resist coat. Such freezing is commonly accomplished by exposing the developed pattern to a surfactant or solvent rinse.[20] The need for an additional chemical-freeze processing step significantly increases the complexity of the double-patterning process with polymer resists. In a thermal-freeze process, the developed resist pattern is simply

baked at an appropriate temperature to render the pattern insoluble. In the case of MSOx, a 5-minute bake at 220 °C is adequate to lock in or “freeze” the pattern. After the 220 °C bake MSOx patterns have been transformed into dense oxides and are no longer soluble in resist or developer. A second lithography process can then be performed on top of the existing pattern. Finally, an etch step can be performed to transfer the doubly exposed pattern. The LFLE process is a commonly proposed method to realize pitch doubling and patterning of contact holes.[20,21]

By implementing a negative-tone LFLE process with a thermal freeze, contact-hole patterns were generated in ZircSOx by electron beam lithography at a dose near 500 $\mu C/cm^2$. SEM images of the crosshatched patterns (Figure 3.3) clearly reveal resolved 30-nm square holes. The features are uniform and exhibit sharp angles – structures that are very difficult to obtain with positive-tone chemically amplified resists.

Application to 193 nm Lithography

Tunability of the optical properties of the MSOx resist platform is a unique capability for optimizing 193-nm lithography. As with typical resist design, the primary objective was to optimize absorbance to balance efficient coupling of the incident radiation with a uniform light distribution through the film. To take advantage of the high etch resistance and to mitigate pattern collapse, the films are

targeted for a thickness of approximately 30 nm. This implies a target absorbance of 3 μm^{-1} and an extinction coefficient (*k*) of approximately 0.1.

To tune the optical properties, Zr, for example, can be readily replaced by Hf without affecting the chemical or mechanical properties of the film. In the $Zr_{1-x}Hf_xSOx$ system, the entire range of compositions, x =0 to x = 1, can be accessed. Variable angle spectroscopic ellipsometry has been used to measure the optical constants across this entire range, cf. Figure 3.4. Indeed the extinction coefficient can be modulated by nearly an order of magnitude across the series. As the fraction of Hf in ZircSOx increases, both the refractive index (*n*) and the extinction coefficient (*k*) decrease. These results demonstrated that while HafSOx is too transparent (*k*~0.01), ZircSOx is a good candidate with $k \sim 0.1$.

Interference exposures at 193 nm were performed on a range of HafSOx/ZircSOx formulations. 60-nm half-pitch lines were written for each condition. As expected, dose improved with the more absorptive Zr-rich formulations. For HafSOx, $E_{1:1}$ = 90 mJ/cm^2, for $Zr_{0.5}Hf_{0.5}SOx$, $E_{1:1}$ = 60 mJ/cm^2, and for ZircSOx, $E_{1:1}$ = 25 mJ/cm^2. Representative SEM images of 60-nm lines on a 60-nm half-pitch in ZircSOx exposed at a dose of 25 mJ/cm^2 are shown in Figure 3.5.

An additional benefit of the MSOx family is the ability to access indices of refraction above 1.8, as such a resist provides additional process latitude stemming from increased depth of focus.[22,23] Typically, achieving an index of refraction

above 1.8 with an organic resist forces an unacceptably high absorbance. ZircSOx has the appropriate absorbance and an index of approximately 1.9. The magnitude of the improvement in process latitude has not yet been quantified.

Not only can Hf and Zr be substituted within the resist, but so too can other metals. A unique aspect of the MSOx systems is that their chemistries allow for inclusion of a variety of both transition and *p*-block metals in varying amounts. Substitution of additional metals into organometallic systems is often difficult, if not impossible, because of to differing rates of ligand exchange, hydrolysis and solubility. An advantage to compositional variability is a larger potential range of optical properties than the ZircSOx-HafSOx system alone. Therefore, MSOx represents a unique platform that allows the tuning of optical and etch properties appropriate for a variety of processes including electron-beam, 193-nm and extreme ultraviolet (EUV) lithography. For example, sub-20nm EUV patterning using this platform has been described elsewhere.[24]

The MSOx materials are aqueous systems, so extension to 193 nm immersion lithography requires a water impermeable topcoat. In addition, a hydrophobic surface appropriate for scanning, i.e., contact angle > 70 degrees, is required. To test immersion capabilities and to avoid the need for a topcoat, initial experiments were performed with cyclohexane as the immersion fluid. However, as no bottom antireflective coating was used, a significant intensity drop at the bottom of the resist became evident as partial delamination was observed.

Evidence for 40 nm half-pitch lines was observed in spite of this issue.. Given the high-resolution patterning shown by electron beam lithography, there is a path to features < 40 nm with 193nm immersion lithography with appropriate topcoat and reflection management.

Conclusion

The solution-deposited MSOx platform has been developed as high performance electron beam and 193-nm resists. With electron-beam exposures, 18-nm half-pitch lines and spaces wth LWR values < 2 nm at 30 keV have been realized at a modest dose of 244 uC/cm^2. The materials also function as sensitive, high-resolution, negative-tone photopatternable hardmasks. At 193 nm, 60-nm half-pitch features were readily written at a dose of 25 mJ/cm^2. A negative-tone LFLE double patterning process was demonstrated showing extendibility to 30 nm and below. A method to tailor the optical and chemical properties of the MSOx platform was shown by alloying ZircSOx and HafSOx. Extending such capabilitiesto other metals provides a new route to effectively managing the interactions among resist optical properties, exposure chemistries, and development processes. Altogether, the MSOx platform presents an unprecedented approach to resist performance optimization.

References

(1) ITRS Roadmap, 2009 Edition, http://www.itrs.net/.

(2) Gibbons, F. P.; Manyam, J.; Diegoli, S.; Manickam, M.; Preece, J. A.; Palmer, R. E.; Robinson, A. P. G. *Microelectronic Engineering* **2008**, *85*, 764–767.

(3) Sailer, H. *Microelectronic Engineering* **2004**, *73-74*, 228–232
.

(4) Lawson, R. A.; Lee, C.-T.; Yueh, W.; Tolbert, L.; Henderson, C. L. *Microelectronic Engineering* **2008**, *85*, 959–962.

(5) Itani, T.; Yoshino, H.; Hashimoto, S.; Yamana, M.; Samoto, N.; Kasama, K. *Microelectronic Engineering* **1997**, *35*, 149–152.

(6) Kratschmer, E. *Journal of Vacuum Science & Technology B: Microelectronics and Nanometer Structures* **1986**, *4*, 361.

(7) Kratschmer, E. *Journal of Vacuum Science & Technology B: Microelectronics and Nanometer Structures* **1987**, *5*, 369.

(8) Lavine, J. M. *Journal of Vacuum Science & Technology B: Microelectronics and Nanometer Structures* **1996**, *14*, 3489.

(9) Teteris, J. *Journal of Non-Crystalline Solids* **2002**, *299-302*, 978–982.

(10) Chern, G. C. *Journal of Applied Physics* **1982**, *53*, 6979.

(11) Baba, M.; Ikeda, T. *Japanese Journal of Applied Physics* **1981**, *20*, L149–L152.

(12) Ridaoui, H.; Wieder, F.; Ponche, A.; Soppera, O. *Nanotechnology* **2010**, *21*, 065303.

(13) Trikeriotis, M.; Bae, W. J.; Schwartz, E.; Krysak, M.; Lafferty, N.; Xie, P.; Smith, B.; Zimmerman, P. A.; Ober, C. K.; Giannelis, E. P. 2010; p. 76390E–76390E–10.

(14) Stowers, J.; Keszler, D. A. *Microelectronic Engineering* **2009**, *86*, 730–733.

(15) Anderson, J. T.; Munsee, C. L.; Hung, C. M.; Phung, T. M.; Herman, G. S.; Johnson, D. C.; Wager, J. F.; Keszler, D. A. *Advanced Functional Materials* **2007**, *17*, 2117–2124.

(16) Pauliac-Vaujour, S.; Brianceau, P.; Comboroure, C.; Faynot, O. *Microelectronic Engineering* **2008**, *85*, 800–804.

(17) Weimer, M.; Wang, Y.; Neef, C. J.; Claypool, J.; Edwards, K.; Zu, Z. SPIE, 2007; Vol. 6519, p. 65192S–65192S–8.

(18) Smith, B. W. SPIE, 2004; Vol. 5754, pp. 751–759.

(19) Namatsu, H. *Journal of Vacuum Science & Technology B: Microelectronics and Nanometer Structures* **1998**, *16*, 69.

(20) Guerrero, D. J.; Sullivan, D. M.; Mercado, R.-M. L. 2009; p. 75200M–75200M–8.

(21) Sakamoto, R.; Endo, T.; Ho, B.-C.; Kimura, S.; Ishida, T.; Kato, M.; Fujitani, N.; Onishi, R.; Hiroi, Y.; Maruyama, D. 2009; p. 75201Y–75201Y–10.

(22) Blakey, I.; Chen, L.; Dargaville, B.; Liu, H.; Whittaker, A.; Conley, W.; Piscani, E.; Rich, G.; Williams, A.; Zimmerman, P. SPIE, 2007; Vol. 6519, p. 651909–651909–9.

(23) Grenville, A. *Future Fab Intl.* **2007**, *20*.

(24) Naulleau, P.; Anderson, C. N.; Baclea-an, L.-M.; Chan, D.; Denham, P.; George, S.; Goldberg, K. A.; Hoef, B.; Jones, G.; Koh, C.; La Fontaine, B.; McClinton, B.; Miyakawa, R.; Montgomery, W.; Rekawa, S.; Wallow, T. 2010; p. 76361J–76361J–9.

Figures

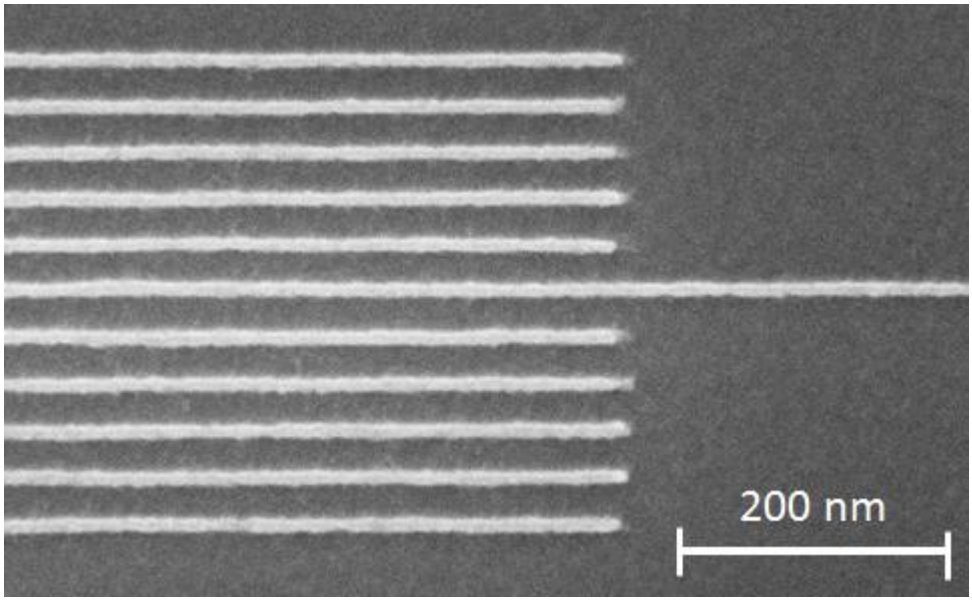

Figure 3.1: SEM image showing 18 nm lines and spaces written in MSOx at a dose of 244 uC/cm^2 with a 30 keV electron beam.

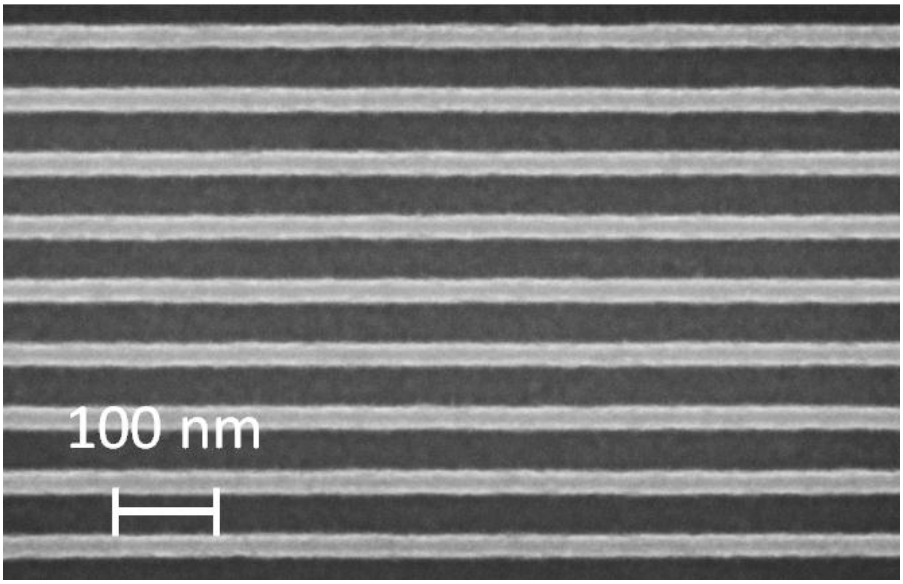

Figure 3.2: SEM image of MSOx written with a 30 keV electron beam at a dose of 436 uC/cm^2 showing LWR of 1.6-1.8 nm for 21 nm lines on 60 nm pitch.

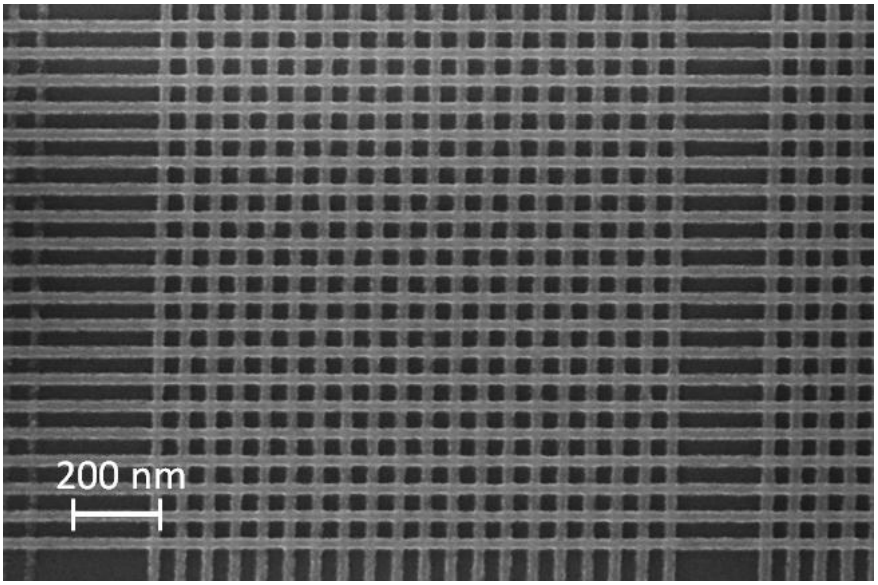

Figure 3.3: Well-resolved 30-nm contact holes achieved using LFLE double-patterning process with a 30 keV electron beam at 500 μC/cm^2.

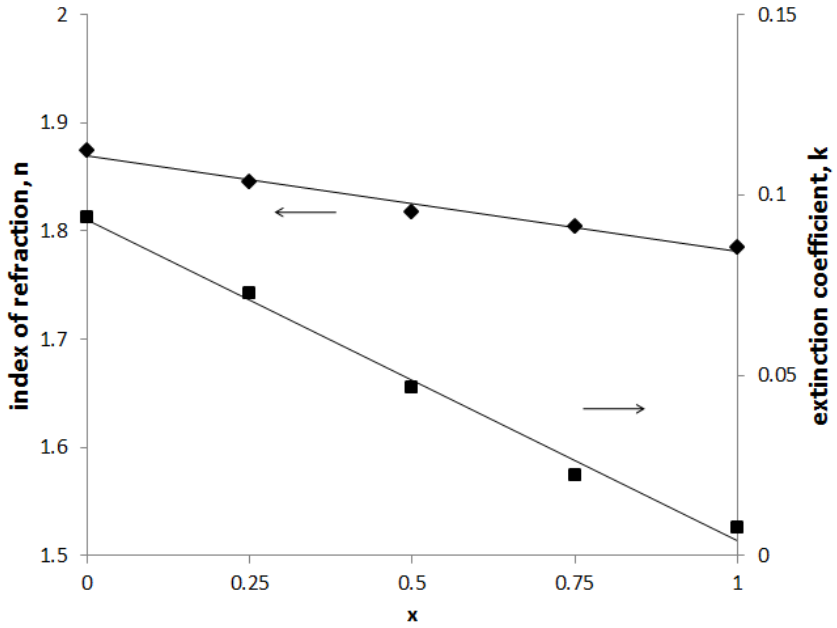

Figure 3.4: Index of refraction and extinction coefficient as a function of *x* in $Zr_{1-x}Hf_xSOx$ resist.

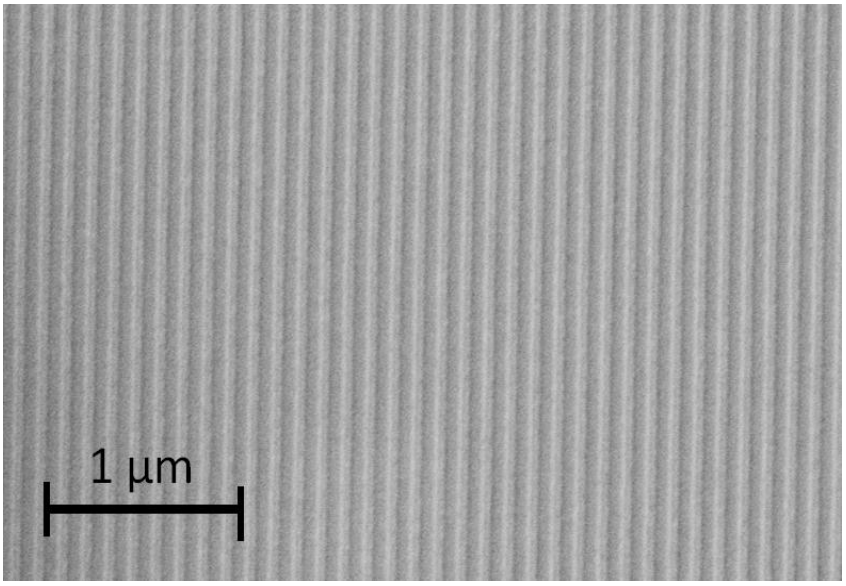

Figure 3.5: 60-nm lines on a 60-nm half-pitch written in ZircSOx using 193 nm optical interference lithography at a dose of 25 mJ/cm^2.

CHAPTER 4

EFFECTS OF METAL SUBSTITUTION ON THE ELECTRON-BEAM PATTERNING OF HAFSOX

Abstract

The resolution, line width roughness and sensitivity (RLS) tradeoffs of HafSOx and HafSOx:M (M = Y, La, Mo and W) resists patterned by electron beams are investigated. The sensitivity HafSOx:M resists is found to be highly dependent upon the identity of the metal: Y and La both create a more sensitive resist, whereas Mo and W lower the sensitivity. Line width roughness is also found to depend upon the identity of the metal. Resolution effects were difficult to analyze due to the limited resolution of the patterning instrument.

Introduction

HafSOx resists, represented by the composition $HfO_{2-x}(SO_4)_x$, offer unparalleled resolution for an oxide material with electron beam and extreme ultraviolet (EUV) lithographies.[1,2] A major advantage to HafSOx resists is their extreme compositional variability that allows for tuning of resist sensitivity, solubility and etch resistance through simple manipulation of the material's composition. While HafSOx is a high resolution electron beam and EUV resist in its own right, much interest exists in substituting other metals into HafSOx to vary the resist properties in order to realize better sensitivity, lower line width roughness (LWR) and higher resolution. A mixed metal system may also open up more possibilities in the choice of developer solution or concentration.

As a first order investigation the effects of substituting either slightly lighter or slightly heavier d-block metals for Hf, namely Y, La, Mo and W. Yttrium and lanthanum are early d-block metals that are known to have an extensive solubility in ZrO_2 and HfO_2. Yttrium, in particular, is a common additive to stabilize the thermodynamically unstable cubic ZrO_2 phase due to its use as an ionic conductor, among others.[3,4,5] Lanthanum was a chosen dopant because it, like yttrium, is a group III element and would serve as a good comparison point.

Tungsten and molybdenum were chosen as constituents for a number of reasons. The solution chemistry of W and Mo oxides is amenable to HafSOx. Both elements form well-known and extremely stable aquo-peroxo species in the

presence of H_2O_2, a component of HafSOx resist solutions, to readily form polyperoxometallates.[6,7] These polyperoxometallates are sensitive to electron and ion beams as well as to ultraviolet radiation. The exposure mechanism of these materials is driven by the radiation-induced decomposition of peroxide groups, resulting to crosslinking between MO_6 octahedra to form dense oxide frameworks that become insoluble in developer solution, such as water or dilute base.[8] MoO_3 and WO_3 have also both shown to be sensitive to electron beams in their own right.[9,10] In these systems, an amorphous to crystalline phase change induced by incident radiation results in a marked difference in solubility in aqueous base.

Furthermore, the addition of other metal oxides provides a means to alter the dissolution properties of HafSOx in the developer solution, which is typically an aqueous tetramethyl ammonium hydroxide (TMAH) solution. Yttrium oxide and lanthanum oxide are highly insoluble in base whereas molybdenum and tungsten oxide are highly soluble, an important consideration because during development two processes occur: neutralization and dissolution. The balance of both processes is crucial to creating high-resolution and high-fidelity patterns. Neutralization of HafSOx occurs due to its acidity, and subsequently protons and anions are lost into solution and the material is converted to a hydrous HfO_2 framework. Dissolution also occurs because of the high solubility of the hydrated peroxo-containing HafSOx species. Control over these two competing processes is crucial to reduce scumming (i.e, improving resolution) and to improve contrast. If neutralization occurs too rapidly then the material becomes insoluble and image

contrast decreases; conversely, if dissolution occurs too quickly then the sensitivity of the material decreases since more energy will be required to reach a material density that is insoluble in TMAH. Therefore by introducing different concentrations of each metal into HafSOx, significant differences of solubility and reactivity in developer can be readily observed and, as a consequence, differences in sensitivity and resolution.

The inherent sensitivity of mixed-metal oxides to electron beams is expected to be influenced by the presence of other metal atoms within the M:HafSOx matrix. The energy deposited within a given distance travelled by an electron decreases with increasing electron density according to the Bethe equation.[11,12] Therefore the substitution of Hf with other metals presumably will change the material's stopping power and, consequently, the resist sensitivity and resolution.

Experimental

Solutions of HafSOx:Y and HafSOx:La were prepared from aqueous solutions of $HfOCl_2$:Y, $HfOCl_2$:La, H_2O_2 and H_2SO_4. $HfOCl_2$:Y,La was prepared by dissolving appropriate molar amounts of Y_2O_3 or La_2O_3 powder into ~1M $HfOCl_2$ solution at room temperature with stirring for 1 day. HafSOx:Mo and HafSOx:W were prepared by mixing appropriate molar amounts of peroxo solutions of Mo and W into $HfOCl_2$, followed by addition of H_2O_2 and H_2SO_4. All

HafSOx and HafSOx:M solutions were diluted to reach a 0.2 M solution of total metal.

Films of HafSOx and HafSOx:M were prepared by spin coating the aqueous solutions at 3000 rpm for 30s on 2.5 cm^2 silicon substrates. Si substrates were prepared for spin coating by sonication in Contrad-70 solution for 60 minutes at 45 ^oC, following by thorough rinsing with DI water.

The films underwent an 80 ^oC post-application bake (PAB) for 3 minutes before exposures. Electron beam exposures were conducted on a Zeiss Ultra-55 Scanning Electron Microscope using a 30 keV accelerating voltage equipped with Nabity Lithography hardware. Following exposure, the films underwent a post-exposure bake (PEB) at 80 ^oC for 1 minute. Development of HafSOx and HafSOx:M samples was conducted in 25% tetramethyl ammonium hydroxide for 15 seconds, followed by thorough rinsing with DI water.

Results and Discussion

Not surprisingly, substituting metals into HafSOx has a marked effect on the sensitivity of the material towards electron beams. The inclusion of La and Y into HafSOx resulted in an overall increase in sensitivity of the resist by about 20%, as is evidenced by the contrast curve in Figure 4.1. Mo and W, on the other hand, result in a material with substantially less sensitivity as seen in the contrast curves in Figure 4.2.

The change in sensitivity of the resist can be interpreted in a couple of ways. First, the solubility of the resist in aqueous base changes because both La_2O_3 and Y_2O_3 are more insoluble in base than is HfO_2, thus it requires less energy in order to convert the resist into an insoluble form. The opposite is true for the inclusion of W and Mo in HafSOx. Tungsten and molybdenum oxides have a high solubility in aqueous base and therefore more energy is needed to convert them into an insoluble form.

A second possible explanation for the differences in sensitivity is that the photoactive species (peroxo groups in this case) are further destabilized by the presence of larger La and Y atoms, thus requiring less energy to decompose and to convert the material to an insoluble form. Conversely, the more stable molybdenum and tungsten peroxide species require more energy to decompose. A similar argument has been made by Okamoto et. al to explain the increase in sensitivity seen in polyperxotungstate when doped with small amounts of Nb or Ta.[13]

In addition to the change in sensitivity, the resolution and LWR of the mixed-metal HafSOx is also affect in relation to that of undoped HafSOx resists. The ultimate resolution of all the samples could not be accurately measured on the electron beam writer in this study due to the its limited resolution of ~18 nm. Representative SEM images of 22 nm line and space elbow features patterned in HafSOx, HafSOx:Y and HafSOx:La are shown in Figure 4.3, Figure 4.4 and

Figure 4.5, respectively.LWR values for HafSOx and M:HafSOx resists measured on 30 nm half-pitch lines are around 4 to 6 nm for all samples. Table 4.1 shows LWR and dose-to-size values for 30 nm half-pitch features patterned in HafSOx and HafSOx:M.

Table 4.1. LWR values of 30 nm line and space features patterned in HafSOx:M (M = Y, La, Mo and W) and HafSOx.

Resist:	HafSOx	HafSOx:Y	HafSOx:La	HafSOx:Mo	HafSOx:W
LWR:	4.4 nm	6.2 nm	5.3 nm	5.9 nm	4.0 nm
$E_{1:1}$	553 μC/cm^2	384 μC/cm^2	442 μC/cm^2	>1 mC/cm^2	>1 mC/cm^2

Conclusion

Electron beam patterning was conducted on HafSOx and HafSOx:M (M = Y, La, Mo, W) resists to determine the relationship between metal content and resist performance in terms of resolution, sensitivity and line-width-roughness. Resist sensitivity was significantly affected by inclusion of metals other than Hf. A sensitivity of 243 μC/cm^2 was shown for non-substituted HafSOx. An increase in sensitivity to 199 μC/cm^2 was shown for both HafSOx:Y (5 at. %) and HafSOx:La (5 at.%), respectively, while a decrease in sensitivity to 443 μC/cm^2 and 297 μC/cm^2 and was shown for HafSOx:Mo (5 at. %) and HafSOx:W (5 at. %), respectively.

These results indicate that metal substitution in HafSOx provides a simple means to manipulate sensitivity and access higher performance dose regimes while not adversely or significantly affecting the resolution or line-width-roughness of the resist for features with critical dimensions larger than 20 nm. Further work on higher resolution capable electron beam writing tools is warranted.

References:

(1) Stowers, J.; Keszler, D. A. *Microelectronic Engineering* **2009**, *86*, 730–733.

(2) Telecky, A.; Xie, P.; Stowers, J.; Grenville, A.; Smith, B.; Keszler, D. A. *Journal of Vacuum Science & Technology B: Microelectronics and Nanometer Structures* **2010**, *28*, C6S19.

(3) Butz, B.; Störmer, H.; Gerthsen, D.; Bockmeyer, M.; Krüger, R.; Ivers-Tiffée, E.; Luysberg, M. *Journal of the American Ceramic Society* **2008**, *91*, 2281–2289.

(4) Sillassen, M.; Eklund, P.; Pryds, N.; Johnson, E.; Helmersson, U.; Bøttiger, J. *Advanced Functional Materials* **2010**, *20*, 2071–2076.

(5) Miyahara, Y. *Journal of Applied Physics* **1992**, *71*, 2309.

(6) Campbell, N. J.; Dengel, A. C.; Edwards, C. J.; Griffith, W. P. *Journal of the Chemical Society, Dalton Transactions* **1989**, 1203.

(7) Okamoto, H.; Iwayanagi, T.; Mochiji, K.; Umezaki, H.; Kudo, T. *Applied Physics Letters* **1986**, *49*, 298.

(8) Okamoto, H.; Ishikawa, A.; Kudo, T. *Journal of Photochemistry and Photobiology A: Chemistry* **1989**, *49*, 377–385.

(9) Hashimoto, M.; Watanuki, S.; Koshida, N.; Komuro, M.; Atoda, N. *Japanese Journal of Applied Physics* **1996**, *35*, 3665–3669.

(10) Koshida, N.; Tomita, O. *Japanese Journal of Applied Physics* **1985**, *24*, 92–94.

(11) Grigor'ev, E. I.; Trachtenberg, L. I. *Radiation chemical processes in solid phase : theory and application*; CRC Press: Boca Raton, Fla. [u.a.], 1996.

(12) Joy, D. C.; Luo, S. *Scanning* **1989**, *11*, 176–180.

(13) Okamoto, H.; Ishikawa, A.; Kudo, T. *Thin Solid Films* **1989**, *172*, L97–L99.

Figures

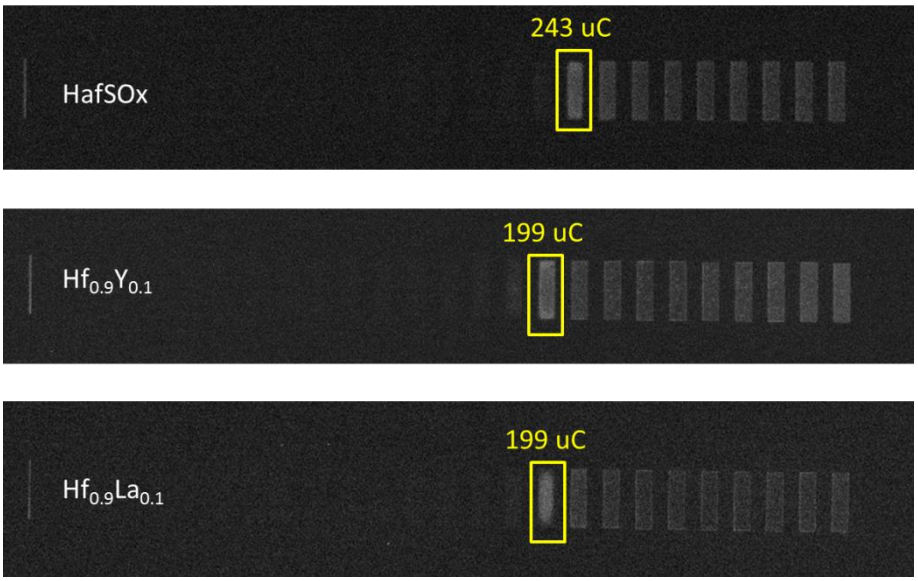

Figure 4.1: Contrast curve consisting of 2 μm x 4 μm rectangles patterned in HafSOx, HafSOx:Y and HafSOx:La resists as a function of increasing dose from left to right.

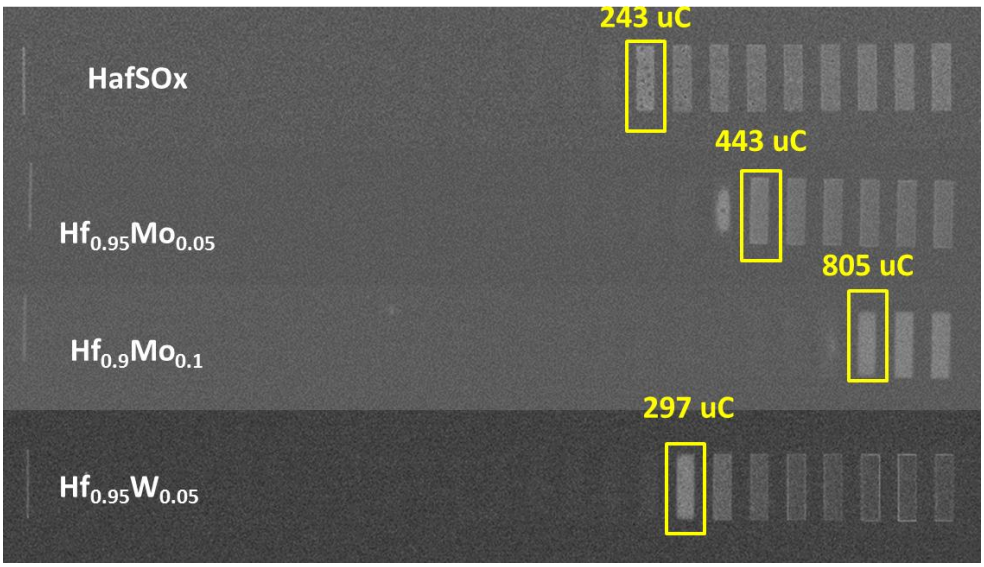

Figure 4.2: Contrast curve consisting of 2 μm x 4 μm rectangles patterned in HafSOx, HafSOx:Mo and HafSOx:W resists as a function of increasing dose from left to right.

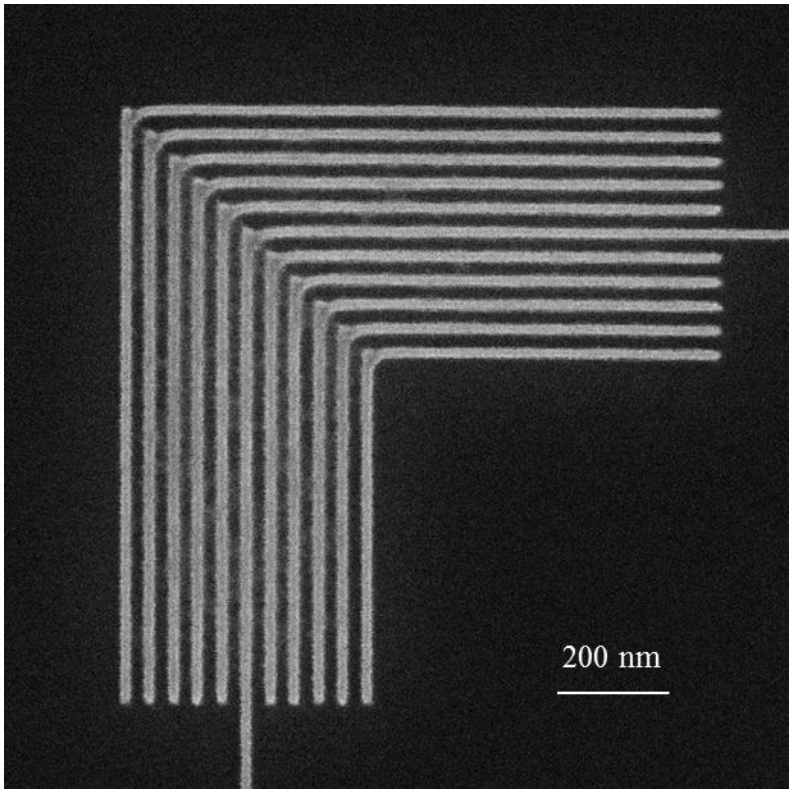

Figure 4.3: HafSOx 22 nm line and space elbow pattern written at a dose of 691 $\mu C/cm^2$.

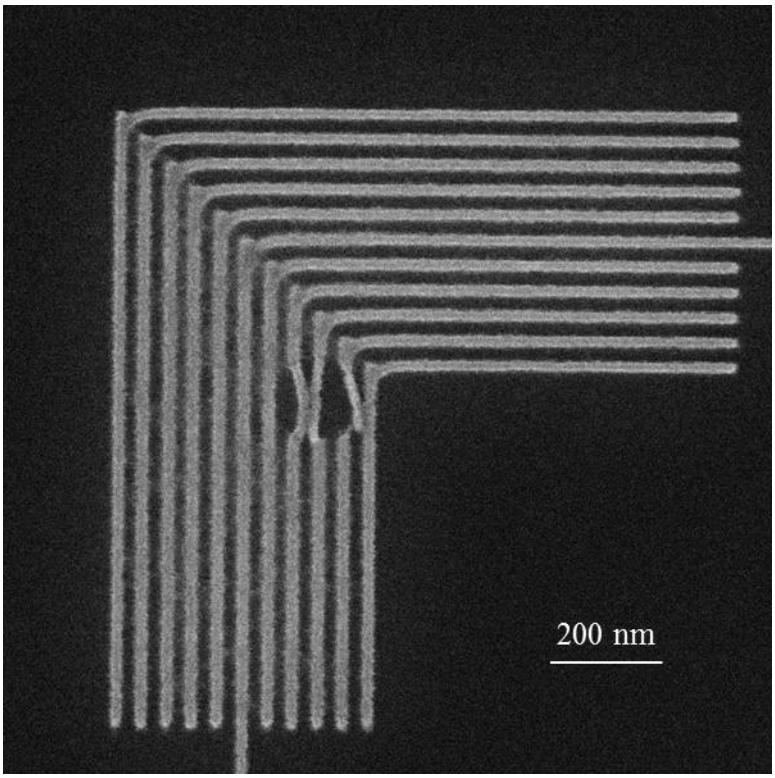

Figure 4.4: HafSOx:Y 10% 22 nm line and space elbow pattern written at a dose of 553 μC/cm^2.

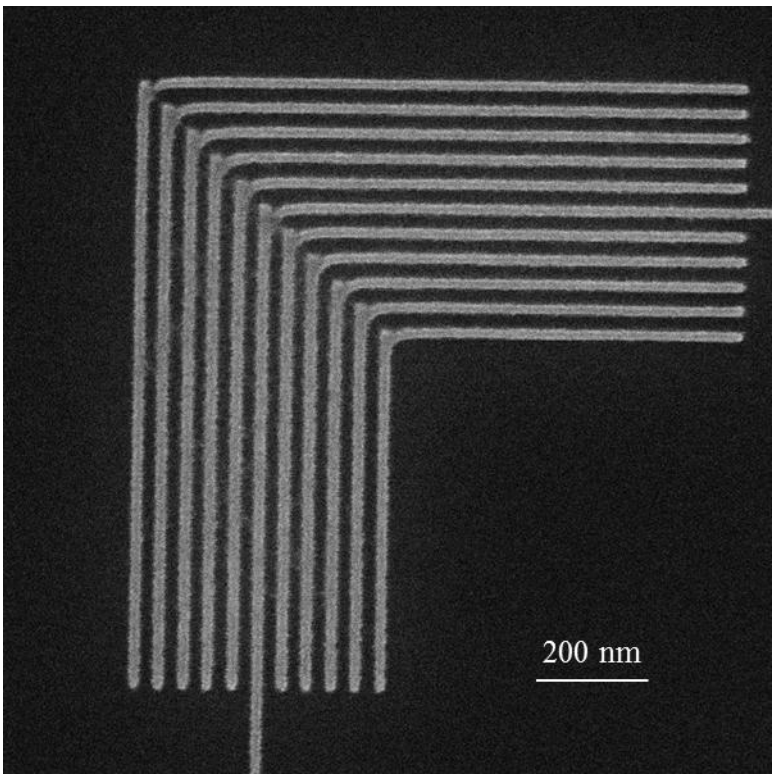

Figure 4.5: HafSOx:La 10% 22 nm line and space elbow pattern written at a dose of 553 μC/cm^2.

CHAPTER 5

NEUTRALIZAITON OF THIN HAFSOX FILMS AND THEIR ANION EXCHANGE CHARACTER

Abstract

HafSOx ($HfO_{2-x}(SO_4)_x$) films are shown to undergo neutralization and ion exchange upon immersion in NaOH solutions. Neutralization results in the complete removal of sulfate and chloride anions from the film to leave a hydrous hafnia ($HfO_x(OH)_{4-2x}$) film which can then undergo a second exchange, or can be readily dehydrated by thermal annealing to form HfO_2. Changes in film thickness and refractive index due to neutralization were characterized by variable angle spectroscopic ellipsometry and elemental analysis was conducted on neutralized films using TOF-SIMS and EPMA techniques to further characterize the extent of ion exchange.

Introduction

Understanding the processes that occur at the interface between solids and aqueous solutions is of fundamental interest. It is well known that metal oxides and minerals in contact with water will undergo chemical changes over time associated with leaching of soluble species, ion exchange, and rearrangement of metal-oxide bonds in concert with solubilization and condensation.[1,2,3,4,5] In fact a major focus of environmental chemistry is on understanding the reactions and nature of the chemistry between water and the surfaces of naturally occurring oxides, such as clays, silicates, and aluminates. Additionally, significant research has gone into understanding the corrosion and leaching behavior of a number of transition metal oxides because of their use as corrosion-resistant barrier layers.[6,7]

Metal oxide films and coatings are pervasive in the technologies that surround us, from lighting to solar cells, from computer components to windows. Within the semiconductor industry alone, understanding the chemistries of metal oxides has been crucial to enabling current devices and devising pathways to future generations of devices. SiO_2, for example, has been the ubiquitous gate oxide material since the beginning of planar processing of transistors, but recently interest and focus has shifted towards other oxides such as HfO_2, Y_2O_3, and Al_2O_3, collectively known as high-K dielectrics, due to their superior dielectric constants compared to SiO_2.[8,9] These materials are routinely deposited using physical methods like atomic layer deposition (ALD), sputtering, and chemical vapor

deposition (CVD) which generally produce very high quality films and coatings. However, such methods are often slow, expensive, energy intensive, and require high vacuum, high temperatures or both.

It is thus of considerable interest to develop chemical techniques and methodologies needed to enable solution routes to oxide materials as solution processing possess numerous advantages. Solution techniques offer relatively simple deposition methods, low-cost and low-temperature processing. In recent years, our lab has demonstrated aqueous chemistries that enable the deposition of a number of oxide materials, including $Al_2O_{3-3x}(PO_4)_{2x}$ (AlPO), HfO_2, TiO_2 and $HfO_{2-x}(SO_4)_x$ (HafSOx).[10,11,12,13] HafSOx is an amorphous oxide that has been shown to be an effective gate oxide material in thin film transistors, as well as a high-resolution inorganic photoresist for extreme ultraviolet (EUV), 193 nm optical and electron beam lithographies.[14,15] In this chapter the ion-exchange and neutralization of "living" HafSOx films will be described. These HafSOx films are labeled as living because they continue to be chemically reactive after deposition. A variety of straightforward solution chemistries can be employed to realize compositions or morphologies that differ significantly from the initially deposited material. Here, the conversion of HafSOx films to amorphous hydrated HfO_2 films has been achieved via acid-base neutralization through immersion of films in aqueous base. A subsequent second ion-exchange reaction can also be performed where sulfate and phosphate anions can be reintroduced into the films, further demonstrating a platform for living film chemistry.

Ion exchange behavior, both cationic and anionic, has been well documented for hydrous zirconia where the exchange process is mediated by reactive and labile adsorbed surface species such as protons, water or halides that can be replaced by other ions.[1617] Similarly it is known that removal of foreign anions from ZrO_2 precipitates can be achieved by washing with aqueous base.[18] A few groups have also published reports describing the preparation of zirconia coatings via hydrolysis and condensation of aqueous $Zr(SO_4)_2$ solutions.[19] Therefore, neutralization and ion exchange of ZircSOx and HafSOx films is expected.

A major impetus for this work was to gain insight into the processes that occur during basic development of HafSOx resist films. Since development is typically done in aqueous solutions of tetramethylammonium hydroxide both processes of dissolution and neutralization are expected to occur. Descriptions of the development of conventional polymer films is often described as proceeding by a reactive dissolution mechanism, where neutralization of weakly acidic polymer-bound moieties are necessary before solvation of the polymer can occur, but much less information exists for inorganic systems.[20,21] By understanding the chemistry and process of neutralization, new approaches to optimizing inorganic resist chemistry may be enabled.

Experimental

Solution and film preparation: Solutions of HafSOx and ZircSOx were prepared by mixing stoichiometric amounts of $HfOCl_2$ and H_2SO_4 followed by dilution with DI water to achieve a final metal concentration of between 0.05M and 0.6M. Films were deposited by spin-coating these solutions at 2000 – 3000 rpm for 45 seconds, followed by a 2-minute hotplate anneal at selected temperatures between 75 and 300 ^{o}C. Si substrates were prepared for spin-coating by immersion in piranha solution (3:1 mixture of concentrated H_2SO_4 (aq) and H_2O_2 (aq)) for 10 minutes. Wafers of thermally grown SiO_2 on Si were prepared for spin coating by sonication in Contrad 70 solution for 60-90 minutes at 45 ^{o}C.

Characterization: Electron micro probe analysis (EPMA) data were collected on a Cameca SX-100. Intensities of O Ka, Si Ka, Cl Ka, Hf Ma, S Ka, and Zr La were collected using wavelength dispersive spectrometers. Data were collected at three different accelerating voltages (10, 15, and 20 kV) with experimental intensities determined from the average of ten proximate positions on each sample. $Ca_{10}(PO_4)_6Cl_2$, $CaSO_4$, Hf, Si, Zr, and MgO were used as standards. Raw intensities were corrected by a procedure detailed by Donovan and Tingle.[22] Quantitative elemental analysis was determined by comparing experimental *K*-ratios to simulated values using StrataGEM thin-film composition analysis software, which employs the PAP formalism developed by Pouchou and Pichoir.[23]

Time-of-Flight Secondary Ion Mass Spectrometry (TOF-SIMS) measurements were conducted on an ION-TOF IV TOF-SIMS instrument with a polyatomic Bi^+ source. Cs^+ ions were used as the primary sputtering source for the depth profiling of positively charged species and O^{2+} ions were used for negatively charged species. Electron flood gun neutralization was used in between every sputter cycle to minimize the charging effects.

Variable angle spectroscopic ellipsometry was conducted on a J.A. Woollam V.A.S.E 32 system. Modeling was conducted on WVASE32 software using Cauchy fitting parameters.

Results and Discussion

Two precursor solution compositions were used to prepare HafSOx films: a solution with a 1 : 0.5 Hf : H_2SO_4 ratio (S50) and a solution with a 1 : 0.7 Hf : H_2SO_4 ratio (S70). These two solutions were selected to study relationships among precursor sulfate content, film sulfate content, and neutralization behavior. The neutralization process is shown schematically in Figure 5.1.

Following immersion in NaOH (aq), no changes were observed in films with respect to color change and delamination, indicating no dissolution occurred. After a subsequent anneal, however, a color difference was observed. This color change is associated with optical interference effects resulting from a change in film thickness, a change in film density, or both. To properly characterize the

nature of the change that occurs in the film due to immersion in NaOH (aq) a number of analytical techniques were employed.

Electron probe micro analysis (EPMA) was used to analyze films for the elements Hf, O, S, Cl, and Na. Analysis of films deposited from S50 and S70 precursor solutions reveal film compositions of $HfO_{1.195}(SO_4)_{0.56}Cl_{0.49}$ and $HfO_{1.065}(SO_4)_{0.75}Cl_{0.37}$, respectively. Because of the difficulty in measuring O concentrations, these formulas are expressed as dehydrated formulas with O included for charge balance. Sodium was included in the analysis because cation exchange of H^+ for alkali metals in basic solutions has been demonstrated in both hydrous ZrO_2 and zirconium phosphates.[16,24] After analysis, however, it was revealed that the Na was not detected in any samples. The lack of Na may be expected considering the neutralized films are washed thoroughly with DI water which could drive exchange of Na^+ for H^+. Indeed, such a behavior has been shown with hydrous ZrO_2 where neutral conditions weak basicity of ZrO_2 favors H^+ adsorption.[16]

To examine the effects of thermally driven condensation on the ion-exchange behavior films of S50 were annealed for 3 minutes at 75, 100, 110, 120, 130 and 140 °C, while films of S70 were annealed for 3 minutes at 150, 160, 170, 180, 200, 210 and 220 °C. Following the anneal, the films were then neutralized by immersion for 20 s in 0.1 M NaOH, washed thoroughly with DI water, and

dried under flowing Ar gas. A final anneal of 220 °C for 5-min. was then conducted on each film.

Plots of normalized S:Hf and Cl:Hf ratios for neutralized films deposited from S50 and S70 solutions are shown in Figure 5.2a and Figure 5.2b. As the pre-neutralization anneal temperature is increased, the amount of sulfur and chlorine detected in the films increases. Below pre-neutralization anneal temperatures of 110 °C for S50 samples and 150 °C for S70, very little sulfur or chlorine is detected. As the pre-neutralization anneal temperature increases the magnitude of dehydration increases, driving condensation and oxide framework densification. This loss of water and enhanced crosslinking significantly decreases the gel-like character of the film, which severely hinders mobility of ions. Complete ion-exchange through the bulk of the film slows and eventually ceases. Though EPMA does not provide information about the depth distribution of elemental constituents it is conceivable, that at the surface of the film, ion exchange and sulfate leaching still occurs. To probe such an effect and to determine the depth distribution of the elements Time of Flight Secondary Ion Mass Spectrometry (TOF-SIMS) was employed.

TOF-SIMS was performed on a series of neutralized HafSOx films to determine the depth distribution of sulfur relative to hafnium within the films. Figure 5.3a and 5.3b show the TOF-SIMS spectra for HafSOx films deposited from S50 and S70 precursor solutions. Similar to what is seen in the EPMA data,

complete exchange occurs only below certain temperatures unique to each composition. For S50, complete exchange occurs only when films are annealed at ≤110 °C, whereas this temperature is elevated upwards of 160 °C for S70.

The TOF-SIMS data also confirm that partial neutralization is possible, resulting in inhomogenous films. At pre-neutralization anneals of 125 °C for S50 films and 175 °C for S70 films a sulfur poor region in the top half of the film is evident, whereas the bottom half of the film is essentially identical in sulfur detected in the non-neutralized films. As the pre-neutralization anneal temperature increases further bulk neutralization ceases, though sulfur poor surfaces are evident. It is likely that a condensed layer of $HfO_x(OH)_{4-2x}$ exists only near the surface of HafSOx films annealed at higher temperatures before neutralization with NaOH (aq).

Physical Properties

Interestingly, the film thickness increases immediately after the neutralization process as shown in Table 5.1:

Table 5.1. Ellipsometry data for HafSOx film before and immediately after neutralization in 0.1 M NaOH (aq).

Sample:	HafSOx	HafSOx post neutralization
Thickness:	127 nm	140 nm
Refractive Index (λ=595nm)	1.68	1.61

This increase in thickness is accompanied by a decrease in refractive index, both indicative of swelling and an increase in porosity. As Cl^- and SO_4^{2-} are released from the film the weakly polymerized HfO_2 framework is disrupted, creating water voids within in the film. As the these voids fill with absorbed water the film expands and the overall density decreases. Film swelling is quite common in a number of polymers where water permeates and is absorbed through pores immediately prior or concurrent with dissolution.[21,25] During neutralization of a HafSOx film, a neutralization front is created near the film surface and it continues to move through the depth of the film driven by the large H^+ gradient between film and solution, and creating water voids in its wake. This neutralization front rapidly forces more H^+ towards the surface, which drags sulfate with it.

As mentioned above the neutralization process can be observed to occur macroscopically by comparing the color change of HafSOx films before and after neutralization and a subsequent anneal. Such a color change is typically indicative of a change in either film density or film thickness. To confirm that such changes occur, variable angle spectroscopic ellipsometry was conducted on unneutralized and neutralized HafSOx films to compare their indices of refraction and film thicknesses. Thickness data for neutralized and unneutralized annealed HafSOx films is shown in Figure 5.4.

The refractive indices of S50 and S70 films measured using ellipsometry before and after neutralization and a post-neutralization anneal at 300 °C are

shown in Figure 5.5. For S50 samples annealed at 75 °C before neutralization, an increase in index of refraction from 1.68 to 1.82 at 550 nm is seen after a 1-min anneal at 300 °C. Concurrent with the increase in refractive index a decrease in film thickness is also seen. Together, these physical changes indicate conversion of the hydrous $HfO_{2-x}(SO_4)_x$ film into $HfO_x(OH)_{4-2x}$. As the pre-neutralization temperature increases, the magnitude of changes of film thickness and refractive index decreases until very little or no change is seen at all.

Coupled with the elemental-analysis data, a couple of observations between S50 and S70 films can be made. First, S70 films may undergo neutralization after higher temperature pre-neutralization anneals than the S50 films. Second, the range of pre-neutralization temperatures where the films may undergo significant exchange is extended in the S70 series relative to the S50 series. This extended temperature range may be explained by the higher acidity and higher level of hydration of the S70 films compared to the S50 samples. Furthermore, the action of sulfate as a condensation inhibitor is evident.

Acid Catalyzed Exchange

Ion exchange for cation and anion exchange has generally been shown to be a pH dependent process, with cation exchange occurring at high pH and anion exchange at low pH.[17] In this work the neutralization of HafSOx films at high pH creates a hydrous HfO_2 film that could continue to express ion-exchange character. To test this, immediately following base neutralization freshly created $HfO_x(OH)_{4-}$

$_{2x}$ films were immersed in acidic and neutral solutions containing sulfate and phosphate anions using 1M aqueous solutions of H_2SO_4 (pH=0), $(NH_4)_2SO_4$ (pH=7) H_3PO_4 (pH=1) and $(NH_4)_2HPO_4$ (pH=6-7). Following immersion and rinsing with DI water, films were then analyzed by EPMA and TOF-SIMS.

EPMA results for twice exchanged films, starting with S50 films, are shown in Figure 5.7. It is clear that anion exchange and sulfate or phosphate uptake is more pronounced in acidic H_2SO_4 and H_3PO_4 solutions compared with the more neutral ammonium salt solutions. Films immersed in H_2SO_4 and H_3PO_4 for 20 s after initial neutralization were found to have the compositions $HfO_{1.84}(SO_4)_{0.16}$ and $HfO_{1.835}(PO_4)_{0.11}$, respectively, represented here as dehydrated formulas. Comparing the amount of sulfur and phosphorus present in the acidic exchanged film and the basic exchanged film, clearly an uptake of sulfate and phosphate has occurred. This behavior is consistent with what has been observed before with hydrous ZrO_2, where acidic conditions favor anion uptake and where little exchange occurs at neutral conditions.

It is also of note that the amount of sulfate and phosphate uptake after exchange in acidic solution differs from the amount sulfate present in the original HafSOx film. It is likely that during neutralization with NaOH the average particle size within the film is increased due to base catalyzed condensation, therefore decreasing the area of exchangeable surfaces. Consequently the film becomes saturated with sulfate and phosphate at much lower concentrations.

EPMA, however, provides no information about depth distribution of the elements within the films, and therefore TOF-SIMS was conducted on films exchanged in sulfuric acid and phosphoric acid with the data shown in Figure 5.8 and 2.9. It is apparent that soaking neutralized HafSOx films in 1 M H_2SO_4 (aq) results in reintroduction of sulfate throughout the full depth of the film, whereas soaking in 1 M H_3PO_4 (aq) results in a gradient of phosphate with a large concentration at the surface that quickly decreases through the depth of the film. Phosphate is known to coordinate more strongly with Zr and Hf than sulfate, and, in fact, readily forms gelatinous precipitates in their solutions. It is likely that lability of the to-be-exchanged anions is necessary for quick migration and diffusion through the hydrated hafnium oxide-hydroxide network.

HafSOx films, as envisioned in this work, can therefore be described as low density metal aquo-hydroxo gels whose densities can be modified by thermal annealing. When lightly annealed, HafSOx films are poorly dense metal hydroxide gels comprised of vanishingly small particles bound together by a network of labile hydrogen bonds mediated by hydroxide, water, sulfate, and oxide species. This weakly bound water and network of hydrogen bonds can then facilitate the migration of anions from surfaces within the film-gel to the solution, enabling an ion exchange process in which sulfate and chloride anions are replaced by water and hydroxides, resulting in a quasi amorphous $HfO_x(OH)_{4-2x}$ gel.

Conclusion

HafSOx films were described to possess ion exchange characteristics where sulfate and chloride anions can be removed from the film by neutralization with aqueous base. Neutralization does not delaminate or significantly roughen the films and results in the conversion of HafSOx ($HfO_{2-x}(SO_4)_x$) to hydrous hafnia, ($HfO_x(OH)_{4-2x}$) below temperatures unique to the starting HafSOx composition. An initial sulfate to hafnium ratio of 0.7 : 1 within the film allows neutralization and exchange of SO_4^{2-} and Cl^- for OH^- to occur at temperatures up to 170 °C, whereas a starting sulfate to hafnium ratio of 0.5 : 1 ceases complete exchange at a lower temperature near 110 °C. A second exchange reaction was demonstrated for neutralized films by immersion in acidic solutions of sulfuric and phosphoric acid.

These results demonstrate a portion of the complex chemistry that occurs during the development of HafSOx resists. Exposure drives condensation and densification in the exposed regions, and therefore slows the ion-exchange process similar to annealed films. Similarly, the influence of resist composition clearly plays a significant role in the development chemistry of HafSOx because of its ion-exchange properties. Furthermore, it is known that the sensitivity of HafSOx increases with decreasing sulfate content and may very well be a result of decreased ion-exchange capacity, though more research needs to be conducted.

References

(1) Casey, W. H.; Westrich, H. R.; Banfield, J. F.; Ferruzzi, G.; Arnold, G. W. *Nature* **1993**, *366*, 253–256.

(2) Casey, W. H.; Ludwig, C. *Nature* **1996**, *381*, 506–509.

(3) Tamura, H.; Katayama, N.; Furuichi, R. *Environmental Science & Technology* **1996**, *30*, 1198–1204.

(4) Brown, G. E. *Proceedings of the National Academy of Sciences* **1999**, *96*, 3388–3395.

(5) Cailleteau, C.; Angeli, F.; Devreux, F.; Gin, S.; Jestin, J.; Jollivet, P.; Spalla, O. *Nature Materials* **2008**, *7*, 978–983.

(6) Chick, L. A.; Pederson, L. R. *MRS Proceedings* **2011**, *26*.

(7) Romero Pareja, R.; López Ibáñez, R.; Martín, F.; Ramos-Barrado, J. R.; Leinen, D. *Surface and Coatings Technology* **2006**, *200*, 6606–6610.

(8) Gusev, E. P.; Cabral, C.; Copel, M.; D'Emic, C.; Gribelyuk, M. *Microelectronic Engineering* **2003**, *69*, 145–151.

(9) Mikhaelashvili, V.; Betzer, Y.; Prudnikov, I.; Orenstein, M.; Ritter, D.; Eisenstein, G. *Journal of Applied Physics* **1998**, *84*, 6747.

(10) Meyers, S. T.; Anderson, J. T.; Hong, D.; Hung, C. M.; Wager, J. F.; Keszler, D. A. *Chemistry of Materials* **2007**, *19*, 4023–4029.

(11) Jiang, K.; Zakutayev, A.; Stowers, J.; Anderson, M. D.; Tate, J.; McIntyre, D. H.; Johnson, D. C.; Keszler, D. A. *Solid State Sciences* **2009**, *11*, 1692–1699.

(12) Jiang, K.; Anderson, J. T.; Hoshino, K.; Li, D.; Wager, J. F.; Keszler, D. A. *Chemistry of Materials* **2011**, *23*, 945–952.

(13) Anderson, J. T.; Munsee, C. L.; Hung, C. M.; Phung, T. M.; Herman, G. S.; Johnson, D. C.; Wager, J. F.; Keszler, D. A. *Advanced Functional Materials* **2007**, *17*, 2117–2124.

(14) Stowers, J.; Keszler, D. A. *Microelectronic Engineering* **2009**, *86*, 730–733.

(15) Telecky, A.; Xie, P.; Stowers, J.; Grenville, A.; Smith, B.; Keszler, D. A. *Journal of Vacuum Science & Technology B: Microelectronics and Nanometer Structures* **2010**, *28*, C6S19.

(16) Amphlett, C. B.; McDonald, L. A.; Redman, M. J. *Journal of Inorganic and Nuclear Chemistry* **1958**, *6*, 236–245.

(17) Clearfield, A. *Industrial & Engineering Chemistry Research* **1995**, *34*, 2865–2872.

(18) Clearfield, A. *Reviews of Pure and Applied Chemistry* **1964**, *14*.

(19) Zhao, F.; Gao, Y.; Luo, H. *Langmuir* **2009**, *25*, 6940–6946.

(20) Flanagin, L. W.; McAdams, C. L.; Hinsberg, W. D.; Sanchez, I. C.; Willson, C. G. *Macromolecules* **1999**, *32*, 5337–5343.

(21) Hinsberg, W.; Houle, F. A.; Lee, S.-W.; Ito, H.; Kanazawa, K. *Macromolecules* **2005**, *38*, 1882–1898.

(22) Donovan, J. J.; Tingle, T. N. *Microscopy and Microanalysis* **1996**, *2*, 1–7.

(23) Pouchou, J. L.; Pichoir, F. In *Microbeam Analysis*; Armstrong, J. ., Ed.; San Francisco Press: San Francisco, 1985; pp. 104–106.

(24) Clearfield, A.; Landis, A. L.; Medina, A. S.; Troup, J. M. *Journal of Inorganic and Nuclear Chemistry* **1973**, *35*, 1099–1108.

(25) Hinsberg, W. D. *Journal of The Electrochemical Society* **1986**, *133*, 1448.

Figures

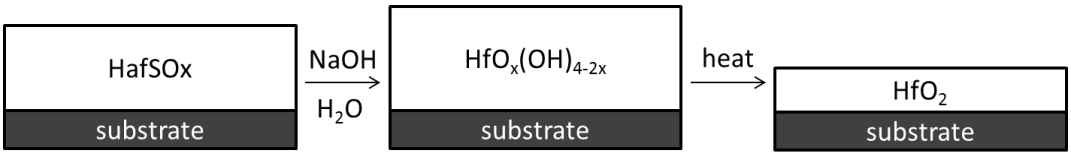

Figure 5.1: Schematic of the process of neutralization of HafSOx films.

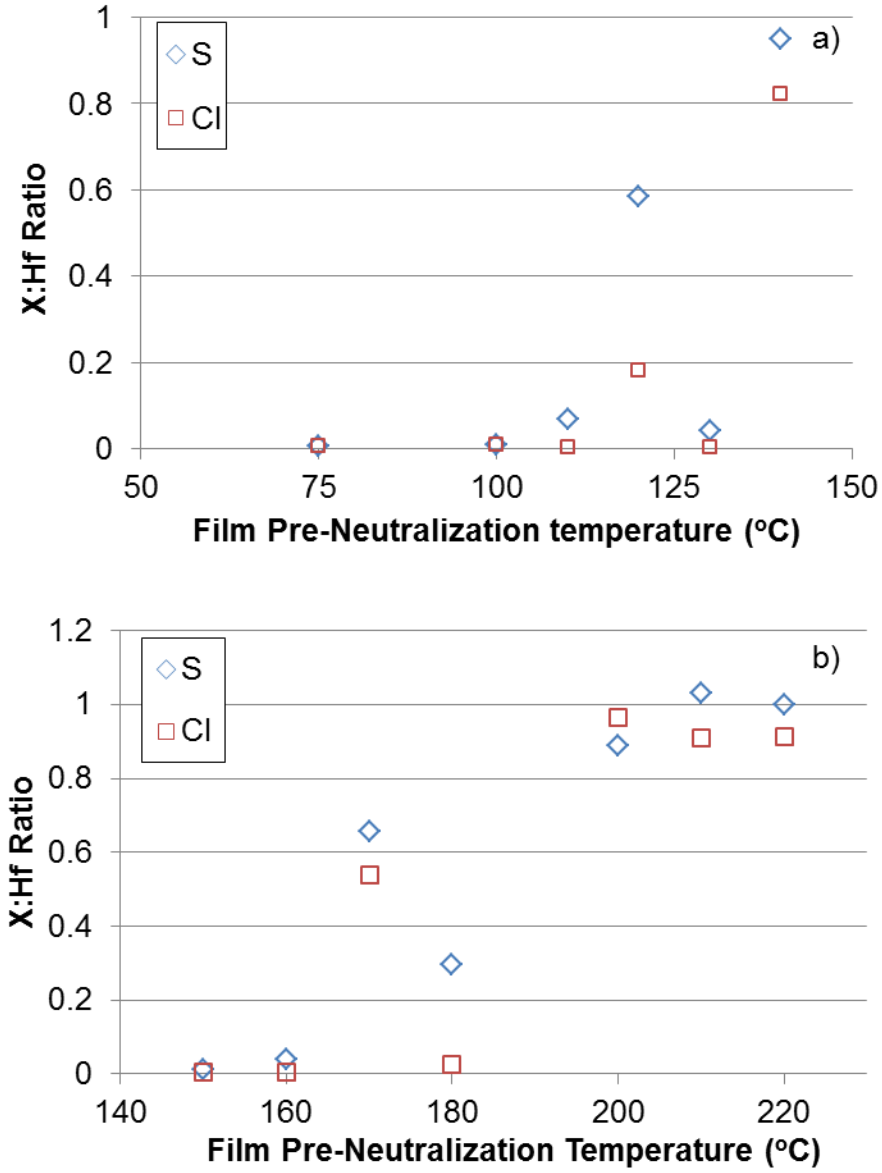

Figure 5.2: EPMA data of normalized S:Hf and Cl:Hf ratios for HafSOx films deposited from a) S50 and b) S70 precursors

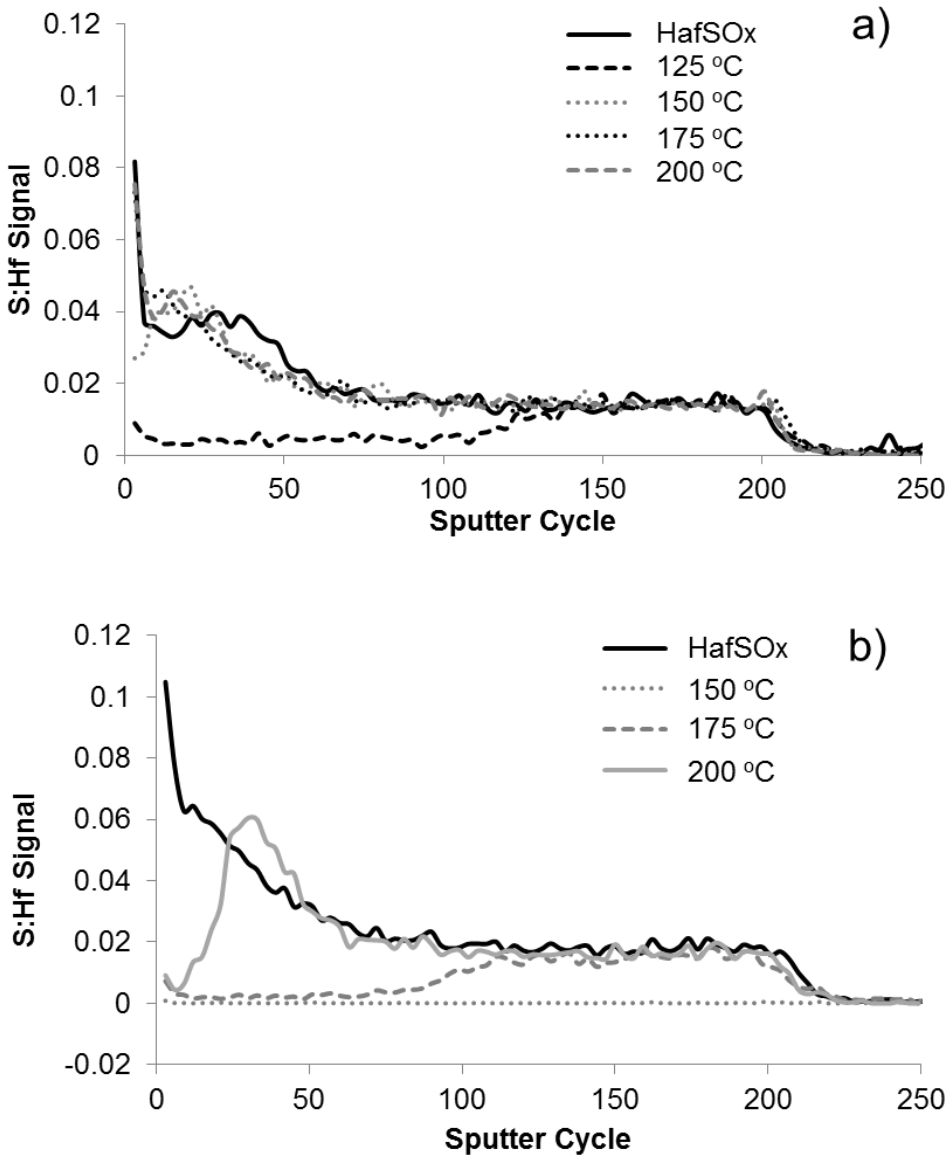

Figure 5.3: Time of Flight Secondary Ion Mass Spectrometry data for HafSOx films prepared at selected temperatures then neutralized with 0.1 M NaOH (aq) for 20s for a) S50 precursor solutions, and b) S70 precursor solutions.

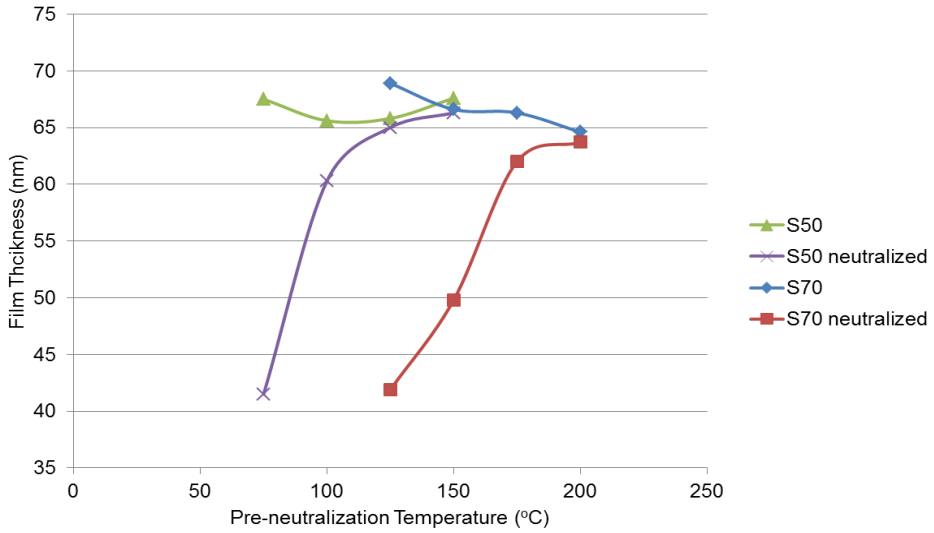

Figure 5.4: Thicknesses of HafSOx films before and after neutralization in 0.1M NaOH as determined by ellipsometry.

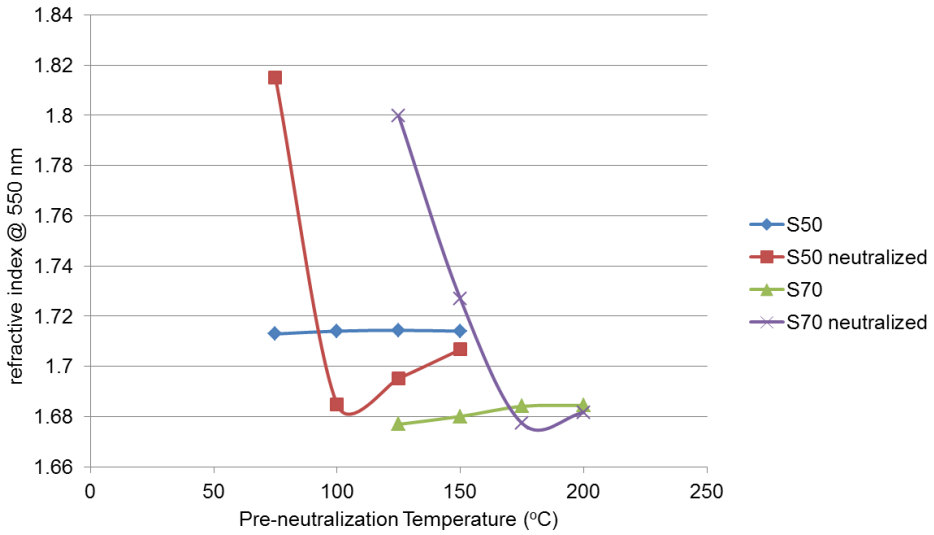

Figure 5.5: Refractive indices of HafSOx before and after neutralization as a function of pre-neutralization anneal temperature.

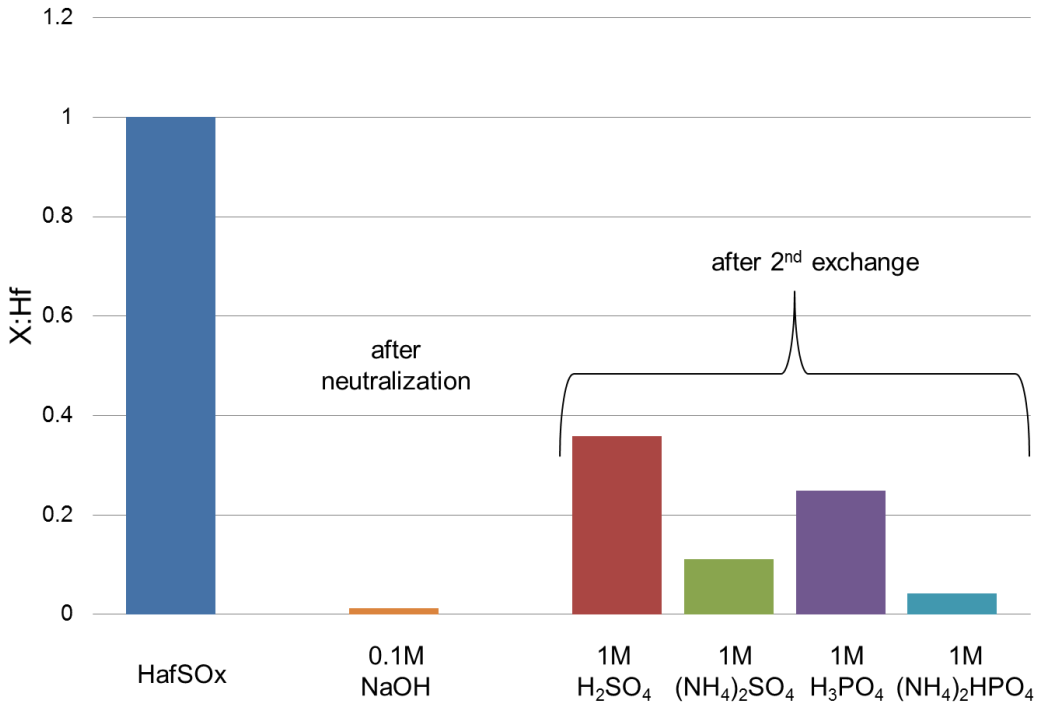

Figure 5.6: EPMA data showing normalized X:Hf ratios for S50 HafSOx films after neutralization and after acid-catalyzed exchange in sulfate and phosphate solutions.

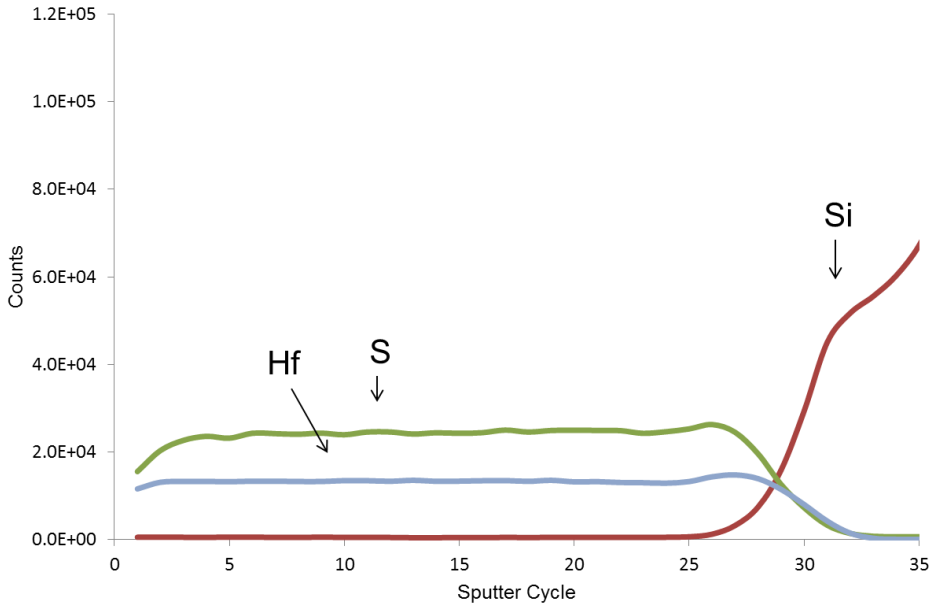

Figure 5.7: TOF-SIMS data of HafSOx films soaked in 1 M H_2SO_4 for 20 seconds following a 20s neutralization in 0.1M NaOH.

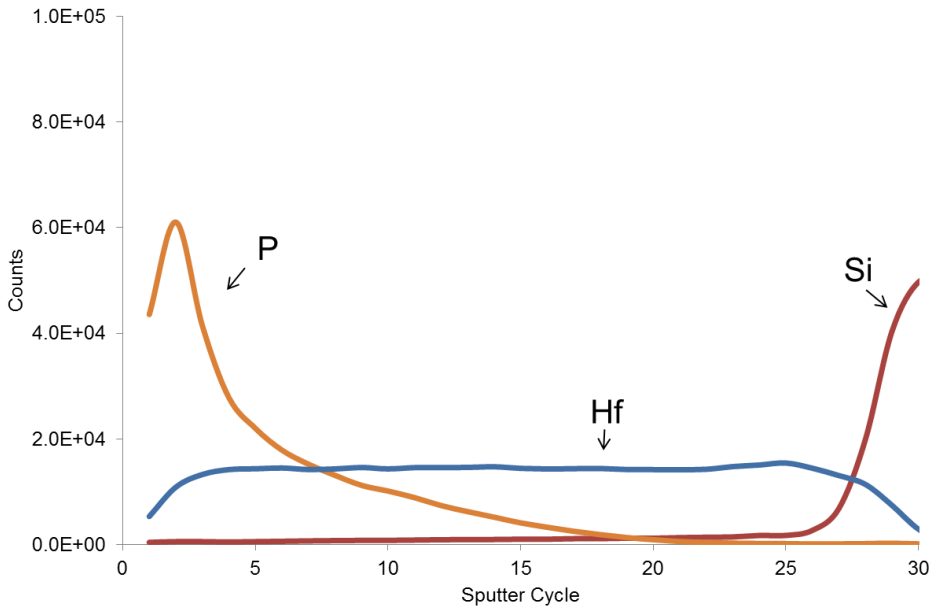

Figure 5.8: TOF-SIMS data of HafSOx films soaked in 1M H_3PO_4 for 20 seconds following a 20s neutralization in 0.1M NaOH.

CHAPTER 6

PROPERTIES AND CHARACTERIZATION OF HfO_2 FILMS PREPARED BY NEUTRALIZATION

Abstract

Films of HfO_2 and ZrO_2 were prepared by neutralization of HafSOx and ZircSOx films with sodium hydroxide. The films were analyzed by x-ray diffraction and were found to crystallize initially in a mixed monoclinic and tetragonal phase from between 500 and 550 ^{o}C, while heating above 550 ^{o}C produced only monoclinic HfO_2 and ZrO_2. The optical properties of HfO_2 films were measured using ellipsometry, and their morphologies were imaged using scanning electron microscopy. Cubic-stabilized hafnia was prepared by doping with Y_2O_3 and nanolaminated structures of cubic HfO_2:Y and monoclinic ZrO_2 were prepared.

Introduction:

Zirconium and hafnium oxide have attracted much interest from chemists, physicists and material scientists for their interesting and applicable properties to catalysis, optical coatings and waveguides, high hardness and high dielectric performance.[1,2,3,4,5] Much interest also exists in the multiple phases of HfO_2 and ZrO_2 due to the physical and chemical differences between them. For example, cubic zirconia and hafnia are well known ion conductors are elevated temperatures, whereas their monoclinic forms are inactive in this respect.[6,7,8] Similarly tetragonal zirconia and hafnia have been theorized to possess superior dielectric properties in comparison to the monoclinic or cubic phases. These phases are stabilized at different temperatures in pure HfO_2 or ZrO_2. The monoclinic phase is the thermodynamically favored phase at low temperatures, while the tetragonal and cubic phases are found at higher temperatures. The tetragonal and cubic phases cannot be quenched in, but they can be stabilized by the addition of lower valent metals, such as Ca^{2+}, Mg^{2+}, La^{3+} or Y^{3+}, into the oxide.[9]

Films of ZrO_2 and HfO_2 are typically deposited from vacuum techniques such as chemical vapor deposition (CVD), sputtering or atomic layer deposition (ALD).[2,10,11] These physical methods often result in high quality films but are slow, expensive and limited in coverage area due to the use of a vacuum chamber. Solution deposition methods have also been used to deposit ZrO_2 and HfO_2 films, though most routes often fail to meet the quality of films deposited via vacuum

methods.[12,13] Most solution deposition routes to ZrO_2 or HfO_2 films employ metal-organic precursors along with aqueous or organic solvents which result in films that contain significant organic impurities. These impurities must then be removed, often by a high temperature anneals, which results in crystallization and the formation of grain boundaries, pores or other phenomena that degrade the quality of the material. Thus, aqueous organic-free routes are desired to avoid the inclusion of organic impurities.

Aqueous routes to all inorganic $HfO_{2-x}(SO_4)_x$ and $ZrO_{2-x}(SO_4)_x$ (HafSOx and ZircSOx) films have been demonstrated by Anderson et al and have been shown to be dense, pinhole free and atomically smooth.[14] Hydrated films of HafSOx retain considerable acidic character and can be neutralized by aqueous base to remove the sulfate anions from the film and resulting in $HfO_{2-x}(OH)_{2x}$, as was demonstrated in the previous chapter. After a subsequent post-neutralization anneal in a furnace or on a hotplate, the hydrous films can be converted to HfO_2 or ZrO_2 by simple dehydration. This chapter will detail the morphologies and properties of HfO_2 films derived from neutralization of HafSOx films.

Experimental

Solution and Film Preparation: HafSOx and ZircSOx solutions were prepared similarly to as was described in chapter 2, where aqueous solutions of $HfOCl_2$, $ZrOCl_2$, H_2SO_4 and H_2O_2 were mixed in stoichiometric ratios and then diluted with deionized water to reach a metal concentration of between 0.1 and

0.6M. Sulfate to metal ratios were between 0.5:1 and 0.7:1. Solutions of HafSOx:Y and ZircSOx:Y were prepared by a similar method by using $HfOCl_2$:Y and $ZrOCl_2$:Y as metal sources. These solutions were prepared by dissolving an Y_2O_3 into $HfOCl_2$ or $ZrOCl_2$ by stirring at room temperature for 24 hours.

Substrates of Si and 200 nm of SiO_2 on Si were prepared for deposition by sonication for 1 hour at 45 ^oC in a Contrad 70 solution. Deposition was carried out by spin coating at 2000 to 3000 rpm for 45s, followed by a hotplate anneal at 125 ^oC for 3 minutes. This process resulted in film thicknesses from 10 to 100 nm per cycle, and was repeated until a desired film thickness was reached. Neutralization was carried out by immersing the films in 0.1M NaOH for 30 seconds, followed by a thorough rinse with DI water and a furnace anneal.

Characterization: X-ray diffraction (XRD) data were collected for thin films using a Rigaku RAPID diffractometer employing Cu Ka radiation generated from a rotating anode at 40 kV and 100 mA. X-ray reflectivity (XRR) data were collected with Cu Ka radiation at 40 kV and 40 mA on a Bruker D8 Discover Diffractometer and a Rigaku Ultima IV Diffractometer. Film thicknesses and mass densities were calculated from XRR data using the software package GlobalFit. SEM images were collected on a Zeiss Ultra-55 Scanning Electron Microscope at beam energies from 3-6 keV. Variable angle spectroscopic ellipsometry was conducted on a J.A. Woollam V.A.S.E 32 system. Modeling was conducted on WVASE32 software using Cauchy fitting parameters.

Results and Discussion

As shown previously HafSOx films begin to crystallize around 700 °C when decomposition of sulfate groups begins to occur. Below 700 °C sulfate groups act as a glass former in the HfO_2 matrix, frustrating crystallization and promoting amorphous character. Neutralized HafSOx films, however, begin to crystallize between 500 °C and 550 °C, a temperature that is consistent with the removal of sulfate groups and in agreement with other reports of HfO_2 thin films deposited by vacuum and sol-gel deposition.[15,16] Figure 6.1 shows the XRD pattern of neutralized HafSOx films as a function of temperature.

Interestingly the thermodynamically favored monoclinic HfO_2 phase is not the only phase present upon incipient crystallization, but rather a mixture of monoclinic and cubic/tetragonal phases is seen at 550 °C. Tetragonal and cubic phases of HfO_2 powders are normally stable only above 1700 °C and 2700 °C, respectively, and cannot be quenched in; however, they may be stabilized by inclusion of lower valent cations such as Ca^{2+}, Y^{3+}, La^{3+} and others.[1718] No such cations were present by EPMA so the appearance of a tetragonal/cubic phase warrants an explanation.

Though the monoclinic phase is the thermodynamically stable phase of ZrO_2 and HfO_2 at room temperature, the cubic and tetragonal phases have been shown to appear upon film crystallization due to a couple of reasons. First is a striking similarity between the structure and environment of zirconium in the

$ZrOCl_2$ and $ZrO(NO_3)_2$ salts and the cubic crystal structure of ZrO_2.[19] In both structures Zr^{4+} exists in 8-coordinate edge sharing Zr polyhedra, such as in the well-known doubly-hydroxy bridged $[Zr(OH)_2{\cdot}4H_2O]_4^{8+}$ tetramer present in aqueous solutions of zirconium salts. Upon base-induced precipitation or refluxing of $ZrOCl_2$ solutions, a gel-like precipitate is generated with a local structure that closely resembles that of the cubic phase of ZrO_2. Second, stabilization of cubic and tetragonal phases of HfO_2 and ZrO_2 has also been attributed to small particle sizes and an increased surface energy that induces lattice strain which stabilizes the otherwise unstable cubic/tetragonal phase.[20,21]

The similarities between Zr and Hf chemistry are vast and extensive, and it is recognized that aqueous hafnium solutions closely resemble those of zirconium. Therefore when HafSOx precursor solutions are prepared using aqueous solutions of $HfOCl_2$, cubic-like tetramers $[Hf(OH)_2{\cdot}4H_2O]_4^{8+}$ are present. It is reasonable to assume that this tetramer is conserved not only after the addition of H_2SO_4, but also after deposition via spin coating. Presumably, spin coating drives rapid solvent loss through evaporation and prompt inorganic condensation processes that can kinetically trap metastable species to result in the rapid polymerization of cubic-like Hf tetramers and oligomers. A subsequent low-temperature hotplate cure provides energy to promote cross-linking and condensation between the metal oxide centers, while limiting long-range diffusion and bond rearrangement. After neutralization and removal of sulfate and chloride anions, the weakly polymerized $HfO_x(OH)_{4-2x}$ framework structure retains the cubic-like Hf local coordination

environment of the oligimeric clusters present in the precursor solution. As thermal annealing drives dehydration and subsequent crystallization a kinetically stable cubic phase may then nucleate through the low-energy path provided by the already cubic-like Hf environment within the film. Finally, increasing the annealing temperature leads to the thermodynamically stable monoclinic HfO_2 phase as atoms and bonds undergo longer range diffusion and rearrangement.

Ellipsometry and X-ray reflectivity (XRR) analyses were conducted on neutralized HafSOx films to elucidate upon the densification and thickness changes that occur during neutralization and subsequent annealing. Following neutralization and after a subsequent hotplate cure a striking reduction in thickness is observed, a result of the conversion of the film from HafSOx to hydrous HfO_2. XRR data was fit by GlobalFit software to collect thickness, mass density, and roughness values. Mass densities are shown in Figure 6.2 for annealed HfO_2 films prepared by neutralization. It is seen that considerable densification occurs by 300 ^{o}C, where the films reach 78% theoretical bulk density, and upwards of 90% theoretical density is achieved by 700 ^{o}C. Roughnesses also track with the crystallinity of the sample, increasing from 0.2 nm for a film annealed at 300 ^{o}C to 0.63 nm for a film annealed at 600 ^{o}C.

It is apparent that a decrease in density accompanies film crystallization. HfO_2 films annealed at 500 ^{o}C, which is around the onset of crystallization, exhibit a lower density and index of refraction than films annealed at 400 ^{o}C, which are

largely amorphous. As the film crystallizes grain growth occurs rapidly which breaks and rearranges bonds to result in porosity and an overall decrease in density. Hf^{+4} ions are present in a cubic environment in solution, a coordination that most likely preserved in the amorphous film, the onset of crystallization necessitates the formation of 7-coordinate (monoclinic) Hf^{+4}, which requires bond rearrangement. As the annealing temperature increases further, sintering occurs to reduce porosity to finally result in films that achieve 90% bulk density by 700 ^{o}C.

Films of neutralized HafSOx were also analyzed by variable angle spectroscopic ellipsometry as a corollary to XRR analysis. The index of refraction of ion exchanged HfO_2 films before neutralization, post neutralization, and after post-neutralization anneals was calculated from ellipsometric data from fitting done through a Cauchy model. Comparing HafSOx films before and after ion-exchange it can be seen in Table 6.1 that the index of refraction decreases for the HafSOx film after ion-exchange, while the film thickness increases. Similar behavior is seen in XRR measurements.

Table 6.1. Thickness and index of refraction for HafSOx film before and immediately after neutralization.

Sample:	HafSOx	HafSOx – post neutralization
Film Thickness:	127 nm	140 nm
Refractive Index (λ = 595 nm)	1.68	1.61

After subsequent post-neutralization anneals, however, the films densify considerably. Figure 6.3 shows the indices of refraction and thicknesses as

calculated from ellipsometric data for HfO_2 films annealed at increasing temperature. Even after a 100 ^oC hotplate anneal the refractive index increases to 1.77 compared to 1.68 for a non-neutralized HafSOx annealed at 135 ^oC. Annealing at higher temperatures leads to further film thickness reduction and an increase in index of refraction. After a 300 ^oC anneal the index of refraction, (λ = 595 nm), is 1.87, and after a 700 ^oC anneal is 1.99. The refractive indices obtained here are in good agreement with that of HfO_2 films prepared by vacuum-deposition methods where values of between 1.85 and 1.98 (at λ = 550 nm) for electron-beam deposited films, and 1.98 (λ = 660 nm) for sputter deposited films have been reported.[222] Estimation of film densities was performed by modeling the film as a combination of two materials, the bulk material (HfO_2) and voids (air or water), by using the effective optical medium approach represented by the equation:[23]

$$\frac{(n^2 - n_2^2)(n^2 + 2n_1^2)}{(n^2 + 2n_2^2)(n_1^2 - n^2)} = \frac{q_1}{1 - q_1}$$

where n is the refractive index for the film, n_1 the refractive index for bulk HfO_2 (n_1 = 2.13), n_2 the refractive index of voids in the form of air (n_2 = 1) or water (n_2 = 1.33), and q_1 is the volume fraction of the bulk. From assuming water voids for films annealed at 300 ^oC and below, and air voids for films annealed at 400 ^oC and above densities matching well with those found from XRR analysis are obtained, and are shown in Table 6.2.

Table 6.2. Relative density of HfO_2 films prepared by neutralization determined by XRR and by ellipsometric data.

Anneal Temp (^oC)	From XRR:	From Ellipsometry:
300	78%	75%
400	86%	88%
600	87%	88%
700	91%	92%

These values also agree very well, and, in fact, are nearly identical with those obtained by Jiang et. al for HfO_2 films prepared by spin coating of an aqueous hafnium peroxide precursor where relative densities of 77% and 88% of bulk HfO_2 were found for films annealed at 300 ^oC and 600 ^oC, respectively.[24] The consistency of these results with those found in this thesis is a testament to the efficiency of conversion of aqueous based precursors to dense oxide films.

Scanning electron microscopy (SEM) was conducted on HfO_2 films annealed at 300 ^oC, 600 ^oC and 800 ^oC. At 300 ^oC the films are x-ray amorphous and top-down imaging in Figure 6.4 reveals a smooth and featureless surface, though some texture can be seen in the cross-section image. At 600 ^oC x-ray diffraction indicates that the film is crystalline, and the SEM images shown in Figure 6.5 substantiate their crystallinity. Cross-section images show large dense grains that can also be observed in the top-down image along with a number of cracks and pores. As the anneal temperature is increased to 800 ^oC, the size of the grains increase and grain boundaries become quite evident, as apparent in Figure

6.6. This collection of images agrees well with the densities obtained from XRR and ellipsometry.

Based on the high quality of HfO_2 films obtained via neutralization of HafSOx films and because the neutralization process results in the selective removal of anions from the film, a method to fabricate mixed metal films can be realized. Normally, both ZrO_2 and HfO_2 crystallize in the their thermodynamically favored monoclinic form, but by doping either with lower-charged cations such as Y^{3+}, the cubic or tetragonal phase can be stabilized at lower temperatures.[25,26,27] It has also been demonstrated that the formation of the tetragonal or cubic phase of ZrO_2:Y is determined by the concentration of $YO_{1.5}$ present in the material, with the cubic phase stabilized by the inclusion of above 8% mol. $YO_{1.5}$.

The use of aqueous precursors and neutralization techniques to achieve cubic stabilized hafnia and zirconia offers a number of advantages over organic sol-gel routes. In addition to the previously-described problems associated with the presence of bulky organic ligands and solvent as film impurities, the differences in hydrolysis rates of metal alkokide precursors used in metal-organic sol-gel routes can lead to inhomogeneity and reproducibility issues for films prepared from such routes. For example, Huang and coworkers reported nanocrystalline yttria-stabilized zirconia particles where Y_2O_3 was largely isolated at the particle surfaces.[27] The metal organic sol-gel polymerization processes are highly dependent upon the rates of hydrolysis between Y-alkoxide and Zr-alkoxides, and

these differences are made manifest in the precipitate with the result being the generation of heterogeneous particles with largely ZrO_2-type cores surrounded by Y_2O_3 or ZrO_2:Y at their surfaces. To remedy this situation it becomes necessary to anneal the film or particles at temperatures > 1000 ^oC to force cation diffusion, mixing, and full stabilization of the tetragonal or cubic phase.

On the other hand, the acidic nature of HafSOx precursor solutions accommodates the dissolution of less acidic oxides such as Y_2O_3 or La_2O_3, which negates the problems associated with controlling the hydrolysis of highly reactive metal alkoxides. Thus, solutions of $HfOCl_2$ containing 10% Y^{3+} relative to the total metal concentration were prepared by dissolving Y_2O_3 into $HfOCl_2$ at room temperature. These solutions were then used in the preparation of HafSOx precursor solutions.

Films of Y_2O_3-doped HafSOx were deposited by spin-coating and were then neutralized in 0.1M NaOH. XRD analysis was then conducted on the annealed films. Crystallization of yttria-doped HfO_2 in the cubic phase is observed at 500 ^oC. The observed XRD pattern changes only slightly with increased annealing temperature. Though the observed pattern at all temperatures is consistent with the cubic phase of HfO_2, the position of the diffraction peaks move to lower 2θ values, indicating that an increase in d-spacing is occurring. As the annealing temperature increases, the substitution of Zr^{4+} in favor of larger Y^{3+} cations forces an increase in lattice spacing to accommodate its larger size.

Contrary to the behavior of undoped HfO_2 films, where crystallization of mixed monoclinic and tetragonal phases initially occurs, yttria-doped HfO_2 films appear to be single phase.

On the basis of the non-destructive nature of the neutralization process and the striking similarities between hafnium and zirconium chemistry, a path to structural nanolaminated films was enabled. Nanolaminated structures consisting of alternating layers of ZircSOx and HafSOx with low roughness and high reproducibility have been demonstrated previously. Here, depositing alternating layers of ZircSOx and Y_2O_3-doped HafSOx at low curing temperatures enabled a route to neutralization of the entire stack whereby conversion of the entire film to sulfate-free oxide, e.g. layers of ZrO_2 and HfO_2:Y, was possible. These two materials are known to crystallize in two distinct phases, cubic HfO_2:Y and monoclinic ZrO_2, and therefore facilitate the formation of nanolaminated structures wherein each layer consists of a material in a different crystal strucure. Indeed, after heating the neutralized HafSOx:Y/ZircSOx nanolaminate to 800 ^oC for an hour x-ray diffraction indicates the presence of both monoclinic and cubic phases (Figure 6.7), which is different from the single phase films found when films of either material are crystallized. The presence of two phases is indicative of distinct layers of cubic HfO_2:Y and monoclinic ZrO_2, as shown in an SEM image presented in Figure 6.8. Remarkably, the integrity of each layer appears to be retained through the neutralization process, demonstrating the versatility of the

neutralization process to realize materials and film stacks that would otherwise be difficult to achieve.

Conclusion

The ion exchange and neutralization properties of HafSOx films were employed to fabricate thin HfO_2 films. The neutralized HafSOx films were shown to crystallize between 500 and 550 ^oC in mixed monoclinic and tetragonal phases, with the monoclinic phase becoming stabilized and predominant at 600 ^oC. X-ray reflectivity and ellipsometry were employed to measure the densities, thicknesses and indices of refraction of HfO_2 prepared by neutralization. Around 90% relative density was found for films annealed at 400 ^oC for 1 hour, and refractive indices (λ=595 nm) of between 1.9 and 2.0 were found. SEM images were collected on amorphous and crystalline HfO_2 films. Finally, cubic-stabilized HfO_2:Y films were prepared by neutralization, and nanolaminated structures consisting of cubic-stabilized HfO_2:Y and monoclinic ZrO_2 were fabricated through neutralization routes.

References

(1) Aoki, Y.; Kunitake, T.; Nakao, A. *Chemistry of Materials* **2005**, *17*, 450–458.

(2) Martínez, F. L.; Toledano-Luque, M.; Gandía, J. J.; Cárabe, J.; Bohne, W.; Röhrich, J.; Strub, E.; Mártil, I. *Journal of Physics D: Applied Physics* **2007**, *40*, 5256–5265.

(3) Gao, Y.; Masuda, Y.; Ohta, H.; Koumoto, K. *Chemistry of Materials* **2004**, *16*, 2615–2622.

(4) Urlacher, C.; Marco de Lucas, C.; Bernstein, E.; Jacquier, B.; Mugnier, J. *Optical Materials* **1999**, *12*, 19–25.

(5) Sayama, K.; Arakawa, H. *The Journal of Physical Chemistry* **1993**, *97*, 531–533.

(6) England, W.; Cross, M.; Hamnett, A.; Wiseman, P.; Goodenough, J. *Solid State Ionics* **1980**, *1*, 231–249.

(7) Miyahara, Y. *Journal of Applied Physics* **1992**, *71*, 2309.

(8) Sillassen, M.; Eklund, P.; Pryds, N.; Johnson, E.; Helmersson, U.; Bøttiger, J. *Advanced Functional Materials* **2010**, *20*, 2071–2076.

(9) Álvarez, M. R.; Landa, A. R.; Otero-Díaz, L. C.; Torralvo, M. J. *Journal of the European Ceramic Society* **1998**, *18*, 1201–1210.

(10) Yu, H. Y.; Li, M. F.; Kwong, D. L. *Thin Solid Films* **2004**, *462-463*, 110–113.

(11) Gusev, E. P.; Cabral, C.; Copel, M.; D'Emic, C.; Gribelyuk, M. *Microelectronic Engineering* **2003**, *69*, 145–151.

(12) Schwartz, R. W.; Schneller, T.; Waser, R. *Comptes Rendus Chimie* **2004**, *7*, 433–461.

(13) Mitzi, D. B. *Solution processing of inorganic materials*; Wiley: Hoboken, N.J., 2009.

(14) Anderson, J. T.; Munsee, C. L.; Hung, C. M.; Phung, T. M.; Herman, G. S.; Johnson, D. C.; Wager, J. F.; Keszler, D. A. *Advanced Functional Materials* **2007**, *17*, 2117–2124.

(15) Modreanu, M.; Sancho-Parramon, J.; O'Connell, D.; Justice, J.; Durand, O.; Servet, B. *Materials Science and Engineering: B* **2005**, *118*, 127–131.

(16) Wang, Z. J.; Kumagai, T.; Kokawa, H.; Tsuaur, J.; Ichiki, M.; Maeda, R. *Journal of Crystal Growth* **2005**, *281*, 452–457.

(17) Blanchin, M.-G.; Canut, B.; Lambert, Y.; Teodorescu, V. S.; Barău, A.; Zaharescu, M. *Journal of Sol-Gel Science and Technology* **2008**, *47*, 165–172.

(18) Butz, B.; Störmer, H.; Gerthsen, D.; Bockmeyer, M.; Krüger, R.; Ivers-Tiffée, E.; Luysberg, M. *Journal of the American Ceramic Society* **2008**, *91*, 2281–2289.

(19) Clearfield, A. *Reviews of Pure and Applied Chemistry* **1964**, *14*.

(20) Stichert, W.; Schüth, F. *Chemistry of Materials* **1998**, *10*, 2020–2026.

(21) Garvie, R. C. *The Journal of Physical Chemistry* **1978**, *82*, 218–224.

(22) Jerman, M.; Qiao, Z.; Mergel, D. *Applied Optics* **2005**, *44*, 3006.

(23) Mergel, D. *Thin Solid Films* **2001**, *397*, 216–222.

(24) Jiang, K.; Anderson, J. T.; Hoshino, K.; Li, D.; Wager, J. F.; Keszler, D. A. *Chemistry of Materials* **2011**, *23*, 945–952.

(25) Gutzov, S.; Ponahlo, J.; Lengauer, C. L.; Beran, A. *Journal of the American Ceramic Society* **1994**, *77*, 1649–1652.

(26) Peters, C.; Weber, A.; Butz, B.; Gerthsen, D.; Ivers-Tiffée, E. *Journal of the American Ceramic Society* **2009**, *92*, 2017–2024.

(27) Huang, D.; Venkatachari, K. R.; Stangle, G. C. *Journal of Materials Research* **2011**, *10*, 762–773.

Figures

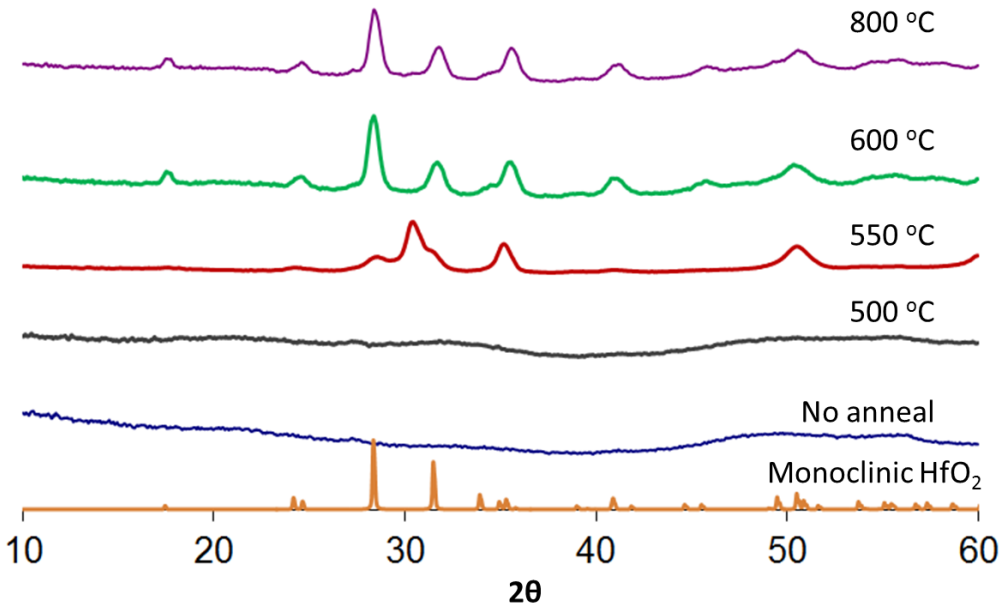

Figure 6.1: XRD patterns and crystallization behavior for neutralized HafSOx as a function of post-neutralization anneal temperature. Freshly neutralized HafSOx films are x-ray amorphous, and crystallization occurs between 500 °C and 550 °C when crystallization of monoclinic and cubic HfO_2 begins to occur.

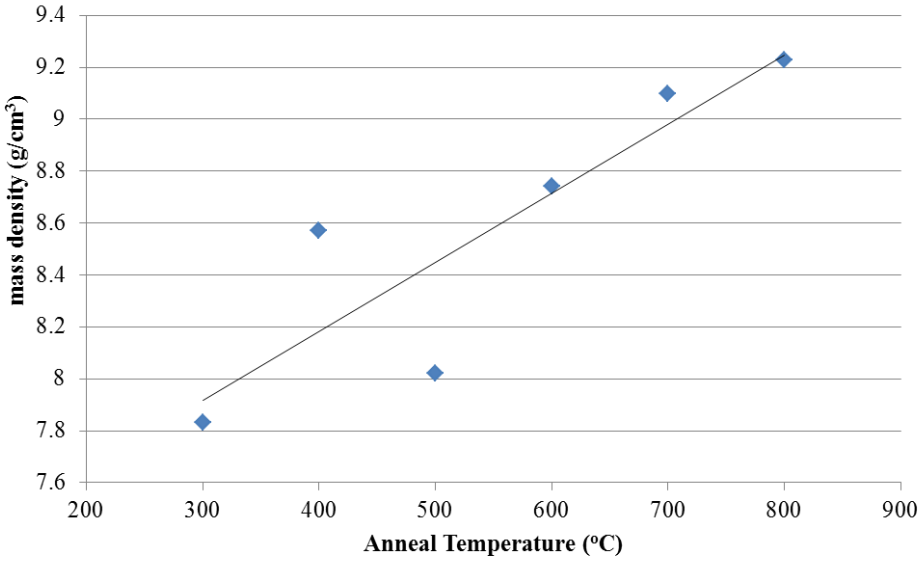

Figure 6.2: Mass densities of HfO_2 films prepared by neutralization and as measured by XRR.

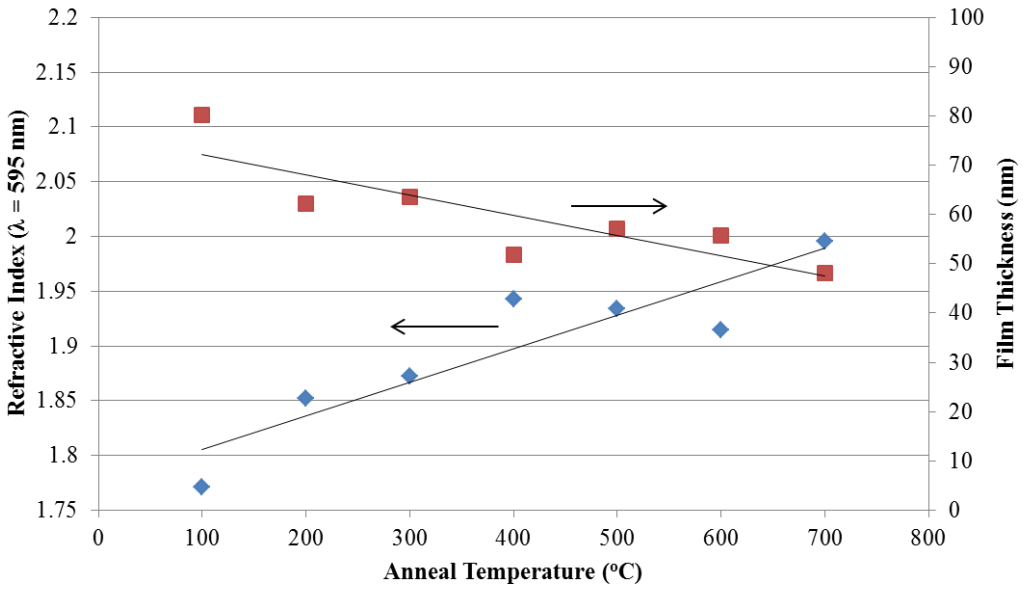

Figure 6.3: Film thicknesses and refractive indices (λ = 595nm) for HfO_2 films prepared by neutralization and as calculated via ellipsometry.

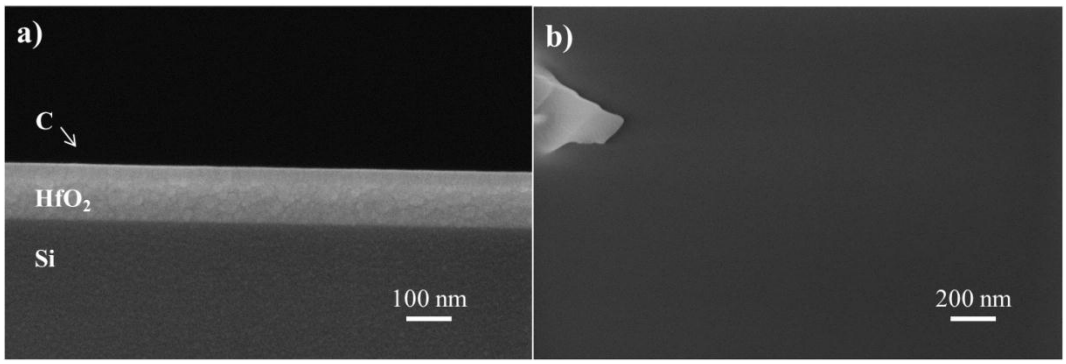

Figure 6.4: a) Cross-section SEM, and b) top-down SEM image of HfO_2 film annealed at 300 ^{o}C for 1 hour.

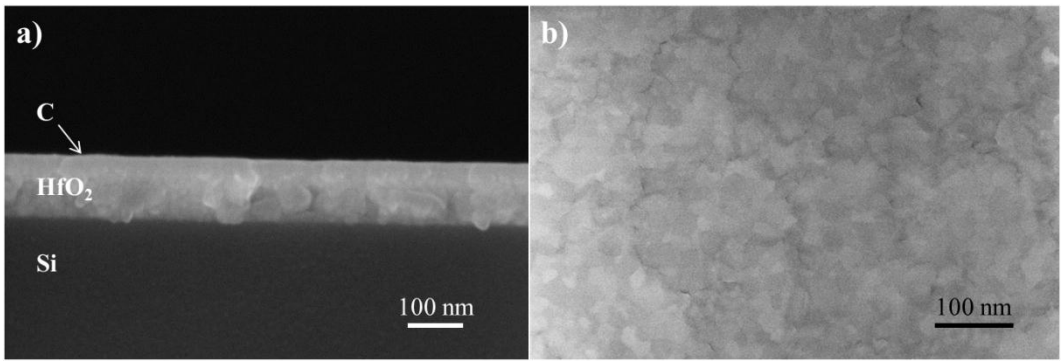

Figure 6.5: a) Cross-section SEM, and b) top-down SEM image of HfO_2 film annealed at 600 ^{o}C for 1 hour.

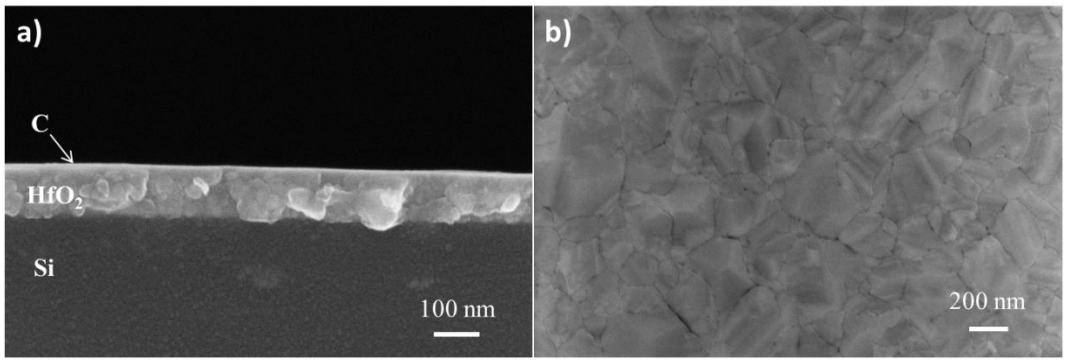

Figure 6.6: a) Cross-section SEM, and b) top-down SEM image of HfO_2 film annealed at 800 ^{o}C for 1 hour.

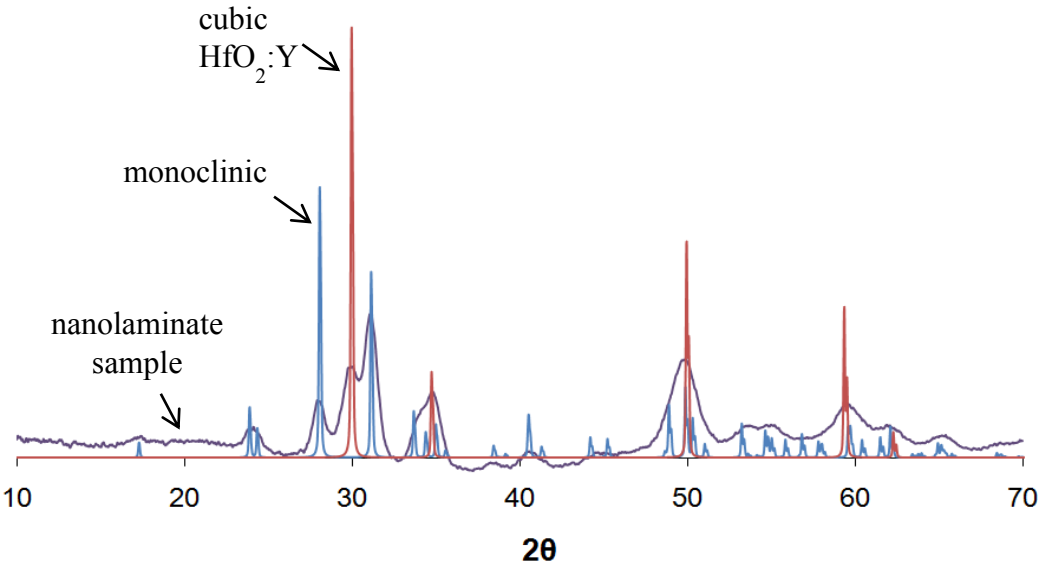

Figure 6.7: XRD pattern of a nanolaminate film stack, consisting of layers of cubic stabilized HfO_2:Y and monoclinic ZrO_2, annealed at 800 ^{o}C.

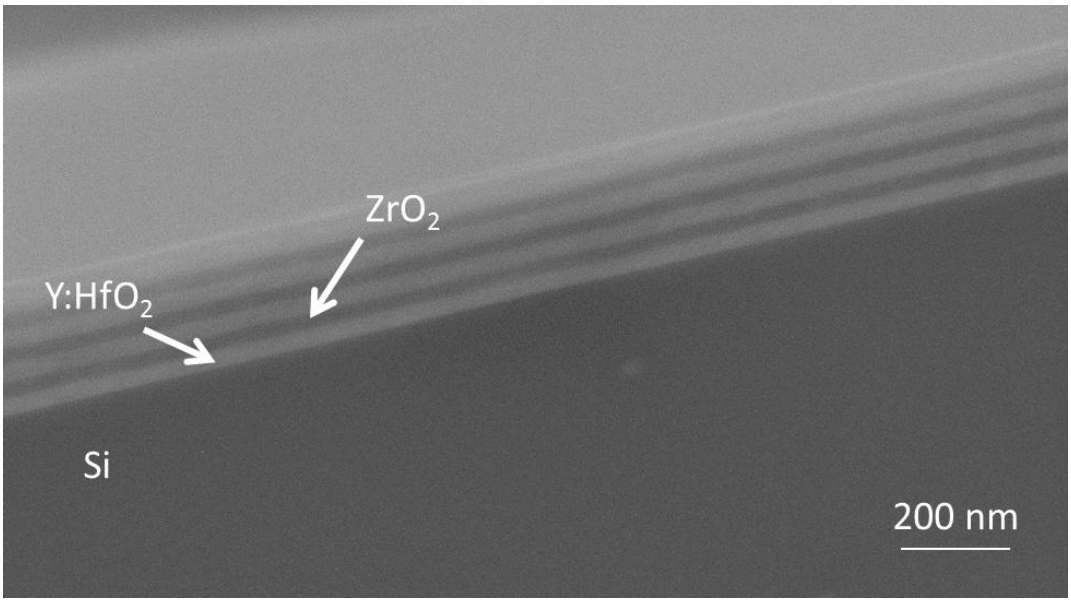

Figure 6.8: Cross-section SEM image of a nanolaminate film stack, consisting of layers of HfO_2:Y and ZrO_2, annealed at 800 ^{o}C.

CHAPTER 7

CONCLUSIONS

Understanding and controlling the chemistry of photoresists is of paramount importance to the success of modern and future lithographic techniques. As resolution requirements continue to push the performance of conventional chemically amplified organic based photoresists to their physical limits, it is becoming increasingly necessary to develop new chemistries and systems to enable future technologies.

Recently, HafSOx resists have proven to be high resolution inorganic photoresists with sensitivity to electron beams, extreme ultraviolet (EUV) radiation, and 193 nm photons. Because of their inorganic nature, HafSOx resists possess a number of advantages over organic resists such as superior etch resistance and higher resolution.

Chapter 2 employed Raman spectroscopy on HafSOx solutions and films to elaborate on the electron beam exposure mechanism in HafSOx resists. Solutions of HafSOx were shown to possess a Raman band at 829 cm^{-1} that was attributed to Hf-peroxo species. Similarly, films of HafSOx were shown to display Raman bands at 840 cm^{-1} corresponding to hafnium bound peroxo groups. HafSOx films were exposed to an electron beam, and a degredation of the Hf-peroxo band at 840 cm^{-1} was seen to decrease.

Chapter 3 demonstrated the use of HafSOx and ZircSOx as photopatternable inorganic hardmasks. Sensitivity to 193 nm light was shown, and was used to produce 60 nm line and space patterns at a dose of 25 mJ/cm^2 using

interference lithography. Based on the differences in optical properties, the sensitivity of $Hf_{1-x}Zr_xSOx$ films were found to be directly related to the ratio of hafnium and zirconium within the film. Furthermore, proof-of-concept litho-free-litho-etch (LFLE) double patterning process was demonstrated by electron beam lithography whereby 30 nm contact holes were patterned.

In Chapter 4 the effect of metal substitution in HafSOx was explored in the context of effects on resolution, line width roughness, and sensitivity (RLS) tradeoffs. It was shown that the sensitivity of HafSOx to electron beams can be increased by 20% by the inclusion of yttrium or lanthanum in HafSOx, whereas the inclusion of molybdenum or tungsten induced a decrease in sensitivity to electron beams.

The ion exchange properties of HafSOx films were analyzed in Chapter 5 in order to illuminate the mechanisms at play during the development of exposed films in the lithographic process. As consequence of their acidic nature, it was shown that immersion of HafSOx films in basic aqueous solutions results in their neutralization and causes changes in chemical and physical properties, altering their composition, density, and reactivity. It was shown that the product of neutralization is nominally represented by the composition $HfO_x(OH)_{4-2x}$.

Finall,y the properties of the neutralized HafSOx films are explored in Chapter 6. By heating the neutralized HafSOx films dense HfO_2 films were realized, and film densities as high as 90% were demonstrated. These HfO_2 were

characterized by a number of techniques, including x-ray reflectivity (XRR), x-ray diffraction (XRD), spectroscopic ellipsometry, and scanning electron microscopy (SEM). The neutralization process was exploited to achieve cubic-stabilized Y:HfO_2 films, and nanolaminated structures consisting of cubic Y:HfO_2 and monoclinic ZrO_2 were fabricated.

All in all, this thesis explored the chemistry of HafSOx resists. HafSOx resists are unique resists in that they are acidic inorganic materials that undergo a number of unique and correlated processes throughout the lithographic process. For example, the post-application bake (PAB) before exposure drives condensation and densification which in turn influences the exposure and development steps. Exposure induces compositional and density changes via decomposition of peroxide groups which, in turn, drives condensation. During the development step both neutralization and dissolution processes occur that determine the resolution, roughness, and fate of the resist material. If the neutralization process is too quick then an insoluble material is formed and resist performance suffers through poor resolution or line width roughness. Conversely, if the dissolution process is too quick then the sensitivity of the resist suffers and patterning becomes difficult.

In summary, this thesis presented research and results that enlighten the processes that occur during the PAB, exposure, and development steps. Additionally the processes at work during each of these steps were shown to be

highly correlated. Therefore this thesis represents an effort to understand and recognize the mechanisms that influence the performance of acidic inorganic resists such as HafSOx.

Figures

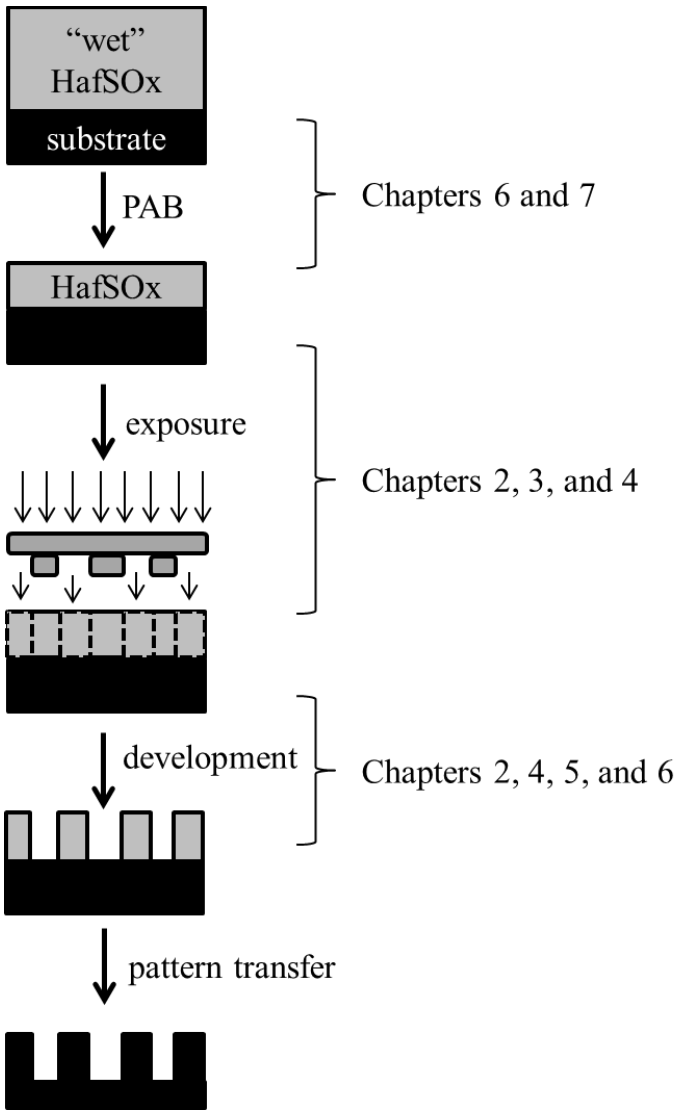

Figure 7.1. Graphical representation of how the research contained within this thesis pertains to HafSOx and the lithographic process.

Bibliography

(1) Moore, G. E. *IEEE Solid-State Circuits Newsletter* **2006**, *20*, 33–35.

(2) Anderson, J. T.; Munsee, C. L.; Hung, C. M.; Phung, T. M.; Herman, G. S.; Johnson, D. C.; Wager, J. F.; Keszler, D. A. *Advanced Functional Materials* **2007**, *17*, 2117–2124.

(3) Gusev, E. P.; Cabral, C.; Copel, M.; D'Emic, C.; Gribelyuk, M. *Microelectronic Engineering* **2003**, *69*, 145–151.

(4) Yu, H. Y.; Li, M. F.; Kwong, D. L. *Thin Solid Films* **2004**, *462-463*, 110–113.

(5) Leskelä, M.; Kukli, K.; Ritala, M. *Journal of Alloys and Compounds* **2006**, *418*, 27–34.

(6) Schwartz, R. W.; Schneller, T.; Waser, R. *Comptes Rendus Chimie* **2004**, *7*, 433–461.

(7) Mitzi, D. B. *Solution processing of inorganic materials*; Wiley: Hoboken, N.J., 2009.

(8) Aoki, Y.; Kunitake, T.; Nakao, A. *Chemistry of Materials* **2005**, *17*, 450–458.

(9) Choi, J. H.; Hwang, S. M.; Lee, C. M.; Kim, J. C.; Park, G. C.; Joo, J.; Lim, J. H. *Journal of Crystal Growth* **2011**, *326*, 175–178.

(10) Lee, K. D. *Thin Solid Films* **1997**, *302*, 84–88.

(11) Burgess, J. *Metal ions in solution*; Ellis Horwood ; distributed by Halsted Press: Chichester; New York, 1978.

(12) Jolivet, J.-P.; Henry, M.; Livage, J. *Metal oxide chemistry and synthesis : from solution to solid state*; Wiley: Chichester [u.a.], 2000.

(13) Henry, M.; Jolivet, J. P.; Livage, J. In *Chemistry, Spectroscopy and Applications of Sol-Gel Glasses*; Reisfeld, R.; JJørgensen, C. K., Eds.; Springer-Verlag: Berlin/Heidelberg; Vol. 77, pp. 153–206.

(14) Sanchez, C.; Livage, J.; Henry, M.; Babonneau, F. *Journal of Non-Crystalline Solids* **1988**, *100*, 65–76.

(15) Helfferich, F. G. *Ion exchange*; Dover Publications: New York, 1995.

(16) Thompson, H. S.; Roy, J. *J. Agric. SOC. Engl.* **1850**, *11*, 68.

(17) Way, J. T.; Roy, J. *J. Agric. Soc. Engl.* **1852**, *13*, 12.

(18) Lemberg, J. *Z. deut. gel. Ges.* **1870**, *22*.

(19) Lemberg, J. *Z. deut. gel. Ges.* **1876**, *28*.

(20) Wiegner, G. *Landwirtsch* **1912**, *60*.

(21) Abrams, I. M.; Millar, J. R. *Reactive and Functional Polymers* **1997**, *35*, 7–22.

(22) Adams, B. A.; Holmes, E. L. *J. Soc. Chem. Ind. (London)* **1935**, *54*.

(23) Clearfield, A. *Inorganic ion exchange materials*; CRC Press: Boca Raton, Fla., 1982.

(24) England, W.; Cross, M.; Hamnett, A.; Wiseman, P.; Goodenough, J. *Solid State Ionics* **1980**, *1*, 231–249.

(25) Clearfield, A. *Chemical Reviews* **1988**, *88*, 125–148.

(26) Amphlett, C. B.; McDonald, L. A.; Redman, M. J. *Journal of Inorganic and Nuclear Chemistry* **1958**, *6*, 236–245.

(27) Clearfield, A. *Inorganic Chemistry* **1964**, *3*, 146–148.

(28) Okoroanyanwu, U. *Chemistry and lithography*; John Wiley: Hoboken, New Jersey, 2010.

(29) Gernsheim, H.; Gernsheim, A. *The history of photography from the camera obscura to the beginning of the modern era,*; Thames & Hudson: London, 1969.

(30) Reiser, A. *Photoreactive Polymers : The Science and technology of Resists*; John Wiley&Sons: New York [etc.], 1989.

(31) Willson, C. G. SPIE, 1997; Vol. 3048, pp. 28–41.

(32) Honda, T.; Kishikawa, Y.; Iwasaki, Y.; Ohkubo, A.; Kawashima, M.; Yoshii, M. *Journal of Microlithography, Microfabrication, and Microsystems* **2006**, *5*, 043004.

(33) Nakamura, J.; Ban, H.; Deguchi, K.; Tanaka, A. *Japanese Journal of Applied Physics* **1991**, *30*, 2619–2625.

(34) Honda, T. SPIE, 2006; Vol. 6154, p. 615422–615422–9.

(35) Shtutina, S.; Klebanov, M.; Lyubin, V.; Rosenwaks, S.; Volterra, V. *Thin Solid Films* **1995**, *261*, 263–265.

(36) Lavine, J. M. *Journal of Vacuum Science & Technology B: Microelectronics and Nanometer Structures* **1996**, *14*, 3489.

(37) Kratschmer, E. *Journal of Vacuum Science & Technology B: Microelectronics and Nanometer Structures* **1987**, *5*, 369.

(38) Isaacson, M.; Muray, A.; Scheinfein, M.; Adesida, I.; Kratschmer, E. *Microelectronic Engineering* **1984**, *2*, 58–64.

(39) Okamoto, H.; Iwayanagi, T.; Mochiji, K.; Umezaki, H.; Kudo, T. *Applied Physics Letters* **1986**, *49*, 298.

(40) Okamoto, H.; Ishikawa, A.; Kudo, T. *Journal of Photochemistry and Photobiology A: Chemistry* **1989**, *49*, 377–385.

(41) Hashimoto, M.; Watanuki, S.; Koshida, N.; Komuro, M.; Atoda, N. *Japanese Journal of Applied Physics* **1996**, *35*, 3665–3669.

(42) Grigorescu, A. E.; Hagen, C. W. *Nanotechnology* **2009**, *20*, 292001.

(43) Grigorescu, A. E.; van der Krogt, M. C.; Hagen, C. W.; Kruit, P. *Microelectronic Engineering* **2007**, *84*, 822–824.

(44) Stowers, J.; Keszler, D. A. *Microelectronic Engineering* **2009**, *86*, 730–733.

(45) Telecky, A.; Xie, P.; Stowers, J.; Grenville, A.; Smith, B.; Keszler, D. A. *Journal of Vacuum Science & Technology B: Microelectronics and Nanometer Structures* **2010**, *28*, C6S19.

(46) Joy, D. C.; Luo, S. *Scanning* **1989**, *11*, 176–180.

(47) Grigor'ev, E. I.; Trachtenberg, L. I. *Radiation chemical processes in solid phase : theory and application*; CRC Press: Boca Raton, Fla. [u.a.], 1996.

(48) Han, G.; Khan, M.; Cerrina, F. *Journal of Vacuum Science & Technology B: Microelectronics and Nanometer Structures* **2003**, *21*, 3166.

(49) Han, G.; Khan, M.; Fang, Y.; Cerrina, F. *Journal of Vacuum Science & Technology B: Microelectronics and Nanometer Structures* **2002**, *20*, 2666.

(50) Casey, W. H.; Westrich, H. R.; Banfield, J. F.; Ferruzzi, G.; Arnold, G. W. *Nature* **1993**, *366*, 253–256.

(51) Casey, W. H.; Ludwig, C. *Nature* **1996**, *381*, 506–509.

(52) Tamura, H.; Katayama, N.; Furuichi, R. *Environmental Science & Technology* **1996**, *30*, 1198–1204.

(53) Brown, G. E. *Proceedings of the National Academy of Sciences* **1999**, *96*, 3388–3395.

(54) Cailleteau, C.; Angeli, F.; Devreux, F.; Gin, S.; Jestin, J.; Jollivet, P.; Spalla, O. *Nature Materials* **2008**, *7*, 978–983.

(55) Chick, L. A.; Pederson, L. R. *MRS Proceedings* **2011**, *26*.

(56) Romero Pareja, R.; López Ibáñez, R.; Martín, F.; Ramos-Barrado, J. R.; Leinen, D. *Surface and Coatings Technology* **2006**, *200*, 6606–6610.

(57) Mikhaelashvili, V.; Betzer, Y.; Prudnikov, I.; Orenstein, M.; Ritter, D.; Eisenstein, G. *Journal of Applied Physics* **1998**, *84*, 6747.

(58) Meyers, S. T.; Anderson, J. T.; Hong, D.; Hung, C. M.; Wager, J. F.; Keszler, D. A. *Chemistry of Materials* **2007**, *19*, 4023–4029.

(59) Jiang, K.; Zakutayev, A.; Stowers, J.; Anderson, M. D.; Tate, J.; McIntyre, D. H.; Johnson, D. C.; Keszler, D. A. *Solid State Sciences* **2009**, *11*, 1692–1699.

(60) Jiang, K.; Anderson, J. T.; Hoshino, K.; Li, D.; Wager, J. F.; Keszler, D. A. *Chemistry of Materials* **2011**, *23*, 945–952.

(61) Clearfield, A. *Industrial & Engineering Chemistry Research* **1995**, *34*, 2865–2872.

(62) Clearfield, A. *Reviews of Pure and Applied Chemistry* **1964**, *14*.

(63) Zhao, F.; Gao, Y.; Luo, H. *Langmuir* **2009**, *25*, 6940–6946.

(64) Flanagin, L. W.; McAdams, C. L.; Hinsberg, W. D.; Sanchez, I. C.; Willson, C. G. *Macromolecules* **1999**, *32*, 5337–5343.

(65) Hinsberg, W.; Houle, F. A.; Lee, S.-W.; Ito, H.; Kanazawa, K. *Macromolecules* **2005**, *38*, 1882–1898.

(66) Donovan, J. J.; Tingle, T. N. *Microscopy and Microanalysis* **1996**, *2*, 1–7.

(67) Pouchou, J. L.; Pichoir, F. In *Microbeam Analysis*; Armstrong, J. ., Ed.; San Francisco Press: San Francisco, 1985; pp. 104–106.

(68) Clearfield, A.; Landis, A. L.; Medina, A. S.; Troup, J. M. *Journal of Inorganic and Nuclear Chemistry* **1973**, *35*, 1099–1108.

(69) Hinsberg, W. D. *Journal of The Electrochemical Society* **1986**, *133*, 1448.

(70) Martínez, F. L.; Toledano-Luque, M.; Gandía, J. J.; Cárabe, J.; Bohne, W.; Röhrich, J.; Strub, E.; Mártil, I. *Journal of Physics D: Applied Physics* **2007**, *40*, 5256–5265.

(71) Gao, Y.; Masuda, Y.; Ohta, H.; Koumoto, K. *Chemistry of Materials* **2004**, *16*, 2615–2622.

(72) Urlacher, C.; Marco de Lucas, C.; Bernstein, E.; Jacquier, B.; Mugnier, J. *Optical Materials* **1999**, *12*, 19–25.

(73) Sayama, K.; Arakawa, H. *The Journal of Physical Chemistry* **1993**, *97*, 531–533.

(74) Miyahara, Y. *Journal of Applied Physics* **1992**, *71*, 2309.

(75) Sillassen, M.; Eklund, P.; Pryds, N.; Johnson, E.; Helmersson, U.; Bøttiger, J. *Advanced Functional Materials* **2010**, *20*, 2071–2076.

(76) Álvarez, M. R.; Landa, A. R.; Otero-Díaz, L. C.; Torralvo, M. J. *Journal of the European Ceramic Society* **1998**, *18*, 1201–1210.

(77) Modreanu, M.; Sancho-Parramon, J.; O'Connell, D.; Justice, J.; Durand, O.; Servet, B. *Materials Science and Engineering: B* **2005**, *118*, 127–131.

(78) Wang, Z. J.; Kumagai, T.; Kokawa, H.; Tsuaur, J.; Ichiki, M.; Maeda, R. *Journal of Crystal Growth* **2005**, *281*, 452–457.

(79) Blanchin, M.-G.; Canut, B.; Lambert, Y.; Teodorescu, V. S.; Barău, A.; Zaharescu, M. *Journal of Sol-Gel Science and Technology* **2008**, *47*, 165–172.

(80) Butz, B.; Störmer, H.; Gerthsen, D.; Bockmeyer, M.; Krüger, R.; Ivers-Tiffée, E.; Luysberg, M. *Journal of the American Ceramic Society* **2008**, *91*, 2281–2289.

(81) Stichert, W.; Schüth, F. *Chemistry of Materials* **1998**, *10*, 2020–2026.

(82) Garvie, R. C. *The Journal of Physical Chemistry* **1978**, *82*, 218–224.

(83) Jerman, M.; Qiao, Z.; Mergel, D. *Applied Optics* **2005**, *44*, 3006.

(84) Mergel, D. *Thin Solid Films* **2001**, *397*, 216–222.

(85) Gutzov, S.; Ponahlo, J.; Lengauer, C. L.; Beran, A. *Journal of the American Ceramic Society* **1994**, *77*, 1649–1652.

(86) Peters, C.; Weber, A.; Butz, B.; Gerthsen, D.; Ivers-Tiffée, E. *Journal of the American Ceramic Society* **2009**, *92*, 2017–2024.

(87) Huang, D.; Venkatachari, K. R.; Stangle, G. C. *Journal of Materials Research* **2011**, *10*, 762–773.

(88) ITRS Roadmap, 2009 Edition, http://www.itrs.net/

(89) Gibbons, F. P.; Manyam, J.; Diegoli, S.; Manickam, M.; Preece, J. A.; Palmer, R. E.; Robinson, A. P. G. *Microelectronic Engineering* **2008**, *85*, 764–767.

(90) Sailer, H. *Microelectronic Engineering* **2004**, *73-74*, 228–232.

(91) Lawson, R. A.; Lee, C.-T.; Yueh, W.; Tolbert, L.; Henderson, C. L. *Microelectronic Engineering* **2008**, *85*, 959–962.

(92) Itani, T.; Yoshino, H.; Hashimoto, S.; Yamana, M.; Samoto, N.; Kasama, K. *Microelectronic Engineering* **1997**, *35*, 149–152.

(93) Kratschmer, E. *Journal of Vacuum Science & Technology B: Microelectronics and Nanometer Structures* **1986**, *4*, 361.

(94) Teteris, J. *Journal of Non-Crystalline Solids* **2002**, *299-302*, 978–982.

(95) Chern, G. C. *Journal of Applied Physics* **1982**, *53*, 6979.

(96) Baba, M.; Ikeda, T. *Japanese Journal of Applied Physics* **1981**, *20*, L149–L152.

(97) Ridaoui, H.; Wieder, F.; Ponche, A.; Soppera, O. *Nanotechnology* **2010**, *21*, 065303.

(98) Trikeriotis, M.; Bae, W. J.; Schwartz, E.; Krysak, M.; Lafferty, N.; Xie, P.; Smith, B.; Zimmerman, P. A.; Ober, C. K.; Giannelis, E. P. 2010; p. 76390E–76390E–10.

(99) Pauliac-Vaujour, S.; Brianceau, P.; Comboroure, C.; Faynot, O. *Microelectronic Engineering* **2008**, *85*, 800–804.

(100) Weimer, M.; Wang, Y.; Neef, C. J.; Claypool, J.; Edwards, K.; Zu, Z. SPIE, 2007; Vol. 6519, p. 65192S–65192S–8.

(101) Smith, B. W. SPIE, 2004; Vol. 5754, pp. 751–759.

(102) Namatsu, H. *Journal of Vacuum Science & Technology B: Microelectronics and Nanometer Structures* **1998**, *16*, 69.

(103) Guerrero, D. J.; Sullivan, D. M.; Mercado, R.-M. L. 2009; p. 75200M–75200M–8.

(104) Sakamoto, R.; Endo, T.; Ho, B.-C.; Kimura, S.; Ishida, T.; Kato, M.; Fujitani, N.; Onishi, R.; Hiroi, Y.; Maruyama, D. 2009; p. 75201Y–75201Y–10.

(105) Blakey, I.; Chen, L.; Dargaville, B.; Liu, H.; Whittaker, A.; Conley, W.; Piscani, E.; Rich, G.; Williams, A.; Zimmerman, P. SPIE, 2007; Vol. 6519, p. 651909–651909–9.

(106) Grenville, A. *Future Fab Intl.* **2007**, *20*.

(107) Naulleau, P.; Anderson, C. N.; Baclea-an, L.-M.; Chan, D.; Denham, P.; George, S.; Goldberg, K. A.; Hoef, B.; Jones, G.; Koh, C.; La Fontaine, B.; McClinton, B.; Miyakawa, R.; Montgomery, W.; Rekawa, S.; Wallow, T. 2010; p. 76361J–76361J–9.

(108) Campbell, N. J.; Dengel, A. C.; Edwards, C. J.; Griffith, W. P. *Journal of the Chemical Society, Dalton Transactions* **1989**, 1203.

(109) Koshida, N.; Tomita, O. *Japanese Journal of Applied Physics* **1985**, *24*, 92–94.

(110) Okamoto, H.; Ishikawa, A.; Kudo, T. *Thin Solid Films* **1989**, *172*, L97–L99.

(111) Ito, H. SPIE, 1999; Vol. 3678, pp. 2–12.

(112) Kozawa, T.; Yoshida, Y.; Uesaka, M.; Tagawa, S. *Japanese Journal of Applied Physics* **1992**, *31*, 4301–4306.

(113) Schwarzenbach, G.; Muehlebach, J.; Mueller, K. *Inorganic Chemistry* **1970**, *9*, 2381–2390.

(114) Butler, A.; Clague, M. J.; Meister, G. E. *Chemical Reviews* **1994**, *94*, 625–638.

(115) Jere, G. V.; Santhamma, M. T. *Inorganica Chimica Acta* **1977**, *24*, 57–61.

(116) Schmidt, R.; Pausewang, G.; Massa, W. *Zeitschrift anorganische und allgemeine Chemie* **1986**, *535*, 135–142.

(117) Bassil, B. S.; Mal, S. S.; Dickman, M. H.; Kortz, U.; Oelrich, H.; Walder, L. *Journal of the American Chemical Society* **2008**, *130*, 6696–6697.

(118) Tarafder, M. T. H.; Miah, M. A. L. *Inorganic Chemistry* **1986**, *25*, 2265–2268.

(119) Dengel, A. C.; Griffith, W. P. *Polyhedron* **1989**, *8*, 1371–1377.

(120) Thompson, R. C. *Inorganic Chemistry* **1985**, *24*, 3542–3547.

(121) Griffith, W. P.; Wickins, T. D. *Journal of the Chemical Society A: Inorganic, Physical, Theoretical* **1968**, 397.

(122) Stowers, J. K.; Telecky, A.; Kocsis, M.; Clark, B. L.; Keszler, D. A.; Grenville, A.; Anderson, C. N.; Naulleau, P. P. 2011; p. 796915–796915–11.